Affecting intracellular iron and copper via transmetalation and study of drug delivery systems to improve the specificity of Ti(IV)-based anticancer compounds

By
Lauren Fernández-Vega

Submitted to the Faculty of Natural Sciences
Department of Chemistry

In partial fulfillment of the requirements for the degree of
Doctor of Philosophy
at the
University of Puerto Rico, Rio Piedras Campus
April 27th, 2022

I

ACCEPTED BY THE FACULTY OF NATURAL SCIENCES
DEPARTMENT OF CHEMISTRY
UNIVERSITY OF PUERTO RICO RIO PIEDRAS CAMPUS
IN PARTIAL FULFILLMENT OF THE REQUIREMENTS FOR THE DEGREE OF
DOCTOR OF PHILOSOPHY
IN THE SUBJECT OF
CHEMISTRY

Arthur D. Tinoco, Ph.D.
THESIS DIRECTOR

DISSERTATION COMMITTEE
Jose M. Rivera Ortiz, Ph.D.
Esther A. Peterson Peguero, Ph.D.
Nestor M. Carballeira, Ph.D.
Jorge L. Colon Rivera, Ph.D.

Table of content

Table captions

Figure captions

Chapter 1

Chapter 2

Abbreviations

ROS   Reactive Oxygen Species

TfR   Transferrin Receptor

PDB   Protein Data Bank

ICP-MS   Inductively coupled plasma mass spectrometry

ICP-OES   Inductively coupled plasma atomic emission spectroscopy

Def   Deferasirox

RNR   Ribonucleotide reductase

ATP   Adenosine triphosphate

ADP   Adenosine diphosphate

AMP   Adenosine monophosphate

DNA   Deoxyribonucleic acid

EPR   Electron Paramagnetic Resonance

Q-TOF   Quadrupole Time of Flight

Abstract

Cancer is the principal cause of death globally, and research and how it works have become crucial. Iron (Fe) and Copper (Cu) are essential metals present in many critical biological processes in the human body. These metals play a part in angiogenesis, metastasis, rapid growth, and cancer survival. Disrupting them can disrupt intracellular processes that could lead to cell death. In this research work, we aim to study how Titanium(IV) Deferasirox $[Ti(Deferasirox)_2]^{2-}$ can affect both Fe and Cu and induce cell death by disrupting metals bioavailability, forming intracellular cytotoxic species, and generation an imbalance in reactive oxygen species (ROS) production. Studies in the concentration-dependent intracellular species of Cu-induced transmetalation showed that the possible intracellular products could generate cytotoxic species under physiological conditions. At the same time, Fe-induced transmetalation formed a redox active intermediate that produces a significant increase in ROS formation. The metals become unavaible for the cancer cell to perform the necessary biological processes to survive in both approaches.

Nonetheless, specificity is still a field that has become important in chemotherapeutics treatments. Since patients suffer many side effects, the idea is to deliver the drug effectively to the desired target. Drug delivery systems (DDS) are being developed to reach this objective. Herein we explored three DDS types to compare their specificity against cancer cells. Interestingly, the protein-based bovine serum albumin (BSA) DDS does not show any improvement in the uptake and activity of the titanocene dichloride (Cp_2TiCl_2) drug. Cancer cells were treated with a high concentration of Cp_2TiCl_2-BSA, and no activity was observed. Results were supported by precipitation during the cell lysate experiment, where compounds interact with intracellular compounds, demonstrating that the conjugate will not survive after entering the cell. A formulate with zirconium phosphate (ZrP) was also prepared, Cp_2TiCl_2@ZrP, and more intracellular Ti(IV) accumulation was observed, but no improvement in specificity or activity was observed. For the $[Ti(Deferasirox)_2]^{2-}$-Substance P (TDSP), more Ti(IV) accumulation was observed as in the formulate but again, no specificity improvement. Some researchers demonstrate that even when SP has been used as a drug carrier, this peptide can also increase viable cancer cells, playing against the compound anticancer activity. Finally, the peptide-directed DDS by the HAIPYRHK (P7) peptide seems more efficient in delivering the Ti(IV) ion and releasing it intracellularly as a still stable compound. Previous studies confirm the stability and activity of TD against cancer cells, but no selectivity was observed. The bioactive peptide TDP7 increases the intracellular Ti(IV) and improves the specificity against cancer cells.

Anticancer bioinorganic research is a pretty new research field compared to the past most used chemo-agents that are mainly organic molecules. In inorganic

research, these organic molecules are coordinated to a metal that often changes the drugs' biological performance. Metals can affect different biological targets depending on their properties, mainly dictated by the hard and soft acid-base (HSAB) theory.

Ti(IV) drugs have been evolving, and today, there are more stable and effective compounds that can display their biological properties against cancer cells. In the past few years, inorganic research has been mainly empirical since we lack the "rules" that dictate a structure-activity relationship. Inorganic compounds often have different geometries, oxidation states, and binding properties. Changing the ligand or the metal is impactful in the compound behavior. Still, after cisplatin, many inorganic molecules had reached clinical trials and became part of the treatment for cancer patients. Now, a new horizon is explored with bimetallic complexes, with two different metals performing their activity. Ti(IV) Deferasirox has been shown to work well with other anticancer drugs such as cisplatin. Both drugs with different mechanistic pathways will generate a synergistic effect to obtain a new generation of Ti(IV)-containing drugs.

Affecting intracellular iron and copper via transmetalation and study of drug delivery systems to improve the specificity of Ti(IV)-based anticancer compounds

Dedication

I dedicate this work to God, to my son, Luis Alejandro, and my husband, Luis Carlos. You are my motivation to be better everyday.

Acknowledgments

Thank God almighty for giving me the life and strength to be here today. I owe you everything in my life, and everything I do is for your glory.

Thanks to my husband, Luis Carlos, I won't be here without your support and encouragement to go forward. Thanks for your patience in every step of my career and my life. Thanks to my family, my mother Marbel Vega, my father Freddy Fernández, my brother Luis Felipe, my aunts and my grandma for always giving me support in every direction I have taken in my studies and my life. Thanks to my pastors, Freddy Palma y Sylvia De Palma, and the Ministerio de la Reconciliación for your prayers and love for my family and me.

Special thanks to my advisor Dr. Arthur D. Tinoco, for your guidance, support, patience, and encouragement to become a better scientist, and above all, thanks for your friendship. Thanks for supporting me as an international student, as a woman in science, as Latina, and as a mom. Without you, I will not be the scientist and the person I have become today. Thanks to Tinoco lab and all my lab mates over the years. Thanks to Josué and Israel, more than lab mates, you're my friends. Thanks for all your help and advice during my research time.

Thanks to the committee members for your advice and guidance in all the Ph. D. requirements. I have learned a lot from you! Thanks to Dra. Liz Diaz, for allowing me to be part of the project of empowering women in STEM. I enjoyed and learned a lot about being part of the event. Thanks to Gilles Gasser for accepting me to stay four months in París as part of my Chateaubriand fellowship. It was a tremendous personal and academic experience. I want to thank to all the funding sources NIH R21 (1R21CA240997-01A1), NIH SC1 (5SC1CA190504), NSF REU PR-CLIMB (2050493), the Chateaubriand Fellowship and Programa de becas de mérito y ejecutorias excepcionales (PBMA).

Thanks to all *mis colombianos*, Luis Alberto, Carolina, Wenndy, Lesly, Yelitce, Vanessa, and Oscar, you are my family! Thanks for being part of my life, supporting me, and loving me the way I am. Especially, thanks to my *chiquitas*, Mariana and Natalia, you bring happiness to my life!

Thanks to Mario Ramos for your friendship and advice on many things I didn't know. You are the best! Thanks to Marielys for being part of that difficult first year, making us part of your family, and showing us how beautiful is Puerto Rico.

Thanks to every person have been involved in my career development.

Last but not least, thanks to my beautiful baby boy Luis Alejandro, you came last, but my life is now complete because you are here with us. My achievements are for you, my baby, to give you everything I can to help you become a good person. Thanks for choosing me as your mom, and I will love you for the rest of my life.

Chapter 1

Introduction

Most chemotherapeutic agents were organic molecules with complex structures and synthesis pathways for a long time.[1] When Barnett Rosenberg accidentally discovered cisplatin in the 1960s, metal-based compounds emerged as anticancer agents.[2] Since then, platinum (Pt)-based complexes have been the best-selling anticancer drugs in the market.[3] Other metals than Pt are being researched to improve current anticancer treatments. Bioinorganic research has attracted much attention in developing new and more effective anticancer drugs.

1.1. Metals and cancer

Metals play a critical role in various biological processes in the human body, and the definition of essential metals and non-essential metals is still under study. While metals can maintain a healthy human body, they can also induce toxicity and health issues depending on their concentration or biological role.[4] Generally, what is defined as a non-essential metal is low bioavailability metals that are unnecessary for life. The metals classified as necessary for life are: Mo, Na, Zn, K, Cu, Co, Mg, Ca, Mn and Fe, and elements such as V, Ni, and Sn are presumed to be essential.[4]

1.1.1. Iron and copper

The metal homeostasis in living creatures is a delicate mechanism to maintain the metal concentration at healthy levels.[5] In cancer, these mechanisms are altered, and more consumption and high levels of certain metals are observed in cancer patients.[6-7] Fe and Cu are highly required in cancer development since they are involved in cancer's rapid progression and survival.[5] Both metals are closely related in their biological role. Cu has a redox cycling ability that enables this metal to be a catalytic co-factor in critical enzymes part of the Fe uptake process.[8-9] Fe is an active redox metal involved in cellular respiration, enzymes functions, DNA synthesis, and cell cycle progression.[10-11] Higher transferrin receptor 1 (TfR) levels are observed in cancer cells.[12-13] Hence, Fe plays an essential role in cancer cells' progression and survival as they have a higher requirement for Fe since their rapid progression requires it.[10] Fe is also involved in reactive oxygen species (ROS) production in cancerous and non-cancerous cells. Fe-dependent ROS production imbalance has been associated with the metastatic cascade facilitating migration and invasion of cancer cells to other tissues.[14] Similarly, Cu levels in cancer cells are higher than in non-cancer cells. The redox cycling properties of this metal appear to have a strong link with metastasis. Elevated Cu levels have been associated with malignancy, facilitating angiogenesis and metastasis.[15]

Treatment of metal overload diseases has led to a new perspective on mental deprivation as an anticancer treatment. FDA-approved chelation therapy has been designed as an anticancer approach (**Fig 1.1**).[16-18]
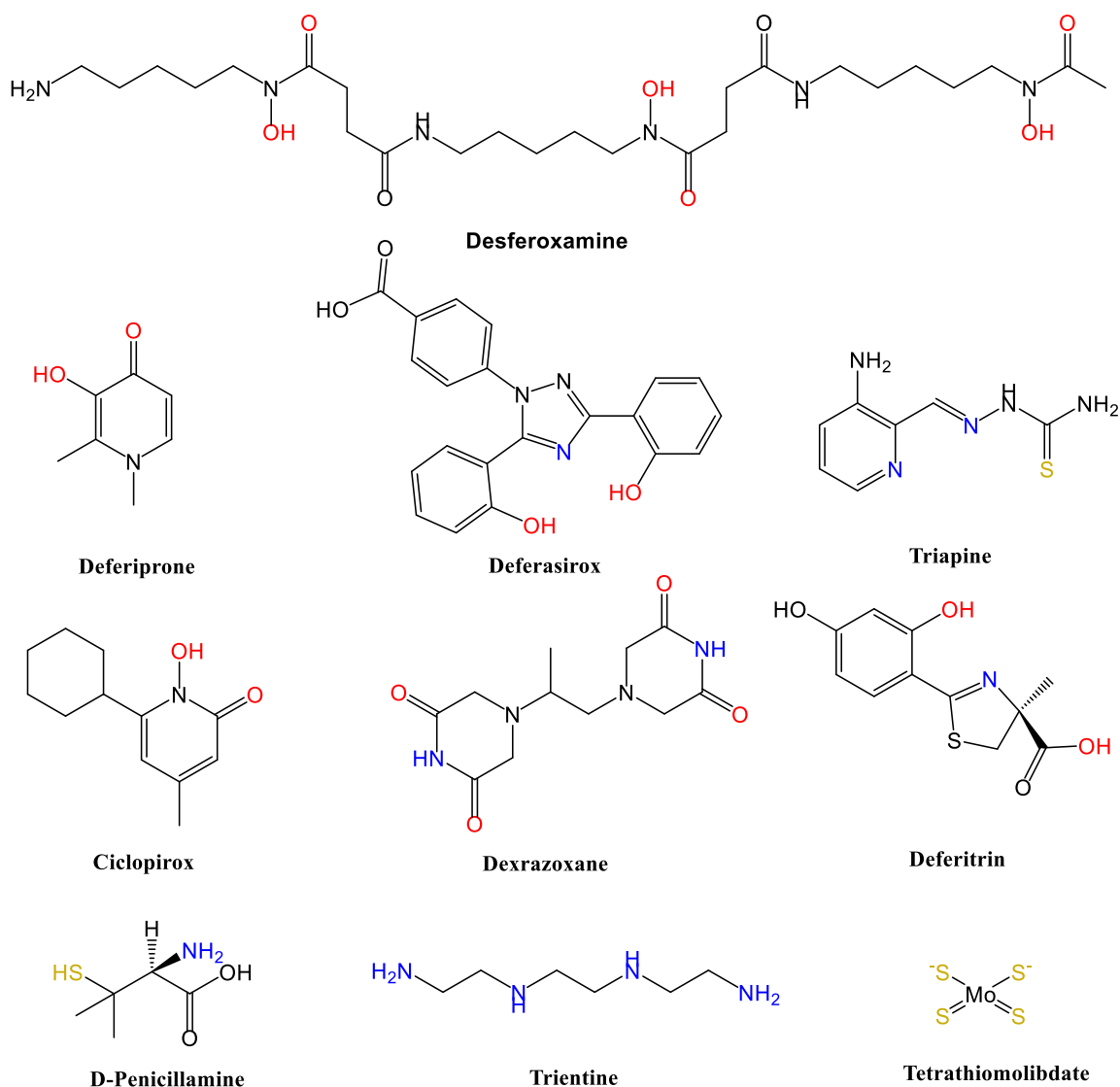
Figure 1.1 Iron chelators in clinical use: Deferoxamine, Deferiprone, Deferasirox, Triapine, Ciclopirox, Dexrazoxane, and Deferritin. Copper chelators in clinical use: D-penicillamine, Trientine, and tetrathiomolybdate.

Cu and Fe chelation therapy has the potential to become primary anticancer treatment but still lacks selectivity and potency. Using non-toxic non-essential metals coordinated with biologically active ligands that can disrupt their biological processes is a path to study the mechanistic impact of Ti(IV)-containing anticancer chelation therapy. Titanium(IV) is considered a non-toxic and non-essential metal in the human body.

1.1.2. Titanium in the human body

Ti is considered a non-essential metal for humans due to the lack of knowledge about any function this metal plays in the human body. Still, there is a daily ingestion of 200-300 µg Ti/day.[19] Ti have very low solubility at pH 7.4 with a $K_{sp} = 1 \times 10^{-29}$ (0.2 fM for the proposed soluble species $TiO(OH)_2$).[20-21] In blood plasma, Ti is found at an approximate 100 µM, which is a significantly high concentration for a non-essential metal and without showing any toxicity.[22] Ti can enter the human body in different ways, by food or drink ingestion, inhalation, and exposition of daily products. For example, Ti(IV) citrate and Ti(IV) ascorbate are used in agriculture and be founded in food.[23] TiO_2 is a food additive in sweets, chewing gum, milk products, bakery, and other consumables. Humans are also exposed to TiO_2 through paint, toothpaste, sun lotion, and cosmetics.[19, 24-25] In its metal form, Ti has the capacity of osteointegration, which is very desirable in fixation systems for humans such as prosthetics, dental and, orthopedics implants.[26] People with these types of implants present a much higher concentration of Ti (50 times higher) than people without them.[27-29] Follow-ups in Ti implant patients have found high success in using Ti in different after-fixation studies compared to other materials and Ti alloys.[29-32] At present, the toxicity of Ti implant is not common but still is a topic to be aware of.[30] Until today, the toxicity of Ti is associated with photo-induced reactions, which are not possibly happening in the human body.[24]
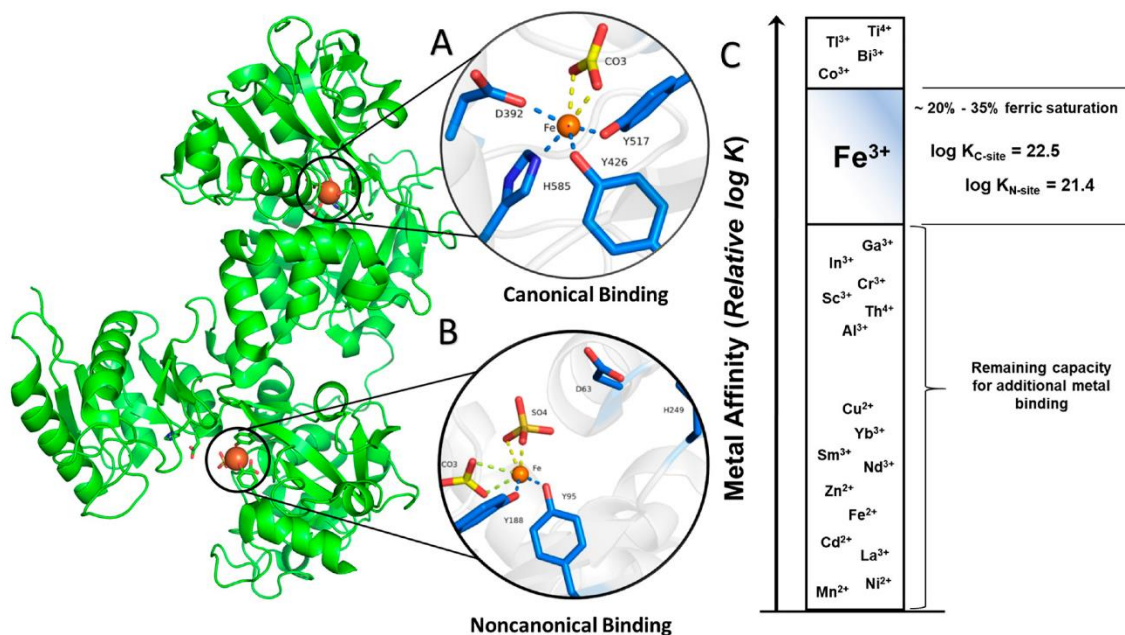
Figure 1.2. Canonical (closed, **A**) and non-canonical (open, **B**) Fe(III) binding to serum transferrin (sTf). (**C**) Representation of sTf metal affinity suggests the capacity for additional nonferric metal binding. The relative positions were taken from experimental values[33-34] and references within. PDB code: 3QYT.[35] *Inorganics is an open access article distributed under the Creative Commons Attribution License which permits unrestricted use, distribution, and reproduction in any medium, provided the original work is properly cited (See appendix 1).*

1.1.3. Titanium transport

High concentrations of Ti in the human body mean natural ways of transporting the metal and remain soluble. Ti was found to be captured or bound by serum transferrin (sTf).[20-21] An ICP-MS study was performed in blood serum, different samples from patients with and without Ti implants were analyzed. Most of the Ti was bound to the sTf protein in both populations. sTf is a bilobal (N and C terminus) glycoprotein that maintains the Fe (Fe) homeostasis. Histidine, aspartic acid, and two tyrosines are involved in the Fe coordination, and coordination is fulfilled by a carbonate anion (**Fig 1.2**). Closed conformation, also known as canonical, is as described before (**Fig 1.2A**) fulfilled by the four aminoacids and the carbonate anion. A non-canonical conformation occurs when alternate aminoacids and the anion bind the Fe. An open conformation is observed (**Fig 1.2B**).
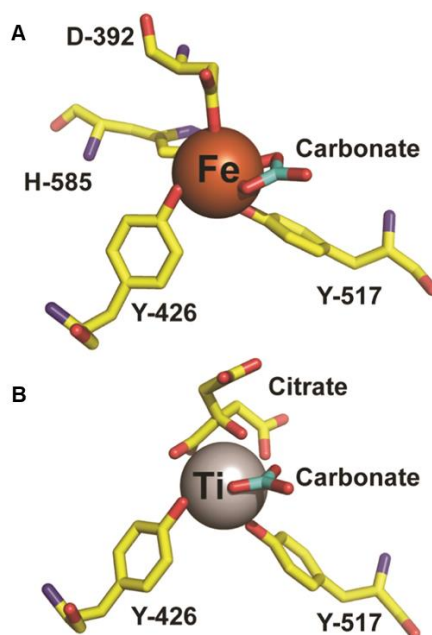
Figure 1.3 X-ray characterization of Fe(iii) and Ti(iv) coordination by serum transferrin. **A**) The C-lobe metal binding site of serum transferrin (3QYT) shows Fe(iii) bound to two tyrosine, one histidine, and one aspartate residue and to the synergistic anion carbonate. Fe(iii) is bound in a closed protein conformation. **B**) Ti(iv), however, is bound by citrate in place of the histidine and aspartate residues resulting in an open conformation (5DYH). Adapted with permission from Journal of the American Chemical Society, 138(17), 5659–5665. Copyright 2016 American Chemical Society.[36] See appendix 2.

sTf appears to have some preferences by Lewis acidic metals (**Fig 1.2C**), but it is not true to all metals. But for Ti(IV), sTf can bind it by the two tyrosines, the anion and citrate, to fulfill the coordination sphere as a non-canonical conformation (**Fig 1.3**). The sTf-Ti$_2$ complex formed has a high affinity by the transferrin receptor (TfR) (log K_A= 14.6). As expected, sTf-Fe$_2$ affinity is stronger (log K_A= 17.5).[35] Besides sTf, Ti(IV) can be bound by nitrogen and oxygen-containing biological chelators (**Fig 1.4 and 1.5**). The bioinorganic coordination chemistry in most of

these chelators mimics Fe's coordination (III). Ti(IV) and Fe(III) share many chemical similarities that make Ti(IV) compatible with the same biological molecules as Fe(III). Both are highly Lewis acidic metals, have a similar ionic radio (Ti(IV) 0.605 vs. Fe(III) 0.65), their most common coordination number is six, and have low water solubility.[37]
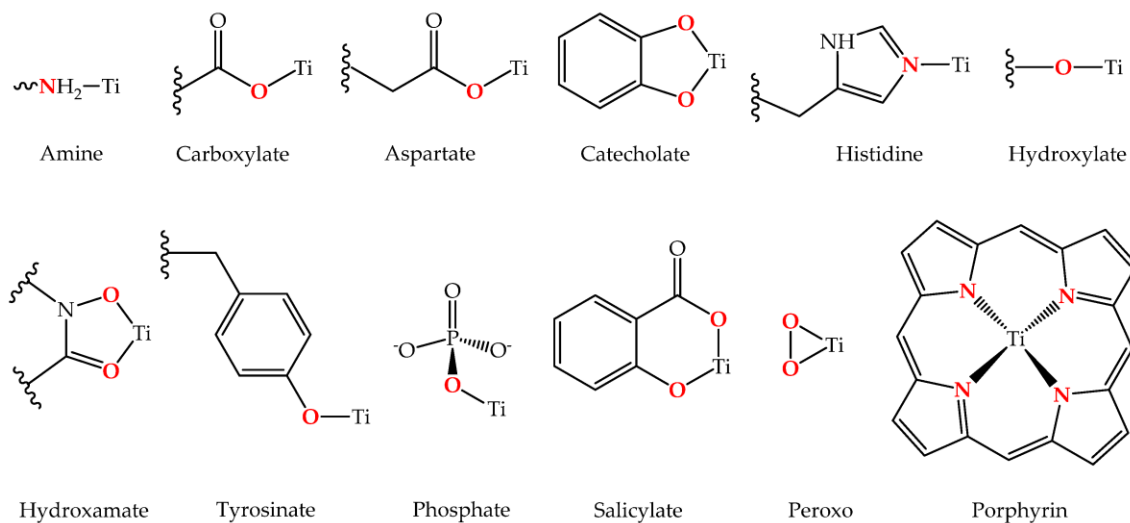
Figure 1.4. Typical Ti(IV) binding moieties of endogenous ligands with some representative coordination modalities. Reprinted from Coordination Chemistry Reviews, 363, M. Saxena, S.A. Loza-Rosas, K. Gaur, S. Sharma, S.C. Pérez Otero, A.D. Tinoco, Exploring titanium(IV) chemical proximity to Fe(III) to elucidate a function for Ti(IV) in the human body, 109–125, Copyright (2018), with permission from Elsevier. See appendix 3.
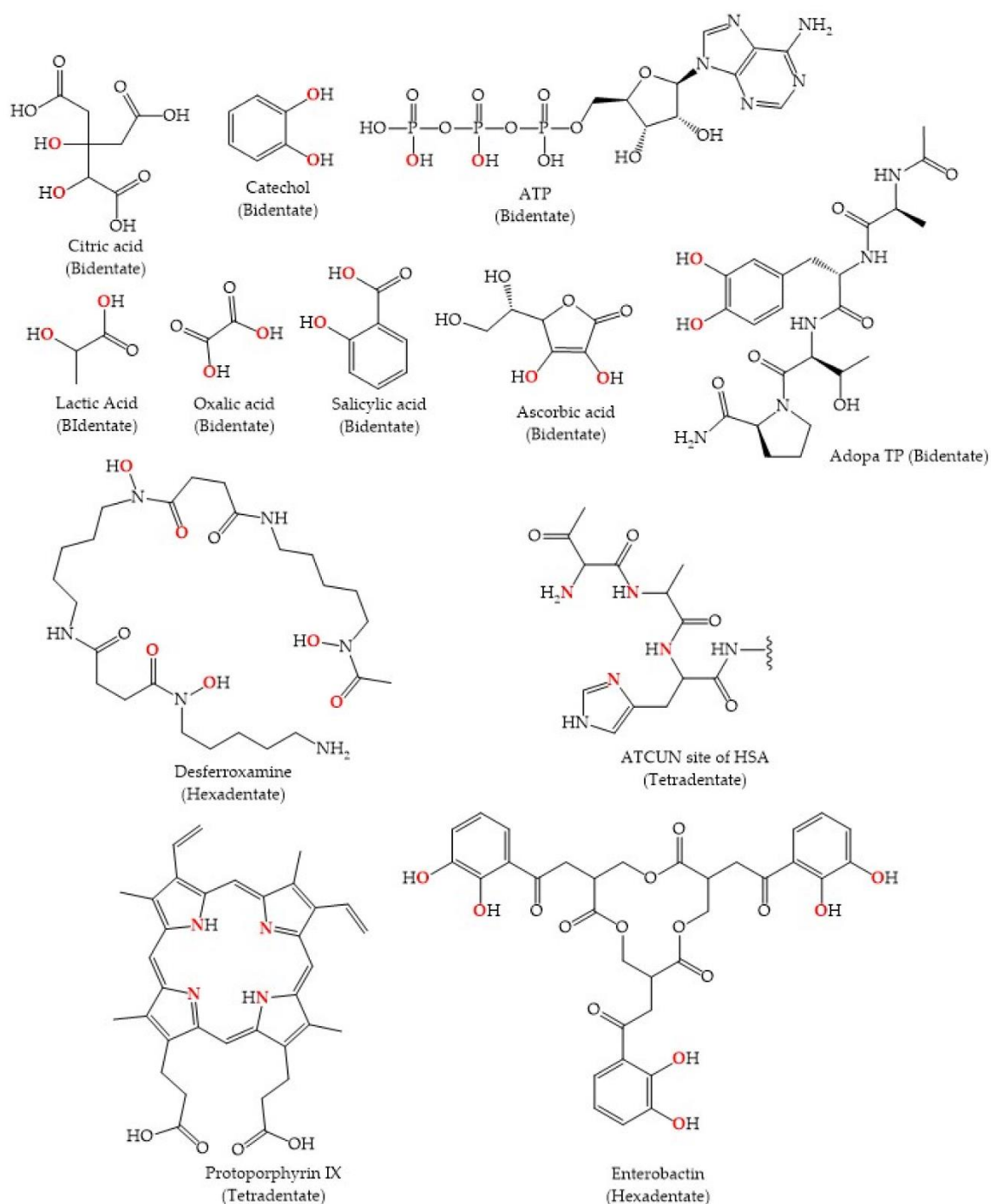
Figure 1.5. Some endogenous (or proposed) biological Ti(IV) chelators. Typical Ti(IV) binding moieties of endogenous ligands with representative coordination modalities. Reprinted from Coordination Chemistry Reviews, 363, M. Saxena, S.A. Loza-Rosas, K. Gaur, S. Sharma, S.C. Pérez Otero, A.D. Tinoco, Exploring titanium(IV) chemical proximity to Fe(III) to elucidate a function for Ti(IV) in the human body, 109–125, Copyright (2018), with permission from Elsevier. See appendix 3.

1.2. Titanium and Cancer

After the discovery of cisplatin, the anticancer research focused on metal-centered compounds. In the 1970s, complexes' appearance generated great expectations by showing great antiproliferative capacity *in vitro*.[38] Since there have been multiple studies showing promise antiproliferative activity against tumors with lower side effects and no cellular acquired resistance to the compound, which is a significant disadvantage in commercial metal-based anticancer drugs like cisplatin.[39-41] However, the compounds' aqueous instability and solubility issues proved to be the main disadvantage to overcome. Once in preclinical studies, these compounds lost their effectiveness in their in vitro studies.[42-47] Since then, multiple approaches have appeared, with a promising increase in biological activity and solubility. Although the new generation of compounds has shown improvement in aqueous stability, it remains in a range of hours. Therefore, greater attention should be paid to the stability and chelating capacity of the ligands.

1.2.1. Development of Ti complexes after the discovery of cisplatin

Titanocene dichloride (Cp_2TiCl_2) and budotitane (**Fig 1.6**) were the first to reach clinical trials after cisplatin.[48] Cp_2TiCl_2 was active against melanoma and colon carcinoma, and budotitane shows a considerable antitumor activity and less toxicity than cisplatin.[49-50] The suspension of the clinical trials of these two Ti-complexes was due to the lack of stability. These results led to the development of new Ti-based anticancer drugs.

Titanocene Dichloride   Budotitane
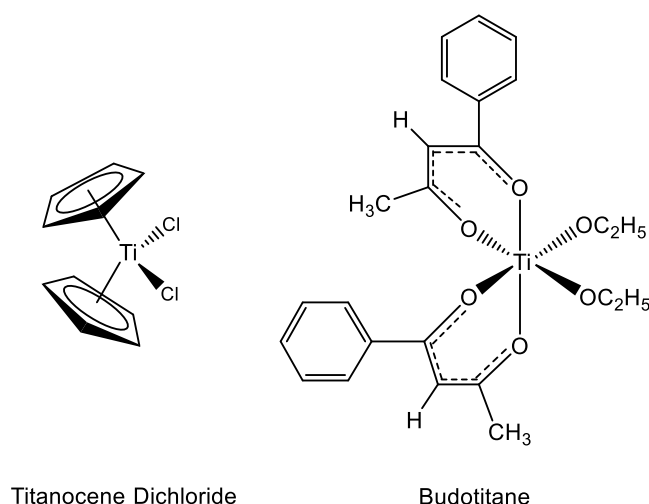
Figure 1.6. Structures of Titanocene dichloride and budotitane.

As previously described, the most common oxidation state of Ti is 4+. However, upon exposure to air or water, it can quickly react with oxygen to form TiO_2.[50] Ti(IV) compounds that have demonstrated excellent potential as anticancer drugs to attack a broad spectrum of tumors.[50-52] Nonetheless, Ti(IV) is highly prone to hydrolysis at physiological pH. This property results in the dissociation of drug candidates and the irreversible formation of insoluble TiO_2 coupled with the loss of anticancer activity.[33] To explain how Ti(IV) compounds that are highly unstable in solution can demonstrate cytotoxic activity, the serum Fe(III) transport protein,

transferrin (Tf), has been implicated in the mechanism of action of these compounds.[33] The favored hypothesis is that the compounds deliver Ti(IV) to sTf, which then chelates the metal ion and transports it to cancer cells via the Fe(III) endocytotic route.[33] The structural characteristics of the human sTf binding site moiety serve as a valuable template for designing biomimicking ligands capable of stably chelating Ti(IV) and facilitating the transport of the metal into cancer cells (**Fig 1.3**).[53]

Currently, many studies are being developed to enhance the stability of Ti(IV) drugs in water.[33, 54-55] Different researchers worldwide are trying to improve the poor water solubility and instability of the Ti anticancer drugs. For example, the second generation of budotitane complexes was synthesized by McGowan and Lord, improving the aqueous stability of the parent compound (**Fig 1.7**).[56] Tshuva and Huhn are developing different types of Ti(IV) compounds to achieve the stability of the metal at physiological pH to avoid the precipitation or interaction with proteins in the bloodstream (**Fig 1.7**).[52-53, 57]

1.2.2. New generation of Ti complexes that mimics human sTf binding site

Tinoco and coworkers found that the Fe(III) blood transport protein, serum transferrin (STf), works in synergism with the small anion citrate to stabilize Ti(IV). STf can transport Ti(IV) into cells and regulate its activity so that it is not toxic to the cells43 and might participate in cellular functions (**Fig 1.3**). This Ti(IV) stabilizing property by the transferrin binding site offers insights to develop a new drug design strategy. The structural characteristics of the human Tf binding site moiety serve as a valuable template for designing biomimicking ligands capable of stably chelating Ti(IV) and facilitating the transport of the metal into cancer cells. The chemical transferrin mimetic (cTfm) ligands are a new class of ligands with similar structural characteristics to the human sTf. They can chelate with Ti(IV) to form stable complexes. The effectiveness of cTfm ligands comes from their higher affinity for Fe(III) and lower for Ti(IV). The cTfm ligands can coordinate the free metal Fe, promoting a synergistic anticancer effect—cell death pathways by Fe depletion and Ti(IV) anticancer activity. The ability of cTfm ligands to protect Ti(IV) from hydrolysis at physiological conditions and transport Ti(IV) into cancer cells can give us insights to develop new drugs.[43] Def (Def) (4-[3,5-bis(2-hydroxyphenyl)-1,2,4-triazole-1-yl] benzoic acid, $C_{21}H_{15}N_3O_4$) is an excellent cTfm mimetic ligand, which is being used to treat Fe overload diseases and can stabilize Ti(IV). Similarly, HBED (N,N'-di(2-hydroxybenzyl)ethylenediamine-N,N'-diacetic acid monohydrochloride) has been observed to stabilize Ti(IV) as cTfm ligand.

The $[Ti(Def)_2]^{2-}$ complex (**Fig 1.7**, Tinoco Ti complex) showed stability at physiological pH, which is supported by the cell viability data (**Fig 1.8 and Table 1.1**). The complex showed a dose-dependent antiproliferative behavior effect against both cell lines.[53] The synergistic capability of $[Ti(Def)_2]^{2-}$ was tested with cisplatin against Jurkat cells (leukemia cell line). Results prove that a 1:1 ratio of both compounds, cisplatin: $[Ti(Def)_2]^{2-}$, has a modestly synergistic effect, but a 2:1 ratio has a strong synergistic effect. A synergistic effect could mean lower

treatment dosages, reduced side effects, and the capability to work with other drugs to improve anticancer treatments in different tissues.
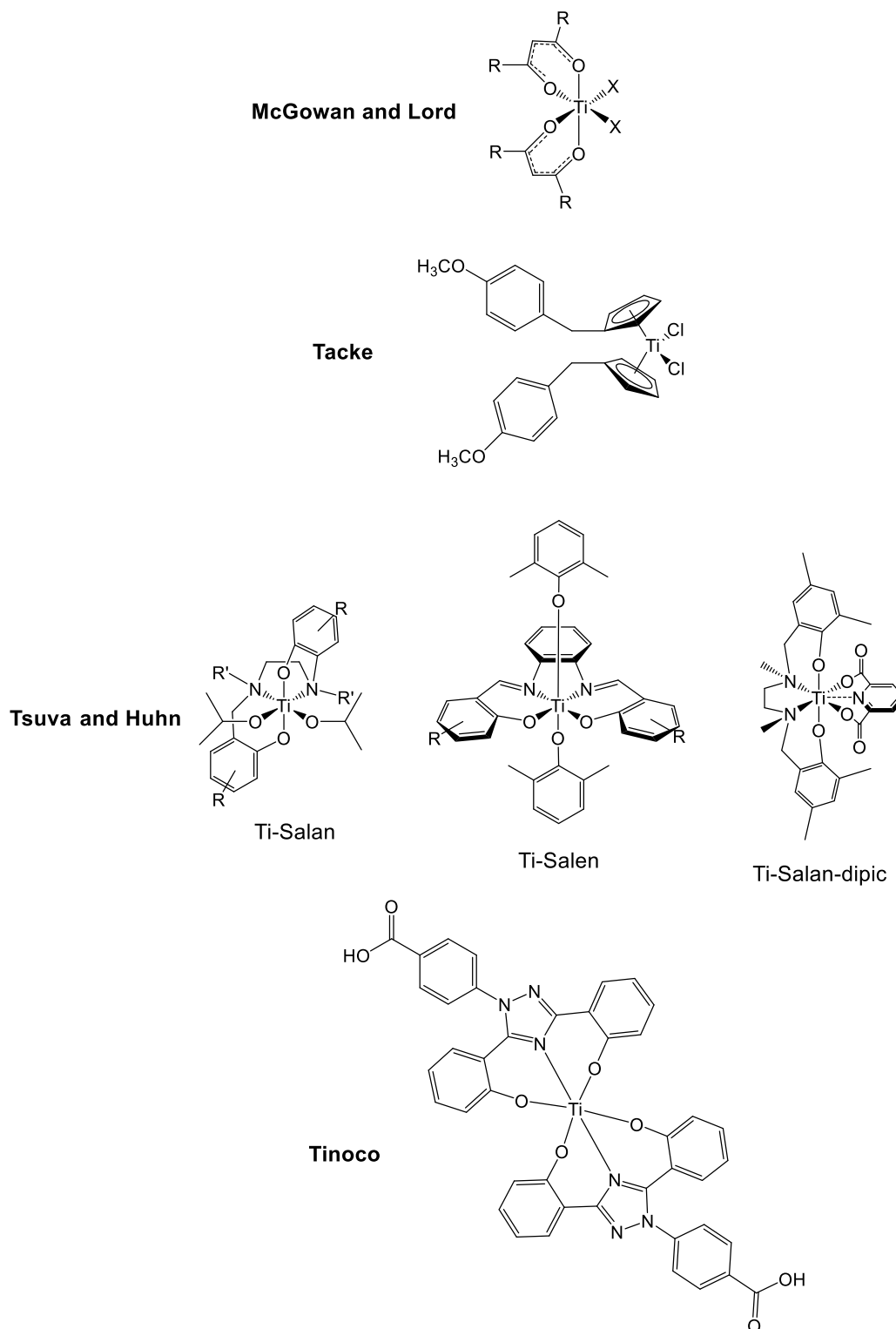
Figure 1.7. Development of new Ti complexes by different researchers with different ligands to improve the aqueous metal stability.
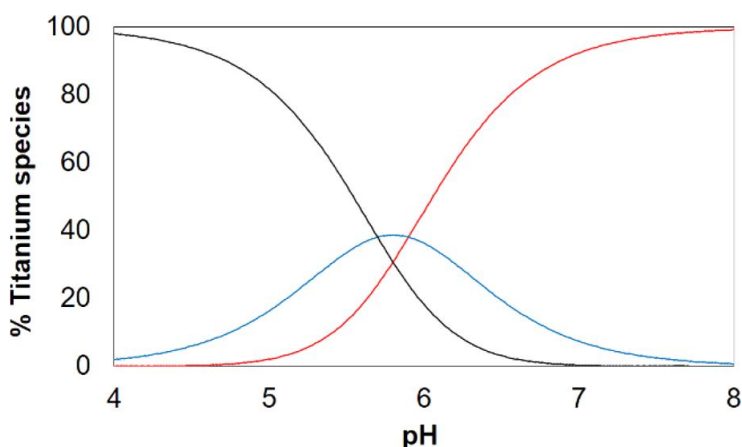
Figure 1.8. Ti(IV) Def aqueous speciation from pH 4 to 8 using 50 µM Ti(IV)/100 µM Def: (black line) $[Ti(Def)_2]^0$; (blue line) $[Ti(Def)_2]^-$; (red line) $[Ti(Def)_2]^{2-}$. Adapted with permission from Journal of the American Chemical Society, 56, 14, 7788-7802. Copyright 2017. See appendix 4.

Table 1.1 IC$_{50}$ Values of Ti(Def)$_2$$^{2-}$ complexes against A549 and MRC5 cells[53]

	IC$_{50}$ (µM)	
	A549	**MRC5**
[Ti(Def)$_2$]$^{2-}$	20 ± 1	25 ± 1
Def	12.1 ± 1	a

a A proliferative behavior was observed

1.2.3. Current proposed mechanism of Ti-based complexes

Ti biological activity is still under the focus of many researchers. Transmetalation is a new term introduced by Tinoco et al. This terminology refers to the ability of some Ti-complexes to interchange Ti(IV) with Fe(III) under cellular conditions. The reaction is favored by the higher preference of the ligand by one metal than the other. Transmetalation studies were performed between $[Ti(Def)_2]^{2-}$ and a Fe(III) intracellular source under physiological conditions. The reaction was monitored by UV-vis and mass spectrometry (M.S.) to follow the response below:[53]

$$Ti(Def)_2{}^{2-} + Fe(Cit)_2{}^{5-} + 2\,H_2O \rightleftharpoons Fe(Def)_2{}^{3-} + Ti(Cit)_2(OH)_2{}^{6-} + 2H^+$$

The Def ligand prefers to bind Fe(III), which promotes the displacement of Ti(IV). By MS, a multi-species transmetalation process was observed, indicating that not only one species is present during the process, as follows:[53] Supplementation Fe(III) studies highlight the importance of Fe to cancer cells.[53]

The proposed mechanism for the transmetalation between Ti(Def)$_2$ and labile Fe(III) without excess citrate background:[53]

$$\text{Ti(Def)}_2{}^{2-} + \text{Fe(Cit)}_2{}^{5-} \rightleftharpoons [\text{Ti(Def)}_2\text{Fe(Cit)}_2]^{7-}$$

$$[\text{Ti(Def)}_2\text{Fe(Cit)}_2]^{7-} \rightarrow [\text{Ti(Def)Fe(Cit)}_2]^{4-} + \text{Def}^- + 2\text{OH}^-$$

$$[\text{Ti(Def)Fe(Cit)}_2]^{4-} + \text{Def}^- \rightarrow [\text{Ti(Def)(Cit)}]^{3-} + [\text{Fe(Def)(Cit)}]^{4-}$$

$$[\text{Ti(Def)(Cit)}]^{3-} + [\text{Fe(Def)(Cit)}]^{4-} + 2\text{H}_2\text{O} \rightleftharpoons [\text{Ti(Cit)}_2(\text{OH})_2]^{6-} + \text{Fe(Def)}_2{}^{3-} + 2\text{H}^+$$

Data suggest that the cell death pathway triggered by Fe depletion is happening, and the Ti(IV)-based complexes are stable enough to reach the intracellular envFement and deliver Ti intracellularly.

Jurkat cells were used as a model to test Fe(III) transmetalation and its effect on the ribonucleotide (RNR) enzyme. RNR is a Fe-dependent enzyme important in DNA synthesis and facilitates metastasis via Fe-based metalloproteinases in cancer cells.[58-60] Electron paramagnetic resonance (EPR) was used to analyze the inhibition of the tyrosyl radical, a characteristic signal of R2 RNR. The absence of the signal means the inhibition of the enzyme activity. Being a Fe-dependent enzyme, the Fe(III) depletion by the Ti(IV)-based ligand should decrease the tyrosyl signal. In **figure 1.9**, the tyrosyl signal is reduced after a 3h treatment with the Ti(IV)-based complexes and their metal-free ligands.[61] The decrease of the signal can be possible due to the bioavailable Fe(III) chelation, a redox activity performed by the compound that could reduce the tyrosyl radical formation, and the possibility of Ti(IV)-based complexes could sequester the Fe(III)-bound to the RNR enzyme.[61]

Other RNR inhibition was studied; the capability of Ti to be bound by phosphates groups could indicate that the nucleotides, the building blocks in DNA synthesis, could be affected. ^{13}P NMR analysis showed that Ti(IV) could interact with adenosine triphosphate (ATP), adenosine diphosphate (ADP), and adenosine monophosphate (AMP) at pH 7.4. These results indicate that Ti(IV) can interact with nucleotides, affecting DNA synthesis. Further studies have to be done, but Ti(IV)-based complexes could be interacting with the nucleotides pool of the RNR enzyme, inactivating it in the process.[61]

Figure 1.9. Whole-cell EPR spectra for the 3 h treatment of Jurkat cells with 50 µM $[Ti(Def)_2]^{2-}$, Def^-, $TiO(H^+-HBED)]^{1-}$, and $HBED^{2-}$ and also the buffer control. The EPR signal corresponds to (a) the tyrosyl radical of the RNR enzyme ($g \approx 2$) and to the (b) intracellular high-spin Fe(III) ($S = 5/2$; $g \approx 4.3$). Experimental conditions: microwave frequency, 9.338 GHz; microwave power, 2 mW; magnetic field modulation amplitude, 0.5 mT for the tyrosyl radical and 1 mT for high-spin Fe(III) ($S = 5/2$), temperature: 20 K. All EPR spectra were baseline-corrected. *Jacs Au is an open access article distributed under the Creative Commons Attribution License which permits unrestricted use, distribution, and reproduction in any medium, provided the original work is properly cited (See appendix 5).*

1.3 Conclusion

Ti is an intriguing metal able to be in the human body in high concentrations and be part of biological processes that we are still trying to understand. The development of Ti(IV)-based complexes has led to a first understanding of how these compounds work. But still exits many unanswered questions, and having more information about the mechanism of these compounds will lead to a more focused and more effective preparation of Ti anticancer complexes. One of the most interesting features of Ti(IV)-based complexes is the ability to perform transmetalation. Thus, the study of their interaction with essential metals such as Fe and Cu in cancer development is required.

This research project focuses on studying the mechanistic insight of the Ti(IV)-based complexes and their interaction with Fe and Cu, ROS production and their role in cell death pathways, and how different drug delivery systems work in Ti(IV) delivery. Finally, an analysis of how the ligand-metal relationship impacts the development of new anticancer drugs.

1.4 References

1.   Nardon, C.; Boscutti, G.; Fregona, D., *Anticancer Res.* **2014,** *34* (1), 487-492.

2.   Rosenberg, B.; Van Camp, L.; Krigas, T., *Nature* **1965,** *205* (4972), 698-699.

3.   Dilruba, S.; Kalayda, G. V., *Cancer Chemother. Pharmacol.* **2016,** *77* (6), 1103-24.

4.   Zoroddu, M. A.; Aaseth, J.; Crisponi, G.; Medici, S.; Peana, M.; Nurchi, V. M., *J. Inorg. Biochem.* **2019,** *195*, 120-129.

5.   Arredondo, M.; Núñez, M. T., *Mol. Asp. Med.* **2005,** *26* (4–5), 313-327.

6.   Ibrahim, O.; O'Sullivan, J., *Biometals* **2020,** *33* (4-5), 201-215.

7.   Merlot, A. M.; Kalinowski, D. S.; Kovacevic, Z.; Jansson, P. J.; Sahni, S.; Huang, M. L.-H.; Lane, D. J.; Lok, H.; Richardson, D. R., *Curr. Med. Chem.* **2019,** *26* (2), 302-322.

8.   Denoyer, D.; Masaldan, S.; La Fontaine, S.; Cater, M. A., *Metallomics* **2015,** *7* (11), 1459-1476.

9.   Vashchenko, G.; MacGillivray, R., *Nutrients* **2013,** *5* (7), 2289-2313.

10.   Chanvorachote, P.; Luanpitpong, S., *Am. J. Physiol. Cell Physiol.* **2016,** *310* (9), C728-C739.

11.   Koppenol, W.; Hider, R., *Free Radic. Biol. Med.* **2018**.

12.   Daniels, T. R.; Delgado, T.; Rodriguez, J. A.; Helguera, G.; Penichet, M. L., *Clin. Immunol.* **2006,** *121* (2), 144-58.

13.   Seymour, G. J.; Walsh, M. D.; Lavin, M. F.; Strutton, G.; Gardiner, R. A., *Urol. Res.* **1987,** *15* (6), 341-344.

14.   Kwok, J. C.; Richardson, D. R., *Crit. Rev. Oncol. Hematol.* **2002,** *42* (1), 65-78.

15.   Gupte, A.; Mumper, R. J., *Cancer Treat. Rev.* **2009,** *35* (1), 32-46.

16.   Birch, N.; Wang, X.; Chong, H. S., *Expert Opin. Ther. Pat.* **2006,** *16* (11), 1533-1556.

17.   Gaur, K.; Vázquez-Salgado, A. M.; Duran-Camacho, G.; Dominguez-Martinez, I.; Benjamín-Rivera, J. A.; Fernández-Vega, L.; Carmona Sarabia, L.; Cruz García, A.; Pérez-Deliz, F.; Méndez Román, J. A.; Vega-Cartagena, M.; Loza-Rosas, S. A.; Rodriguez Acevedo, X.; Tinoco, A. D., *Inorganics* **2018,** *6* (4), 126.

18.   Goodman, V. L.; Brewer, G. J.; Merajver, S. D., *Curr. Cancer Drug Targets* **2005,** *5* (7), 543-549.

19.   Buettner, K. M.; Valentine, A. M., *Chem. Rev.* **2012,** *112* (3), 1863-1881.

20.   Knauss, K. G.; Dibley, M. J.; Bourcier, W. L.; Shaw, H. F., *J. Appl. Geochem.* **2001,** *16* (9-10), 1115-1128.

21.   Loza-Rosas, S. A.; Saxena, M.; Delgado, Y.; Gaur, K.; Pandrala, M.; Tinoco, A. D., *Metallomics* **2017,** *9* (4), 346-356.

22.   Suwalsky, M.; Villena, F.; Norris, B.; Soto, M.; Sotomayor, C.; Messori, L.; Zatta, P., *J. Inorg. Biochem.* **2005,** *99* (3), 764-770.

23.   Kužel, S.; Hruby, M.; Cígler, P.; Tlustoš, P.; Van Nguyen, P., *Biol. Trace Elem. Res.* **2003,** *91* (2), 179-189.

24.   Saxena, M.; Loza-Rosas, S. A.; Gaur, K.; Sharma, S.; Otero, S. C. P.; Tinoco, A. D., *Coord. Chem. Rev.* **2018,** *363*, 109-125.

25. Fiordaliso, F.; Foray, C.; Salio, M.; Salmona, M.; Diomede, L., *J. Agric. Food Chem.* **2018,** *66* (26), 6860-6868.

26. Wang, Q.; Zhou, P.; Liu, S.; Attarilar, S.; Ma, R. L.-W.; Zhong, Y.; Wang, L., *Nanomaterials* **2020,** *10* (6), 1244.

27. Curtin, J. P.; Wang, M.; Cheng, T.; Jin, L.; Sun, H., *J. Biol. Inorg. Chem.* **2018,** *23* (3), 471-480.

28. Suárez-López del Amo, F.; Garaicoa-Pazmiño, C.; Fretwurst, T.; Castilho, R. M.; Squarize, C. H., *Clin. Oral Implants Res.* **2018,** *29* (11), 1085-1100.

29. Swiatkowska, I.; Martin, N. G.; Henckel, J.; Apthorp, H.; Hamshere, J.; Hart, A. J., *J. Trace Elem. Med. Biol.* **2020,** *57*, 9-17.

30. Kim, K. T.; Eo, M. Y.; Nguyen, T. T. H.; Kim, S. M., *Int. J. Implant Dent.* **2019,** *5* (1), 1-12.

31. Gulati, K.; Scimeca, J.-C.; Ivanovski, S.; Verron, E., *Drug Discov.* **2021**.

32. Darr, E.; Cher, D., *Med. Device* **2018,** *11*, 287.

33. Tinoco, A. D.; Saxena, M.; Sharma, S.; Noinaj, N.; Delgado, Y.; Quiñones González, E. P.; Conklin, S. E.; Zambrana, N.; Loza-Rosas, S. A.; Parks, T. B., *JACS* **2016,** *138* (17), 5659-5665.

34. Li, H.; Sadler, P. J.; Sun, H., *Eur. J. Biochem.* **1996,** *242* (2), 387-393.

35. Benjamín-Rivera, J. A.; Cardona-Rivera, A. E.; Vázquez-Maldonado, Á. L.; Dones-Lassalle, C. Y.; Pabón-Colon, H. L.; Rodríguez-Rivera, H. M.; Rodríguez, I.; González-Espiet, J. C.; Pazol, J.; Pérez-Ríos, J. D., *Inorganics* **2020,** *8* (9), 48.

36. Panagiotidis, P.; Kefalas, E. T.; Raptopoulou, C. P.; Terzis, A.; Mavromoustakos, T.; Salifoglou, A., *Inorganica Chim. Acta* **2008,** *361* (8), 2210-2224.

37. Cotton, F. A.; Wilkinson, G.; Murillo, C. A.; Bochmann, M.; Grimes, R., *Adv. Inorg. Chem.* **1988**; Vol. 6.

38. Brintzinger, H.; Bercaw, J. E., *JACS* **1970,** *92* (21), 6182-6185.

39. Majumdar, S.; Siahaan, T. J., *Med. Res. Rev.* **2012,** *32* (3), 637-58.

40. Muppidi, A.; Doi, K.; Edwardraja, S.; Pulavarti, S. V.; Szyperski, T.; Wang, H. G.; Lin, Q., *Bioconjugate Chem.* **2014,** *25* (2), 424-32.

41. Maxwell, K. L.; Kowdley, K. V., *Curr. Opin. Gastroenterol.* **2012,** *28* (3), 217-222.

42. Liang, J. F.; Yang, V. C., *Bioorg. Med. Chem. Lett.* **2005,** *15* (22), 5071-5.

43. Parks, T. B.; Cruz, Y. M.; Tinoco, A. D., *Inorg. Chem.* **2014,** *53* (3), 1743-9.

44. Mitchell, A. J.; Lone, A. M.; Tinoco, A. D.; Saghatelian, A., *PLoS One* **2013,** *8* (7), e68638.

45. Feistritzer, C.; Clausen, J.; Sturn, D. H.; Djanani, A.; Gunsilius, E.; Wiedermann, C. J.; Kähler, C. M., *Regul. Pept.* **2003,** *116* (1-3), 119-126.

46. Unal, S.; Bas, M.; Hazirolan, T.; Tuncer, A. M.; Cetin, M.; Gumruk, F., *Blood* **2014,** *124* (21), 3.

47. Davies, G. I.; Davies, D.; Charles, S.; Bowden, D.; Barnes, S., *Intern. Med. J.* **2014,** *44*, 8-8.

48. Köpf, H.; Köpf-Maier, P., *Angew. Chem., Int. Ed. Engl.* **1979,** *18* (6), 477-478.

49. Lümmen, G.; Sperling, H.; Luboldt, H.; Otto, T.; Rübben, H., *Cancer Chemother. Pharmacol.* **1998,** *42* (5), 415-417.

50.   Schilling, T.; Keppler, K.; Heim, M.; Niebch, G.; Dietzfelbinger, H.; Rastetter, J.; Hanauske, A.-R., *Investig. New Drugs* **1995,** *13* (4), 327-332.

51.   Immel, T. A.; Groth, U.; Huhn, T., *Eur. J. Chem.* **2010,** *16* (9), 2775-2789.

52.   Schur, J.; Manna, C. M.; Deally, A.; Köster, R. W.; Tacke, M.; Tshuva, E. Y.; Ott, I., *ChemComm* **2013,** *49* (42), 4785-4787.

53.   Loza-Rosas, S. A.; Vázquez-Salgado, A. M.; Rivero, K. I.; Negrón, L. J.; Delgado, Y.; Benjamín-Rivera, J. A.; Vázquez-Maldonado, A. L.; Parks, T. B.; Munet-Colón, C.; Tinoco, A. D., *Inorg. chem.* **2017,** *56* (14), 7788-7802.

54.   Casañas-Montes, B.; Díaz, A.; Barbosa, C.; Ramos, C.; Collazo, C.; Meléndez, E.; Queffelec, C.; Fayon, F.; Clearfield, A.; Bujoli, B.,   *J. Organomet. Chem.* **2015,** *791*, 34-40.

55.   Speight, J. G., *McGraw-Hill: New York, 2005*; Vol. 1.

56.   Lord, R. M.; Mannion, J. J.; Hebden, A. J.; Nako, A. E.; Crossley, B. D.; McMullon, M. W.; Janeway, F. D.; Phillips, R. M.; McGowan, P. C., *ChemMedChem* **2014,** *9* (6), 1136-1139.

57.   Hartinger, C. G.; Zorbas-Seifried, S.; Jakupec, M. A.; Kynast, B.; Zorbas, H.; Keppler, B. K., *J. Inorg. Biochem.* **2006,** *100* (5-6), 891-904.

58.   Mannargudi, M. B.; Deb, S., *J. Cancer Res. Clin. Oncol.* **2017,** *143* (8), 1499-1529.

59.   Greene, B. L.; Kang, G.; Cui, C.; Bennati, M.; Nocera, D. G.; Drennan, C. L.; Stubbe, J., *Annu. Rev. Biochem.* **2020,** *89*, 45-75.

60.   Agarwal, D.; Goodison, S.; Nicholson, B.; Tarin, D.; Urquidi, V., *Differentiation* **2003,** *71* (2), 114-125.

61.   Gaur, K.; Pérez Otero, S. C.; Benjamín-Rivera, J. A.; Rodríguez, I.; Loza-Rosas, S. A.; Vázquez Salgado, A. M.; Akam, E. A.; Hernández-Matias, L.; Sharma, R. K.; Alicea, N., *JACS Au* **2021**, 1(6), 865-878.

Chapter 2

A Mechanistic Study of Ti(IV) based complexes and their influence in the Cu(II) and Fe(III) homeostasis disturbance producing a ROS intracellular imbalance

2. 1   INTRODUCTION

The accidental discovery of cisplatin led to the development of anticancer metal-based complexes with less complicated structures and a broad spectrum of intracellular targets.[1] Metals play an essential role in numerous biological processes in the human body, and depending on the metal properties; they can be used to attack different intracellular aims.[2] The hard-soft acid-base theory then establishes which target will likely be chosen by the metal ion and which ligands will be compatible with them. Medicinal inorganic chemistry still lacks "rules" that dictate the drug outcome based on the structure-activity relationship. Metals can act differently depending on the ligand type of bonding, metal complex geometry, oxidation states, and ligand substituents.[3] Studies made on groups of ligands and metals to understand their action had brought more understanding to their biological activity.[4-5]

For human health purposes, metals are classified as essential and non-essentials. The "essential" definition is a thin line that depends mainly on bioavailability and concentration. While a metal is necessary for human survival, the same metal can produce toxicity if the concentration is over the amount required.[2] Copper (Cu) and iron (Fe) are classified as essential metals. They shared similarities, such as two normal oxidation states allowing them to participate in each other's oxidation/reduction processes.[6] For instance, multicopper oxidases such as hephaestin (Heph), ceruloplasmin (Cp), and zyklopen (Zp) are essential for cellular iron uptake.[6-8] Cu also plays a part in a Fe-dependent cell death such as ferroptosis. Ferroptosis is mainly characterized by lipid peroxidation, and Cu accumulation leads to higher reactive oxygen species (ROS) production, leading to elevated rates of lipid peroxidation.[9] Both metals can compete for metal transporters such as divalent metal transporters 1 (DMT1) in the intestinal tract and play functions in metalloproteins due to their redox properties.[10-11] Cu deficiency can induce hypochromic anemia that Fe administration cannot resolve, and Fe deficiency promotes an increase in Cu transport to increase Fe absorption.[12]

Cu and Fe have been identified as essential metals in cancer survival, angiogenesis, and progression.[11] As in normal cells, their redox properties affect each other in cancer processes. Then, affecting one or both metals can be used as an anticancer treatment strategy. Cu(II) had recently become the spotlight in anticancer metals depletion therapy. Unlike other metals, Cu(II) showed cytotoxic species' formation with some ligands, such as polypyridyl-type ligands. Among other metals, the trend for Cu(II) tends to be different. In phenantroline mechanistic studies was confirmed that the ligand can inhibit the DNA synthesis, but by adding the metals to the treated cells, such as Ni(II), Fe(II), Zn(II), or Co(II), the effect was reversed, suggesting that pre-binding the metal could affect the compound uptake; with Cu(II) this effect was not observed.[4] In the case of this metal, Cu oxidation states play an essential role in its activity due to the formation of different species and compounds geometries that impact the uptake and activity of the compounds.[4]

Based on the current findings in metal depletion therapy, previous studies on the Titanium(IV) Deferasirox $[Ti(Deferasirox)_2]^{2-}$ compound have shown its ability to affect Fe via a transmetalation approach.[13-14] $[Ti(Deferasirox)_2]^{2-}$ has proved to be active against lung and leukemia cancer cells. An essential feature of $[Ti(Deferasirox)_2]^{2-}$ is that it can perform intracellular transmetalation. Transmetalation refers to a process in which a metal complex can interchange its metal center with another based on ligand-metal affinity. During this process, redox-active species can be formed. $[Ti(Deferasirox)_2]^{2-}$ can impact the intracellular labile Fe pool via transmetalation, resulting in a decreased metal bioavailability. A decrease in Fe bioavailability disrupt the Fe binding to the ribonucleotide reductase (RNR), inactivating the enzyme and preventing DNA synthesis.[13]

Herein, we present how transmetalation $[Ti(Deferasirox)_2]^{2-}$ affects both Fe and Cu intracellular bioavailability. We analyzed the solvent/concentration-dependent speciation of $[Ti(Deferasirox)_2]^{2-}$-Cu(II) possible transmetalation products and how the $[Ti(Deferasirox)_2]^{2-}$-Fe(III) transmetalation species are capable of the formation of intracellular reactive oxygen species (ROS). In this research work, we provide a preliminary model of the intracellular Fe and Cu imbalance mechanism of a Ti(IV)-based complex.

2. 2   MATERIALS AND METHODS

2.2.1 Materials

All aqueous solutions were prepared with autoclaved (121ºC and 18 PSI) high-quality nanopure water (18.2 MΩ cm resistivity, PureLab Ultra Analytic water purification system). Iron(III) Chloride ($FeCl_3$), thionyl chloride ($SOCl_2$), pyridine, xylenes, salicylamide, salicylaldehyde, hexane, ethyl acetate, citratoiron(III) ($Fe(C_6H_5O_7)$), sodium dodecyl sulfate (SDS), and methanol were obtained from

Sigma-Aldrich. Copper chloride ($CuCl_2$) and zinc chloride ($ZnCl_2$) were obtained from Fisher Scientific. Ti(Deferasirox)$_2$ (Ti($C_{42}H_{26}N_6O_8$)) was synthesized as described in the literature.[3]

Dicitratoiron(III) [Fe(Citrate)$_2$]$^{5-}$ (Fe($C_6H_5O_7$)$_2$$^{5-}$) was prepared in situ by mixing equimolar amounts of Fe($C_6H_5O_7$), and Na$_3$Citrate in solution and adjusting the pH to 7.4.[30] Cu(II) citrate ([Cu$_2$(Citrate)$_2$OH]$^{3-}$ (Cu$_2$($C_6H_5O_7$)$_2$(OH)) and Zn(II) citrate ([Zn(Citrate)]$^-$ (Zn($C_6H_5O_7$)$^-$) were prepared in situ by mixing equimolar amounts of $CuCl_2$, $ZnCl_2$, and Na$_3$Citrate in solution and adjusting the pH to 7.4.[31-35] Iron (III) Deferasirox [Fe(Deferasirox)$_2$]$^{3-}$ was prepared in situ by reacting an aqueous solution of $FeCl_3$ with two equivalents of Deferasirox and then diluting the stock solution in a pH 7.4 buffer and validated by UV-vis spectroscopy (see below).[29] A549 human lung cancer cells and MRC5 human lung normal cells were obtained from ATCC® (CCL-185™ and CCL-171™, respectively). Both cell lines were cultured in phenol red DMEM (Sigma, D6429) containing 1% glutamine, 4.5 g/mL of glucose, and sodium pyruvate. Media was supplemented with 10% FBS (HyClone) and 1% of penicillin-streptomycin (Prepared from the solid obtained from Calbiochem, EMD Biosciences Inc. and prepared as follows: Streptomycin 11mg/mL and Penicillin 7mg/mL) at 37ºC in a humidified atmosphere of 5% (v/v) CO_2. Phenol Red-free DMEM (CellGro® REF 17-205-CV) was used during cytotoxicity studies. 3-(4,5-n dimethylthiazole-2-yl)-2,5-diphenyl tetrazolium bromide (MTT) was purchased from Sigma-Aldrich. MALDI TOF was performed using the α-Cyano-4-hydroxycinnamic acid matrix purchased from sigma. All other chemicals were of high purity and used as received.

The determination of the extinction coefficients of [Ti(Deferasirox)$_2$]$^{2-}$,[3] [Fe(Deferasirox)$_2$]$^{3-}$, Cu(II) Deferasirox, and Zn(II) Deferasirox, were calculated preparing in situ standards of every metal compound. Each metal salt was mixed with an excess of deferasirox to guarantee the complete coordination of the metal in the solution. 5 μM $CuCl_2$ and 5 μM $ZnCl_2$ with 50 μM of Deferasirox at pH 7.4 (0.1 M NaCl, 1% DMF. No buffer used; pH value was adjusted with NaOH). 2.5 μM Fe$_2$(SO$_4$)$_3$ with 50 μM of Deferasirox at pH 7.4 (0.1 M NaCl, 1% DMF, and pH adjusted with NaOH). Each reaction was scanned using UV-Vis spectroscopy, and the complexes' 1 M absorbance spectra were obtained by subtracting the residual deferasirox absorbance using ReactLab Equilibria software (Jplus Consulting Pty Ltd).

2.2.2 Instruments

A Cary 300 UV-Vis spectrophotometer was used for kinetics experiments. All pH values were determined using a Thermo Scientific Orion Star A211 and an Orion 9157BNMD electrode, calibrated with standard buffer solutions at pH 4, 7, and 10. Mass spectra were collected on a MALDI TOF/TOF AB SCIEX 4800 Analyzer and a Waters Micromass Q-TOF with electrospray ionization (ESI) at a capillary voltage of 3000 and sample cone voltage of 30. Crystal structure analysis was

performed in a Rigaku Smart Lab III Xray Diffractometer. IR spectra were collected in a Nicolet IS 50 FT-IR Spectrometer. Multiwell plate absorbance was measured in a Tecan Infinite M200 PRO plate reader. Cells were grown in a Revco Elite III RCO5000T-5-ABC incubator. Cell counting and culture viability monitoring were performed using a Nikon Eclipse TS-100 microscope. ICP-OES data was collected in an Optima 8000 (Perkin-Elmer). Continuous-wave (CW)-EPR spectra were recorded at the University of Arizona, EPR Facility on an X-band EPR spectrometer Elexsys E500 (Bruker). For cyclic voltammetric analysis, a VMP3 multi-channel potentiostat (Bio-logic Science Instrument, USA) equipped with EC-Lab software and a three-electrode system was employed.

2.2.3 Synthesis of 4-[(3Z,5E)-3,5-bis(6-oxocyclohexa-2,4-dien-1-ylidene)-1,2,4-triazolidin-1-yl] benzoic acid ($C_{21}H_{15}N_3O_4$), Deferasirox

The intermediate molecule 2-(2-hydroxyphenyl)-4H-benzo[e][1,3]oxazin-4-one was synthesized as follows: Salicylic acid (10.0 g, 72.4 mmol, 1.00 eq.) and salicylamide (8.9 g, 65.0 mmol, 0.90 eq.) were dissolved in 45.0 mL of xylenes under argon atmosphere. The mixture was stirred, and pyridine (1.52 mL, 18.8 mmol, 0.26 eq.) was added. The reaction mixture was heated to reflux, and $SOCl_2$ (8.0 mL, 11.01 mmol, 1.52 eq) was added dropwise over 6 h. The mixture was left to react overnight. The next day, the reaction was cooled down to room temperature, and the precipitated solid was filtered and dried in a high vacuum. No significant impurities were observed by thin-layer chromatography (TLC) (80:20, Hexane: Ethyl acetate), and the following reaction was performed.

Deferasirox was synthesized by reflux using the 2-(2-hydroxyphenyl)-4H-benzo[e][1,3]oxazin-4-one (14.9 g, 62.30 mmol 1.00 eq.) previously synthesized and 4-hydrazine benzoic acid (7.16 g, 4.70 mmol, 0.65 eq) in 140.0 mL of methanol. After a 2h reaction, a pale-yellow solid was observed. The reaction was followed by TLC (80:20, Hexane: Ethyl acetate). After reaction completion, solid was obtained by rotovaporation, resuspended in 200 mL of acetone, and refluxed for 1.5 h. The hot mixture was filtered, and the solid was washed with small amounts of hot water. Solid was dried in high vacuum for 12 h. TLC showed a pure compound (Yield: 16.5 g, 71.3 %). CHN elemental analysis was performed by Atlantic Microlabs (Norcross, GA): C, 67.69 (67.55); H, 4.26 (4.05); N, 11.05 (11.25). ^{1}H NMR (δ ppm d6-DMSO, 500 MHz): 6.88 (d, 1H), 6.97-7.04 (m, 3H), 7.39 (m, 2H), 7.55 (d, 1H), 7.58 (d, 2H), 8.01 (d, 2H), 8.07 (d, 1H), 10.05 (s, OH), 10.80 (s, OH), 13.20 (broad, OH).

2.2.4 Synthesis of Cu(II) Deferasirox ($C_{42}H_{28}N_6O_{10}Cu_2.H_2O$) ($C_{44}H_{30}N_6O_{10}Cu_2$) (M. W. 905,834 g/mol)

18.24 mg (0.11 mmol) of $CuCl_2$ was dissolved in 5 mL of water, and 40.9 mg (0.11 mmol) of deferasirox was dissolved in methanol. The $CuCl_2$ solution was added dropwise to the ligand solution, and a green precipitate was observed. The mixture was stirred overnight. Two washes with methanol were performed, followed by three washes of water. Solid was frozen, lyophilized, and stored

protected from light (yield 81.8 %). CHN elemental analysis was performed by Atlantic Microlabs (Norcross, GA): C, 55,51 (55,69); H, 3,22 (3,34); N, 9,24 (9,28). FTIR data (cm^{-1}) comparison was taken from the ligand and the complex obtaining the following peaks: FT-IR v(Cu-O, Cu-N) 582; v(C=O) 1678, 1607 ligand and 1701, 1601 complex; v(C−O) 1279, 1221 ligand and 1257,1234 complex. UV–vis (Pyridine): λ_{max} 356 nm, ε = 15,808 M^{-1} cm^{-1}, λ_{max} 674 nm, ε = 284.8 M^{-1} cm^{-1}. UV-Vis (H$_2$O, DMF 1%) at pH 7.4 λ_{max} = 330 nm, ε = 21,900 M^{-1}cm^{-1}.

2.2.5 Synthesis of Cu(II) Deferasirox DMF complex (C$_{42}$H$_{28}$N$_6$O$_{10}$Cu$_2$.DMF.H$_2$O).0.5 H$_2$O (C$_{45}$H$_{36}$N$_7$O$_{10.5}$Cu$_2$) (M. W. 969.91 g/mol)

18.24 mg (0.11 mmol) of CuCl$_2$ was dissolved in 5 mL of water, and 40.9 mg (0.11 mmol) of deferasirox was dissolved in dimethylformamide (DMF). The CuCl$_2$ solution was added dropwise to the ligand solution, and a green precipitate was observed. The mixture was stirred overnight. Two washes with DMF were performed, followed by three washes of water. Solid was frozen and lyophilized. CHN elemental analysis was performed by Atlantic Microlabs (Norcross, GA): C, 55.99 (55.73); H, 4.08 (3.74); N, 10.48 (10.11).

2.2.6 Single-crystal X-ray crystallization

A Cu(II) Deferasirox (6.78 mg) sample was weighted and dissolved in pyridine (750 µL). Water was added (736 µL) followed by 1 M HCl (14 µL) to a final 0.1 M concentration of HCl. The solution (200 µL) was let to crystalize at rt by slow evaporation. A green plate crystal of [Cu(deferasirox)(pyridine)]$_2$ ([Cu(Def)(Py)]$_2$) was mounted on a MiTeGen micro loop for structure elucidation. Structural elucidation was performed using a Rigaku XtalLAB SuperNova single micro-focus Cu-Kα radiation (λ = 1.5417 Å) source equipped with a HyPix3000 X-ray detector in transmission mode operating at 50 kV and 1 mA within the CrystAlis^{PRO} software ver. 1.171.39.43c.[15] The data collection was kept at 300 K using an Oxford Cryosystems Cryostream 800 cooler. The crystal structure was solved by Intrinsic Phasing using the program ShelXT[16] and refined by full-matrix least squares on F^2 using ShelXL[17] within the Olex2 (v1.5) software.[18] Multi-scan absorption correction was applied for all data. All non-hydrogen atoms were anisotropically refined. All the H atoms were placed in their calculated positions and then refined using the riding model with Atom—H lengths of 0.95Å (C—H) and 0.82Å (O—H). Isotropic displacement parameters for these atoms were set to 1.2 (C—H) or 1.5 (O—H) times U$_{eq}$ of the parent atom. Idealised tetrahedral OH refined as rotating groups. Large solvent-accessible voids in the crystal structure of [Cu(deferasirox)(pyridine)]$_2$ is occupied by interstitial solvent molecules, whose crystallographic disorder could not be modeled satisfactorily. Consequently, the diffraction data set of [Cu(deferasirox)(pyridine)]$_2$ was modified by the Solvent Mask feature of the OLEX2 program before the final refinement. Crystal data: C$_{52}$H$_{36}$Cu$_2$N$_8$O$_8$, mol wt = 1027.97 g/mol, green plate, 0.148 × 0.108

× 0.01 mm, monoclinic, P2$_1$/c, 16.0148(2) Å, $b =$ 10.46660(10) Å, $c =$ 17.8077(2) Å, α = 90° β = 116.263(2)°, γ = 90°, V = 2383.98(9), 2676.81(7) Å^3, $Z =$ 2, $T =$ 300.01(10) K, μ(Cu Kα) = 1.454 mm^{-1}, ρcalc = 1.275 g/cm^3, 27808 reflections measured (6.154° ≤ 2Θ ≤ 136.802°), 4884 unique (R_{int} = 0.0351, R$_{sigma}$ = 0.0243) which were used in all calculations. The final R_1 was 0.0335 (I > 2σ(I)) and wR_2 was 0.1044 (all data).

2.2.7 EPR analysis of Cu(II) Deferasirox

An EPR experiment was performed on the Cu(II) Deferasirox compound. A sample was prepared by dissolving 6.79 mg (5 mM) in pyridine (750 μL). Water was added (736 μL) and then 1 M HCl (14 μL) to a final 0.1 M concentration of HCl. Samples were transferred to EPR tubes and frozen in liquid N$_2$ before EPR analysis. The EPR experiments were performed using the following conditions: microwave frequency, 9.463 GHz; microwave power, 200 mW; magnetic field modulation amplitude, 0.2 mT for Cu(II) (S =1/2) detection, temperature: 77 K.

2.2.8 Cyclic voltammetry studies of Cu(II) Deferasirox

In situ Cu(II) Deferasirox 2 mM (5% DMF/ 0.1 M KCl, pH 7.4 adjusted with NaOH) was prepared. Samples were purged with N$_2$ for 15 min then analyzed under an N$_2$ stream using a potentiostat with the following conditions number of scans: 4, scan rate: 0.5 V/s, Working electrode: Pt; Reference electrode: Ag/AgCl, NaCl saturated. Before the scanning, the Pt working electrode surface was polished using alumina slurries from higher to lower sized particles on soft surface pads. The electrode was rinsed well with distilled water and sonicated for 10 min using ethanol/distilled water solution (50% v/v) to remove residual abrasive particles. A control of 0.1 M KCl(aq) with 2% DMF at pH 7.4 was run before analyzing the samples to ensure the electrode was properly primed. The cyclic voltammograms were plotted following the IUPAC convention.

2.2.9 Transmetalation studies by UV-Vis spectroscopy and Q-Tof spectrometer

[Ti(Deferasirox)$_2$]$^{2-}$ -Cu(II) transmetalation. The following set of reactions was performed in quadruplicate and at 25 °C. Stocks solutions of [Ti(Deferasirox)$_2$]$^{2-}$ (500 μM) and metal-free ligand (1 mM) were prepared in DMF and diluted with pH 7.4 bicarbonate buffer (5 mM ammonium bicarbonate NH$_4$HCO$_3$, 0.1 M NaCl) to obtain 1% (v/v) DMF. All other solutions were prepared in the pH 7.4 bicarbonate buffer. 5 μM of [Ti(Deferasirox)$_2$]$^{2-}$ and 10 μM of metal-free ligand were reacted with 2.5 μM [Cu$_2$(Citrate)$_2$OH]$^{3-}$ over the course of 48 h and in the presence of 100 μM Na$_3$Citrate. The reactions were monitored by UV-Vis spectroscopy and Q-TOF MS (MS). In the UV-Vis window of 300-650 nm the disappearance of the LMCT band for [Ti(Deferasirox)$_2$]$^{2-}$ (λ$_{max}$ = 365 nm, ε = 11,332 M^{-1} cm^{-1}) was tracked in addition to the formation of the LMCT band for Cu(II) Deferasirox (λ$_{max}$ = 330 nm, ε = 21,900 M^{-1}cm^{-1}). The MS data were collected in negative ion mode, using source and desolvation temperatures of 100 ºC and 250 ºC, respectively. The

mass range was 100-1000 m/z. For the ESI-QTOF-MS experiments, the solutions were prepared in 5 mM ammonium bicarbonate (NH_4HCO_3) volatile buffer (pH 7.4) but without any Na_3Citrate excess salt.

[Fe(Deferasirox)$_2$]$^{3-}$-Cu(II) transmetalation. 2.5 µM of [Fe(Deferasirox)$_2$]$^{3-}$ was reacted with 5 µM of [Cu$_2$(Citrate)$_2$OH]$^{3-}$ in the presence of 100 µM total background of Na_3Citrate, over the course of 72 at 25°C and pH 7.4 (NH_4HCO_3 5 mM, 0.1M NaCl, 1% DMF). The reactions were followed by both UV-Vis spectroscopy. In the UV-Vis window of 250-550 nm the disappearance of the LMCT band for Fe(III) Deferasirox (λ_{max} = 420 nm, ε = 5,720 $M^{-1}cm^{-1}$; λ_{max} = 477 nm, ε = 4,050 $M^{-1}cm^{-1}$) was tracked in addition to the formation of the LMCT band for Cu(II) Deferasirox.

Cu(II) Deferasirox- Fe(III) transmetalation. 5 µM of Cu(II) Deferasirox was reacted with 2.5 µM of [Fe(Citrate)$_2$]$^{5-}$ in the presence of 100 µM total background of Na_3Citrate, over the course of 72 h at 25°C and pH 7.4 (NH_4HCO_3 5 mM, 0.1M NaCl, 1% DMF). Cu(II) Deferasirox was prepared in situ by mixing one equivalent of $CuCl_2$ (dissolved in 10 mM HCl) with one equivalent of deferasirox (dissolved in DMF). The reactions (n= 4) were followed by UV-Vis spectroscopy. In the UV-Vis window of 250-550 nm, the disappearance of the LMCT band for Cu(II) Deferasirox (λ_{max} = 330 nm, ε = 21,900 $M^{-1}cm^{-1}$) was tracked in addition to the formation of the LMCT band for [Fe(Deferasirox)$_2$]$^{3-}$. The Cu(II) Deferasirox LMCT ε value was validated by the titration experiment with [Ti(Deferasirox)$_2$]$^{2-}$ (See below).

[Ti(Deferasirox)$_2$]$^{2-}$ -Cu(II) titration. A titration experiment of [Ti(Deferasirox)$_2$]$^{2-}$ with Cu(II) was performed by preparing separate solutions of 2.5 µM [Ti(Deferasirox)$_2$]$^{2-}$ with $CuCl_2$ (dissolved in 10 mM HCl) at different mole equivalents (from 0.1 to 3.0 equivalents) at room temperature in solution containing 0.1 M NaCl and 1% DMF. These solutions were pH equilibrated to 7.4 and let react for three days. All final solutions were maintained at pH 7.4. No buffer was used to avoid competition from typical Cu(II) coordination by buffers (n= 3).[36] Finally, reactions were monitored by UV-Vis spectroscopy in the range of 250-700 nm.

2.2.10 Transmetalation studies by MALDI-TOF

[Ti(Deferasirox)$_2$]$^{2-}$ (500µM) was reacted with [Cu$_2$(Citrate)$_2$OH]$^{3-}$ (500µM) for 24 h. Fe(III) Deferasirox (500µM) was reacted with [Cu$_2$(Citrate)$_2$OH]$^{3-}$ (500µM) for 24 h. The samples were analyzed by MALDI-TOF. One µL of the α-Cyano-4-hydroxycinnamic acid matrix (5 mg/mL) was placed on the plate before placing the samples and let to crystalize. The solid samples were resuspended in water, and 1 µL of each was spotted on top of the crystallized matrix and allowed to dry. The same approach was used for sample solutions. After, the MALDI-TOF was collected of all the samples in positive ion reflector mode. Mass range was set up from 200 to 1200 m/z. Excel was used to tabulate the data, and Isopro was used

to obtain the theoretical spectra of the species identified. The theoretical and experimental intensities were normalized to a maximum signal of 100.

2.2.11 pH-dependent studies by MALDI TOF/TOF

Deferasirox, 15.5 mg (0.04 mmol, 40 mM) was dissolved in 1mL of DMSO, and 5.5 mg (0.04 mmol, 40 mM) of $CuCl_2$ was dissolved in 1 mL of H_2O. The metal solution (450 µL) was added dropwise to the ligand solution (450 µL) to a final concentration of 18 mM and left to equilibrate for 24 h. To achieve a pH between 5.45-5.7, NaOH and HCl were added as necessary. Similarly, The pH 8.6 samples were prepared at 10 mM, adding to the Deferasirox solution (250 µL) the following: 4.02 µL of 1M NaOH, 14.9 µL of 1M NaCl, and 270 µL of $[Cu_2(Citrate)_2OH]^{3-}$ (dropwise). The pH was measured and confirmed to be at 8.6. Finally, the pH 7.4 samples were prepared at 10 mM, adding to the Deferasirox solution (250 µL) the following: 5 µL of DMF, 5 µL of 1M ammonium bicarbonate (NH_4HCO_3) buffer, and 600 µL of autoclaved water to the deferasirox solution (250 µL). Solution pH was adjusted to 7.4. Lastly, 20µL of 10mM $CuCl_2$ was added dropwise and allowed to react for 24 hours.

2.2.12 Cell viability studies

A549 cells were seeded in 100 x 20 mm Petri dishes and grown in a 5% CO_2 humidified atmosphere. At least three passages were done to ensure the integrity of the cells. When cells reached the 95% confluence, cell solution stock was prepared at 1.0×10^5 cells/mL. A volume of 100 µL was seeded into 96-well plates using phenol red-free DMEM (supplemented with 10 % FBS and 1% Streptomycin/Penicillin). Cells were incubated for 24 h. Cu(II) Deferasirox stock solutions were prepared at a concentration from 2 to 200 µM (1 % DMF), and 100 µL were added to the 96-well plate to a final volume of 200 µL. Each stock's final Cu(II) concentration was half the initial 1 to 100 µM. Controls were treated with the background solution. Cells were incubated for 68 h. MTT solution was added (50 µL) and let it react for 4 hours. After completion, 25 µL of 10 % SDS solution was added. Plates were read after 12 h, at 570 and 800 nm (background absorbance subtraction) on an Infinite M200 PRO Tecan Microplate Reader. The cytotoxic/antiproliferative behavior of the Cu(II) Deferasirox compound was evaluated in A549 cells. Sample absorbance was compared to the 100 % control-containing cells. Origin 8.5 was utilized to fit the growth curve using the pharmacology dose-response equation over the various drug concentrations to determine the half-maximal inhibitory (IC_{50}) and the corresponding standard deviation. All samples were tested six times.

2.2.13 Determining the Cu(II) concentration for the supplementation studies

These studies were performed using A549 cells to get a Cu(II) concentration that does not affect cell proliferation. $[Cu_2(Citrate)_2OH]^{3-}$ was used as a source of Cu(II). A549 cells were cultured as previously described and treated with different

concentrations of $[Cu_2(Citrate)_2OH]^{3-}$ (0, 1, 5, 10, 50, 100, 500, 800, 900, and 1000 nM) for 72 h. An MTT assay was performed as described before.

2.2.14 Cell viability supplementation studies

Two supplementation experiments were performed using two metal sources: $[Cu_2(Citrate)_2OH]^{3-}$ (50 nM) and Zn(II) Citrate (20, 40, and 100 µM). A549 cells were seeded in 100 x 20 mm Petri dishes and grown in a 5% CO_2 humidified atmosphere. At least three passages were done to ensure the integrity of the cells. When cells reached the 95% confluence, cell solution stock was prepared at 1.0 x 10^5 cells/mL. A volume of 100 µL was seeded into 96-well plates using phenol red-free DMEM (supplemented with 10 % FBS and 1% Streptomycin/Penicillin). Cells were incubated for 24 h. Metal sources were added, and cells were incubated for 2h. Free-metal controls were treated with the background solution. $[Ti(Deferasirox)_2]^{2-}$ was added at 23 µM (PBS with 1% DMF) to metal-containing and free-metal-containing samples. Free-compound controls were treated with a background solution. MTT solution was added (50 µL) and let it react for 4 hours. After completion, 25 µL of 10 % SDS solution was added. Plates were read after 12 h, at 570 and 800 nm (background absorbance subtraction) on an Infinite M200 PRO Tecan Microplate Reader. The cytotoxic/antiproliferative behavior of the Cu(II) Deferasirox compound was evaluated in A549 cells. Sample absorbance was compared to the 100 % control-containing cells. Origin 8.5 was utilized to fit the growth curve using the pharmacology dose-response equation over the various drug concentrations to determine the half-maximal inhibitory (IC_{50}) and the corresponding standard deviation. All samples were tested six times.

2.2.15 ROS generation in A549 cells of Titanium(IV) and Copper(II) cTfm complexes

A549 cells were cultured as previously described and seeded in 96 Well Black/Clear Bottom Plate at $1x10^5$ cells/mL. Five compounds (Deferasirox, Titanium HBED [TiHBED]$^-$, $[Ti(Deferasirox)_2]^{2-}$ and titanium citrate $[Ti(Cit)_2]^{4-}$) were tested at the IC_{50} concentrations at 1, 3, 6, 12, 24, and 48 h to evaluate reactive oxygen species (ROS) generation. $[Ti(Cit)_2]^{4-}$ and the positive control (H_2O_2) were tested at 20 µM. All the solutions were prepared using the wash 1X buffer available in the kit and DMF (1%). DMSO was avoided in all preparations because it inactivates ROS formation. The experiment was performed using the ROS/Superoxide Detection Assay Kit (Cell-based) (ab139476), and the protocol was performed as indicated by the manufacturer. The fluorescence increase was monitored at Ex/Em = 485 nm / 535 nm with bottom read mode in an M200 PRO Tecan Microplate Reader. Raw data was processed in excel by subtracting the background signal of controls.

2.2.16 ROS generation of Titanium(IV) and Copper(II) cTfm complexes in solution

All solutions were prepared using PBS to a final concentration of 25 µM for all the metal complexes and glutathione (Glu) stock. The samples were mixed in 96 Well Black/Clear Bottom Plate. The DCF ROS/RNS Assay Kit (biofluids, culture supernatant, cell lysates) (ab238535) was repurposed to measure the ROS generation in PBS (1 % DMF) sample solutions. The experiment was performed as described by the manufacturer. The fluorescence increase was monitored at Ex/Em = 485 nm / 535 nm with bottom read mode in an M200 PRO Tecan Microplate Reader. Raw data was processed in excel by subtracting the background signal of controls

2.2.17 Mitochondrial ROS production of Ti(IV) cTfm complexes in A549 cells

Cells were plated overnight in a growth medium (DMEM, 10% FBS, 1% Penicillin/streptomycin) at 2.5×10^4 cells at 90µL per well. After 24h incubation in a humidified atmosphere (5% CO_2), compounds (HBED, [TiHBED]⁻, Deferasirox, [Ti(Deferasirox)$_2$]$^{2-}$, [Ti(Cit)$_2$]$^{4-}$, and Cu(II) Deferasirox) were added (10 µL) at 10X concentration to a final concentration of 100, 50, 30 and 10 µM and for Cu(II) Deferasirox 40 and 20 µM. After 72 h, the MitoROS 580 stain working solution stock was prepared as indicated by the manufacturer and diluted to 10 mL with the assay buffer. Cells were incubated for an additional 24h, and the fluorescence increase was monitored at Ex/Em = 540 nm / 590nm (cut off 570 nm) with bottom read mode in an M200 PRO Tecan Microplate Reader. Raw data was processed in excel by subtracting the background signal of controls (Compound buffer + MitoROS 580 stain).

2. 3 RESULTS

2.3.1 Characterization of the Cu(II) complexation by deferasirox in solid-state

Deferasirox was synthesized as reported.[13] Elemental analysis and ^{1}H NMR characterization were comparable to the ones observed in the literature (See supporting info). The Cu(II) Deferasirox synthesis was achieved by reacting the Cu(II) source and the ligand at a 1:1 equivalent ratio. Elemental analysis (C, N, H) obtained was in concordance with the molecular structure of Deferasirox. In FT-IR, we observed the characteristic bands of the C=O and C-O groups present in the ligand and its Cu(II) complex (v(C=O) 1678, 1607 ligand and 1701, 1601 complex; v(C−O) 1279, 1221 ligand and 1257,1234 complex), and the Cu-O, Cu-N bands (v(Cu-O, Cu-N) 582) resulted from the complexation. UV vis in pyridine showed two bands, one that agrees with the expected transitions of a metal compound with an ε= 15,808 M^{-1} cm^{-1} and the second corresponding to the blue

color of the copper source λ_{max} 674 nm, ε = 284.8 M^{-1} cm^{-1}. In water similar results were observed λ_{max} = 330 nm, ε = 21,900 $M^{-1}cm^{-1}$.

2.3.2 Cu(II) Deferasirox in solid-state characterization results in a dimer structure

After synthesis, we were able to see that the solid and the dissolved compound were different species based on solubility. When the sample was prepared in situ, it was completely soluble, but when we tried to dissolve the solid, it was not possible until we changed the pH to a basic pH. A MALDI TOF was performed to the Cu(II) Deferasirox solid using a matrix pre-crystalization approach and then placing our solid on top of the pre-crystallized matrix. We obtained two times the mass $[Cu(C_{21}H_{13}N_3O_4)]_2 + H^+$ = 871.78 (**Fig 2.1**) of the expected complex. Maurya et al. reported a dimer conformation of the V(V) Deferasirox complex.[19] We predict that the same could be happening to the Cu(II) Deferasirox complex.
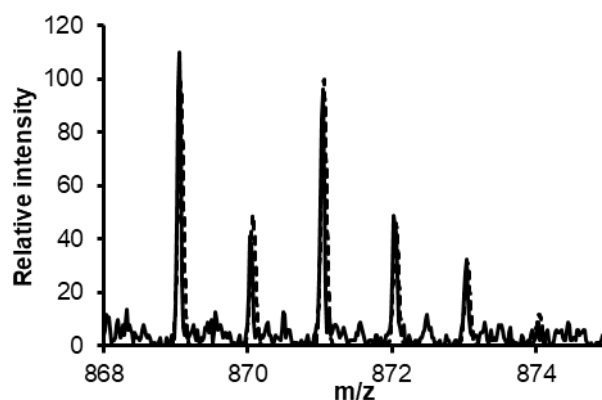
Figure 2.1. MALDI-TOF/TOF mass spectrum of Cu(II)Deferasirox dimer ($[Cu(C_{21}H_{13}N_3O_4)]_2 + H^+$ = 871.78) (solid line) and the theoretical spectrum (dotted line).

Interestingly, the literature previously reported Cu(II) Deferasirox as a mononuclear complex.[20] After a few solubility trials, we found that the complex was easily solubilized in pyridine. A crystalization experiment was designed with a water: pyridine 50:50 mixture. We observed that the presence of water induces the formation of a solid precipitate, and by slow evaporation, we obtained suitable crystals for a single crystal X-ray. A summary of the crystal data, structure solution, and refinement are listed in **Table 2.1**.

Table 2.1. Crystal and structure refinement for [Cu(Def)(Py)]$_2$.

Empirical formula	$C_{52}H_{36}Cu_2N_8O_8$
Formula weight	1027.97
Temperature	300 K
Wavelength	1.54184 Å
Crystal system, space group	Monoclinic, P2$_1$/c
Unit cell dimensions	a = 16.0148(2) Å, α = 90 °
	b = 10.46660(10) Å, β = 116.263(2) °
	c = 17.8077(2) Å, γ = 90 °
Volume	2676.81(7) Å^3
Z, calculated density	2, 1.275 g/cm^3
Absorption coefficient	1.454 mm^{-1}
F(000)	1052.0
Crystal size	0.148 x 0.108 x 0.01 mm
Theta range for data collection	6.154 to 136.802°
Limiting indices	-19 ≤ h ≤ 19, -12 ≤ k ≤ 12, -18 ≤ l ≤ 21
Reflections collected/unique	27,808/4884 (R$_{int}$ = 0.0351)
Completeness to theta = 136.802°	99.9%
Absortion	Multi-scan
Max. And min. transmission	1.000 and 0.882
Refinement method	Full-matrix least squares on F^2
Data/restraints/parameters	4884/0/318
Goodness-of-fit on F^2	1.051
Final R indices [I > 2sigma(I)]	R$_1$ = 0.0335, wR$_2$ = 0.1007
R indices (all data)	R$_1$ = 0.0386, wR$_2$ = 0.1044
Largest diff. peak and hole	0.27 and -0.32 e Å^{-3}

The structure (**Fig 2.2**) contains a dinuclear complex with two Cu ions, two deferasirox, and pyridines in a distorted trigonal bipyramidal coordination geometry. Deferasirox acts as a tridentate ONO ligand in a [Cu^{II}O(μ-Py)$_2$Cu^{II}O] unit, and each Cu(II) is five-coordinated with a deferasirox and pyridine in an anti-coplanar configuration.

Steinhauser et al. established that an entirely planar conformation would generate stress in molecular configuration.[21] Cu(II) Deferasirox complex is not arranged in a meridional configuration as Steinhauser structure, but a distortion in phenol rings is observed (**Fig 2.2**).

The ligand is bound to the Cu(II) ion by the N1 [Cu1-N1 1.9353(14)] from the triazole core, the two oxygens from phenol, one acting as a bridge between the two Cu(II) ions [Cu1-O1 1.9507(13)] and the other as a terminal ligand [Cu1-O2 1.9250(14)], and a pyridine molecule [Cu1-N(4) 2.0288(15)] (**Fig 2.3**, **Table 2.2**). This structure is coherent compared to Maurya et al. for the dinuclear vanadium deferasirox complex.
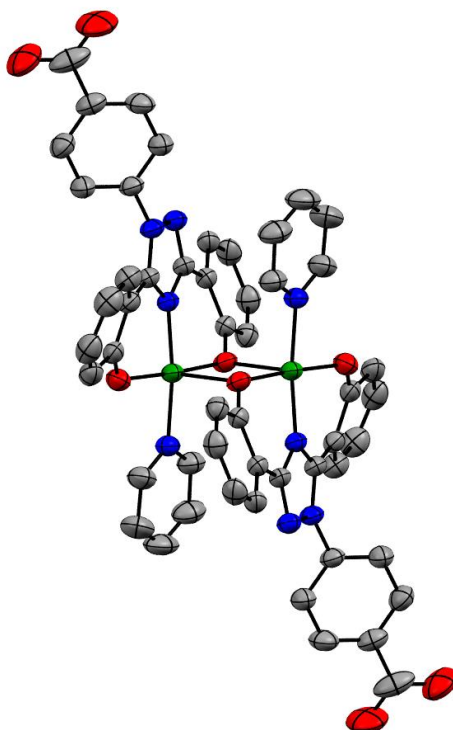
Figure 2.2. Crystal structure of [Cu(Def)(Py)]$_2$. Hydrogen atoms were omitted for clarity. Thermal ellipsoids at 50 % probability.
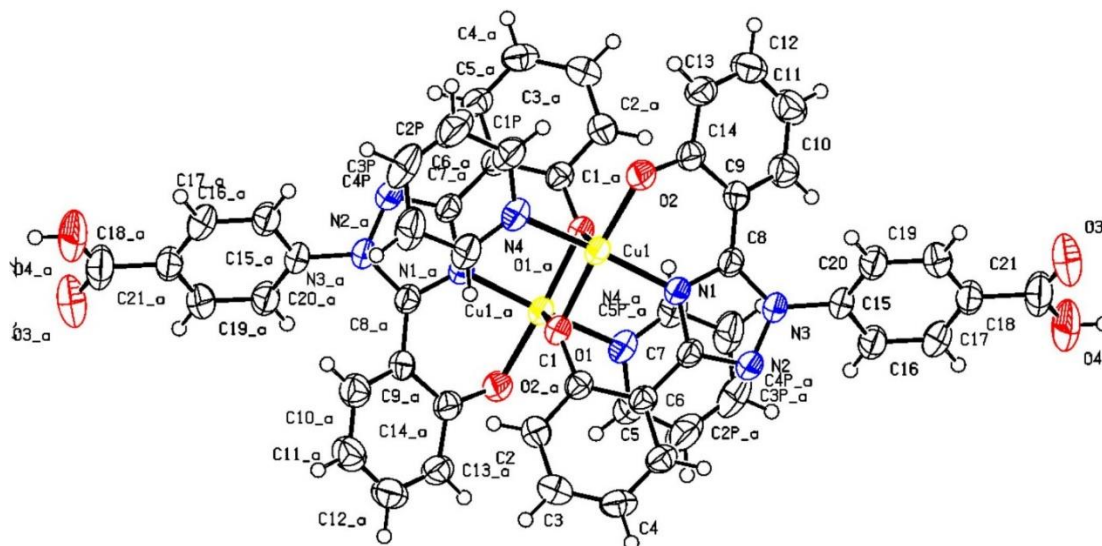
Figure 2.3. Ellipsoid plot (probability 50%) with atom labeling of [Cu(Def)(Py)]$_2$.

Table 2.2. Selected bond lengths (Å) and angles (°) for [Cu(Def)(Py)]$_2$.[a]

Cu(1)—O(1)	1.9507(13)
Cu(1)—O(2)	1.9250(14)
Cu(1)—N(1)	1.9353(14)
Cu(1)—N(4)	2.0288(15)
Cu(1)—O(1)#1	2.3722(14)
O(1)—Cu(1)—N(1)	88.11(6)
O(1)—Cu(1)—O(2)	176.16(5)
O(1)—Cu(1)—N(4)	91.15(6)
O(2)—Cu(1)—N(1)	88.84(6)
O(2)—Cu(1)—N(4)	91.39(6)
N(1)—Cu(1)—N(4)	168.78(7)
O(1)—Cu(1)—O(1)#1	84.08(5)
O(2)—Cu(1)—O(1)#1	98.48(6)
N(1)—Cu(1)—O(1)#1	94.37(5)
N(4)—Cu(1)—O(1)#1	96.69(6)

[a] Symmetry transformation used to generate equivalent atoms: #1 $-x + 1$, $-y + 1$, $-z + 1$.

2.3.3 Cu(II) Deferasirox is a non-redox active mononuclear species in solution

Since Cu(II) Deferasirox appears to have different species in solution and solid-state, and EPR experiment was performed. Single crystal X-ray studies clearly showed a dinuclear complex. However, as previously said, this compound is not soluble in aqueous solutions unless a basic pH is reached, for example, in a solvent such as pyridine. The EPR spectrum was taken from a Cu(II) Deferasirox solid dissolved in a mixture of pyridine and ethylene glycol (**Fig 2.4**). This spectrum is typical for a mononuclear Cu(II) complex. It is characterized by a slightly rhombic g-tensor with (g_x, g_y, g_z) = (2.012, 2.060, 2.261) and near-axial hyperfine interaction (hfi) of the copper nucleus with (A_x, A_y, A_z) = (0, 0, 490) MHz. The observed combination of g_z and A_z values agrees with those expected for square planar copper complexes featuring two nitrogen and two oxygen ligands[22]. The presence of (at least two) coordinated nitrogens is supported by the poorly resolved hyperfine structure of about five lines observed at g_y. The splitting between these lines is about 1.4 mT. The EPR spectrum is thus in general agreement with the monomeric Cu(Def)(Py) species. Cu(II) Deferasirox speciation turns out to be more complex and hence an important topic to understand.
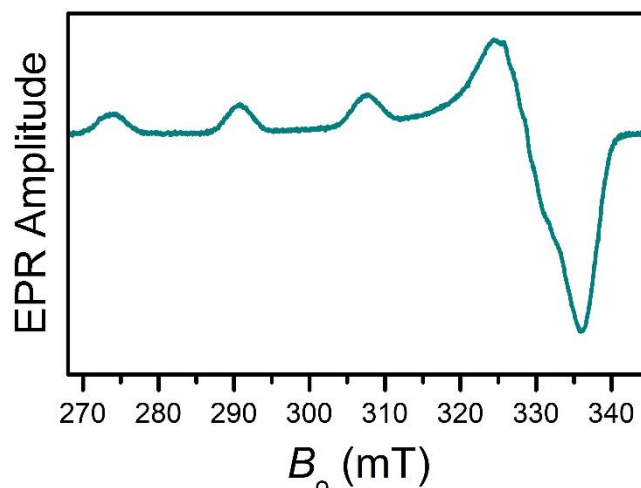
Figure 2.4. EPR spectrum of Cu(II) Deferasirox in frozen pyridine – ethylene glycol solution. Experimental conditions: microwave frequency, 9.463 GHz; microwave power, 200 mW; magnetic field modulation amplitude, 0.2 mT; temperature, 77 K.

Cu(II) is an active redox metal; thus, we expected that Cu(II) Deferasirox can enter redox cycling processes. A cyclic voltammetry study was performed to understand the redox cycling properties of this compound. The reduction potential obtained in the Cu(II) Deferasirox voltammogram was E_c = 0.0398 V (**Fig 5**). This complex is redox active and can be reduced intracellularly but not be able to be oxidized again. Since Cu and Fe are closely related, the capability to be reduced in the intracellular environment can allow this compound to play a role in intracellular processes involving Fe.
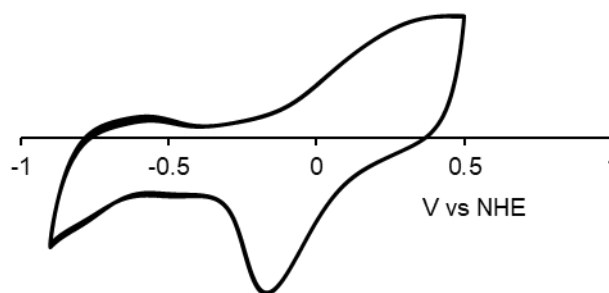
Figure 2.5. Cyclic voltammetry study of the Cu(II) Deferasirox 2 mM (5% DMF/ 0.1 M KCl, pH 7.4 adjusted with NaOH. The reduction potential obtained E_c = 0.0398 V.

2.3.4 Cu(II) Deferasirox is the product of [Ti(Deferasirox)$_2$]$^{2-}$ -Cu(II) transmetalation

Previous studies have shown [Ti(Deferasirox)$_2$]$^{2-}$ can perform transmetalation by an available Fe labile source.[13-14] Since Cu is also involved in numerous intracellular processes, angiogeneses, cancer progression, and survival, affecting

this metal intracellularly could be part of the mechanism of action of the $[Ti(Deferasirox)_2]^{2-}$. Transmetalation and titration experiments were performed (**Fig 2.6 A** and **B**), both were run in excess of Na_3citrate (100 µM) to mimick intracellular conditions. $[Ti(Deferasirox)_2]^{2-}$ (5 µM) and $[Cu_2(Citrate)_2OH]^{3-}$ (2.5 µM) were reacted and monitored for 12 h (720 mins), a green color was observed together with the disappearance of the LMTC band corresponding to the $[Ti(Deferasirox)_2]^{2-}$ complex.[14] The appearance of a new band at 330 nm concordance with the previously obtained maximum absorbance for the Cu(II) Deferasirox complex (H_2O, DMF 1%) at pH 7.4 $\lambda_{max} = 330$ nm, $\varepsilon = 21,900$ $M^{-1}cm^{-1}$. Cu(II)-induced transmetalation is observed (**Fig 2.6 B**), confirming the feasibility of this process occurring intracellularly. By titration in the same conditions, the Cu(II)-induced transmetalation is observed as low as 0.5 equivalents of Cu(II) source against the $[Ti(Deferasirox)_2]^{2-}$ complex. MS data were collected for the same reaction but at a lower concentration to prevent interference from the salt content (**Fig 2.6 C**). The data analysis shows a multistep Cu(II)-induced transmetallation following the suggested following reaction:

$$[Ti(Def)_2]^{2-} + [Cu_2(Cit)_2OH]^{3-} \rightarrow [Cu(Def)(Cit)]^{5-} + [Ti(Def)(OH)]^-$$

$$\rightarrow [Cu(Def)]^- + [Ti(Cit)_2(OH)_2]^{4-}$$
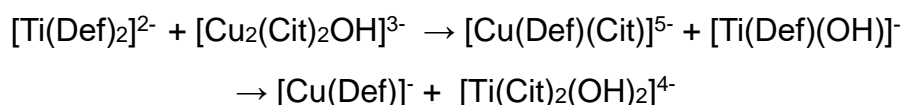
Cu(II)-induced transmetalation can compete with Fe-induced transmetalation, when $[Fe(Deferasirox)_2]^{3-}$ was reacted with 5 µM of $[Cu_2(Citrate)_2OH]^{3-}$, the formation of the Cu(II) Deferasirox band was observed (**Fig 2.7 A**). On the contrary, when 5 µM of Cu(II) Deferasirox was reacted with 2.5 µM of $[Fe(Citrate)_2]^{5-}$ no change in the maximum absorbance was observed (**Fig 2.7 B**), suggesting that Deferasirox have more affinity by Cu(II) than Fe(III) binding. These results support the possibility of Cu(II) intracellular ions to outcompete with Fe(III) binding to Deferasirox via transmetalation. By MALDI-TOF, the dinuclear Cu(II) Deferasirox specie was detected after the transmetalation (**Fig 2.8 A, B, and C**). Changing the pH of the Cu(II) Deferasirox solution, the dimer was also detected (**Fig 2.8 D** and **E**), indicating that the dinuclear complex is found in a wide range of pH from 5.5 -8. Cu(II) Deferasirox electrostatic interactions can be favored to be a dimeric complex, thus forming a more stable compound that the ones formed by the Fe and Ti metals.
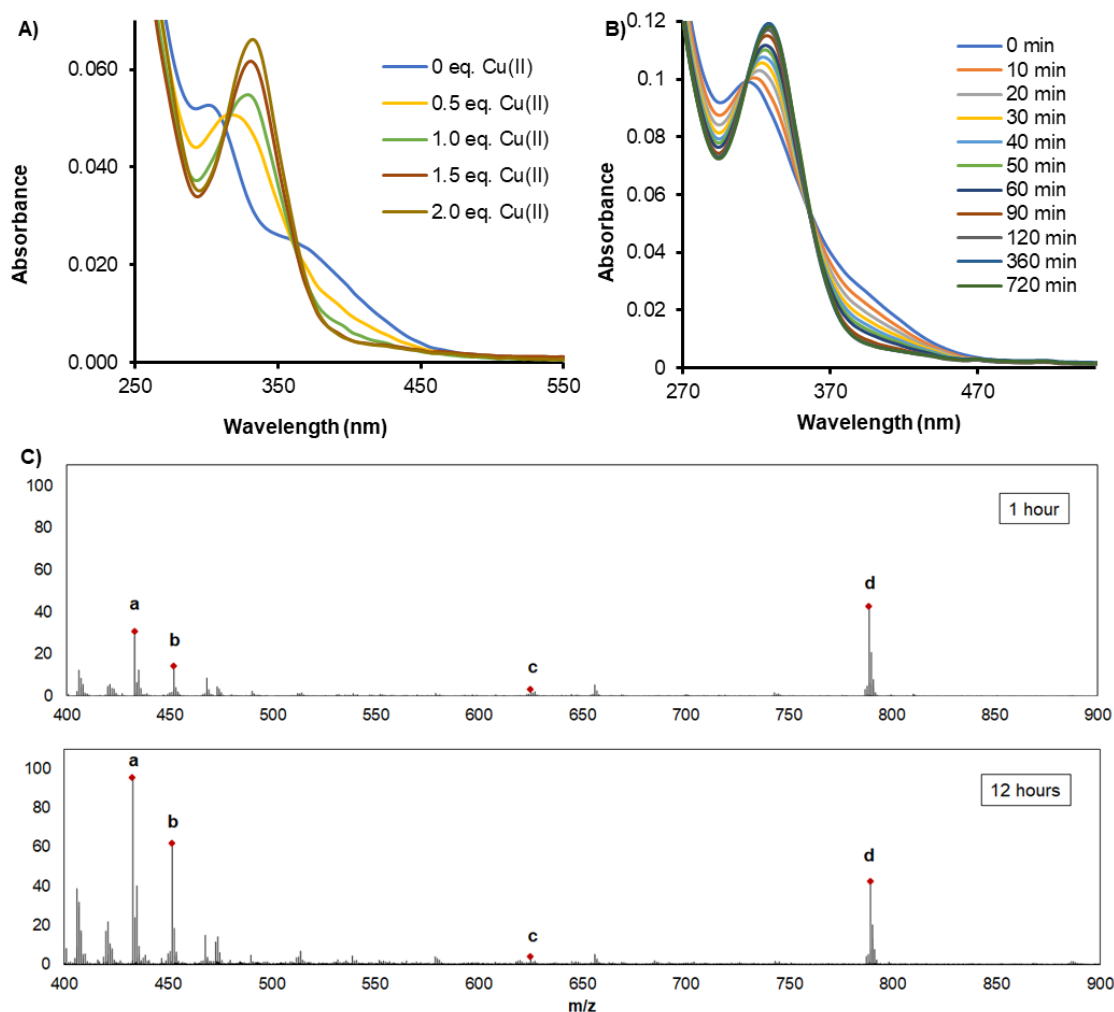
Figure 2.6. (A) UV-Vis absorbance spectra of monitored reaction between 5 µM [Ti(Deferasirox)$_2$]$^{2-}$ and [Cu$_2$(Citrate)$_2$OH]$^{3-}$ variating the Cu(II) equivalents at pH 7.4 (% DMF, NH$_4$HCO$_3$ 5 mM, 0.1M NaCl, 100 µM background citrate). **(B)** UV-Vis absorbance spectra of monitored reaction between 5 µM [Ti(Deferasirox)$_2$]$^{2-}$ and 2.5 µM of [Cu$_2$(Citrate)$_2$OH]$^{3-}$ at pH 7.4 (1% DMF, NH$_4$HCO$_3$ 5 mM, 0.1M NaCl, 100 µM background citrate). **(C)** Negative mode mass spectrum of the reaction between 5 µM [Ti(Deferasirox)$_2$]$^{2-}$ and 2.5 µM [Cu$_2$(Citrate)$_2$OH]$^{3-}$ at pH 7.4. The reaction was monitored at 1 and 12 h. Data suggests a multi-step transmetalation process involving the following species: (a) [Cu(Deferasirox)]$^{-}$, (b) [Ti(Deferasirox)$_2$(OH)$_2$]$^{-}$, (c) [Cu(Deferasirox)(Citrate)]$^{5-}$ and (d) [Ti(Deferasirox)$_2$]$^{2-}$.
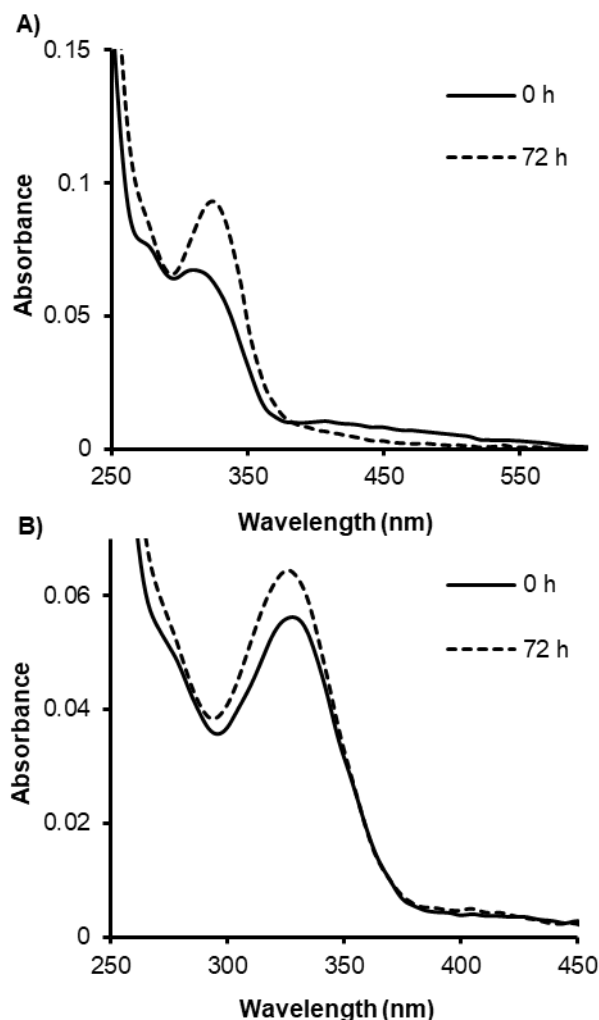
Figure 2.7. (A) UV-Vis absorbance spectra of monitored reaction between 2.5 µM of [Fe(Deferasirox)$_2$]$^{3-}$ was reacted with 5 µM of [Cu$_2$(Citrate)$_2$OH]$^{3-}$ in the presence of 100 µM total background of Na$_3$Citrate, over the course of 72 at 25°C and pH 7.4 (NH$_4$HCO$_3$ 5 mM, 0.1M NaCl, 1% DMF). **(B)** UV-Vis absorbance spectra of monitored reaction between 5 µM of Cu(II) Deferasirox was reacted with 2.5 µM of [Fe(Citrate)$_2$]$^{5-}$ in the presence of 100 µM total background of Na$_3$Citrate, over the course of 72 h at 25°C and pH 7.4 (NH$_4$HCO$_3$ 5 mM, 0.1M NaCl, 1% DMF).
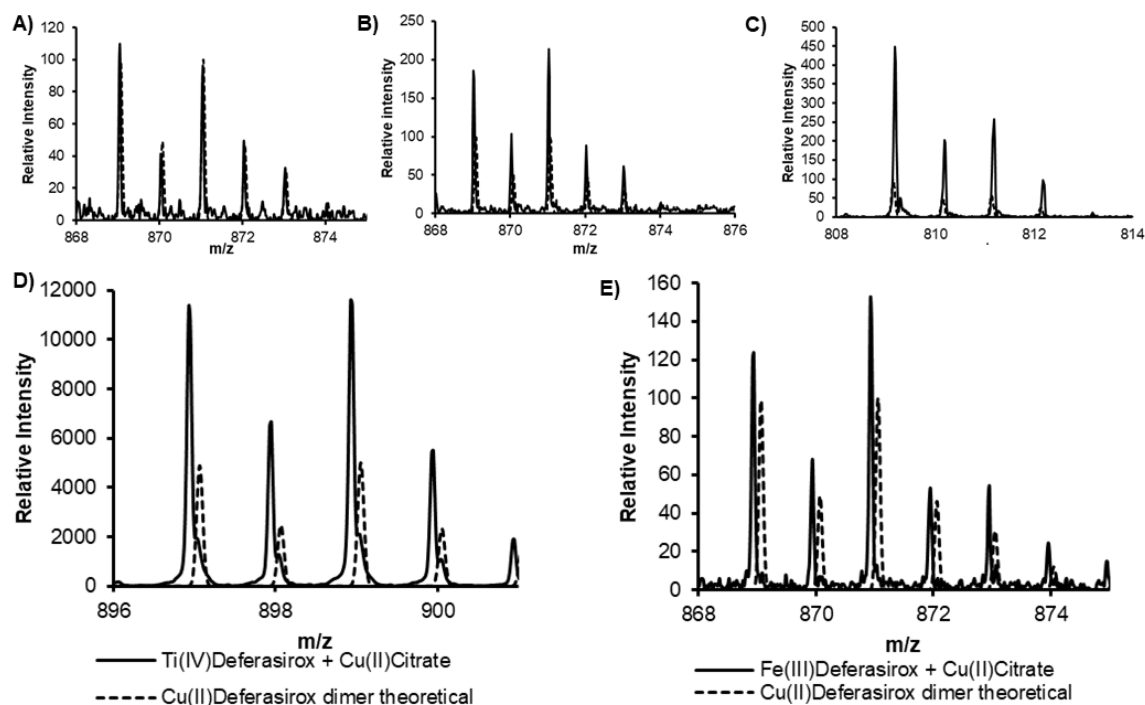
Figure 2.8. MALDI-TOF experiments of Cu(II) Deferasirox [Cu($C_{21}H_{13}N_3O_4$)]$_2$ + H$^+$ = 871.78. pH-dependent Cu(II) Deferasirox species: **A)** pH 5.5, **B)** pH 7.4, **C)** pH 8. Transmetalation product characterization: **D)** Ti(IV) Deferasirox-Cu(II) transmetalation, and **E)** Fe(III) Deferasirox-Cu(II) transmetalation.

2.3.5 Intracellular transmetalation results in a cytotoxic product

Cell viability experiments were performed in lung carcinoma cell line model A549. An antiproliferative behavior was observed with an IC$_{50}$ value of 6.08 ± 1.14 µM (**Fig 2.9**). Interestingly, compared with the previously reported IC$_{50}$ value for Ti(IV) deferasirox (20 ± 1 µM)[3] for A549 cell line, the Cu(II) Deferasirox IC$_{50}$ value is much lower than that. Together with the Cu-induced transmetalation evidence, the presence of labile Cu(II) metal ions results in a transmetalation product that is more active than the initial compound. But, due to low intracellular concentrations of this metal, it has a limited effect.
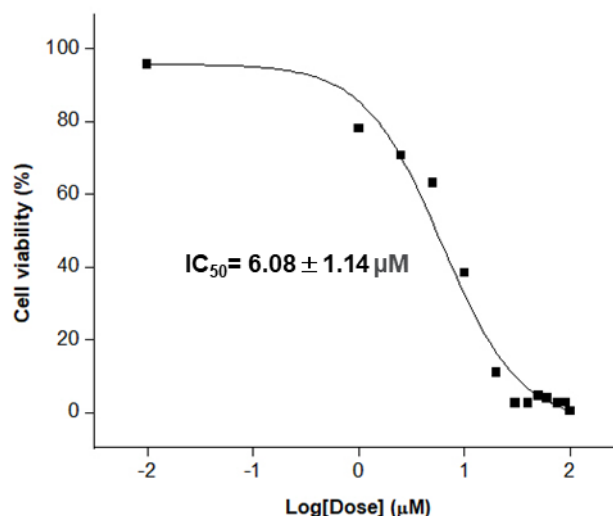
Figure 2.9. Cell viability study of an in situ prepared Cu(II) Deferasirox complex against A549 cell line.

To understand the impact of Cu in cancer cells, a Cu supplementation study was performed. To achieve the right concentration to conduct the study, $[Cu_2(Citrate)_2OH]^{3-}$ was tested at different concentrations to find a concentration that does not affect cell proliferation. From 0 to 1000 nM were tested against A549 cells. The selected concentration was at 50 nM with 97,30 ± 6,19 % of live cells (**Fig 2.10**).
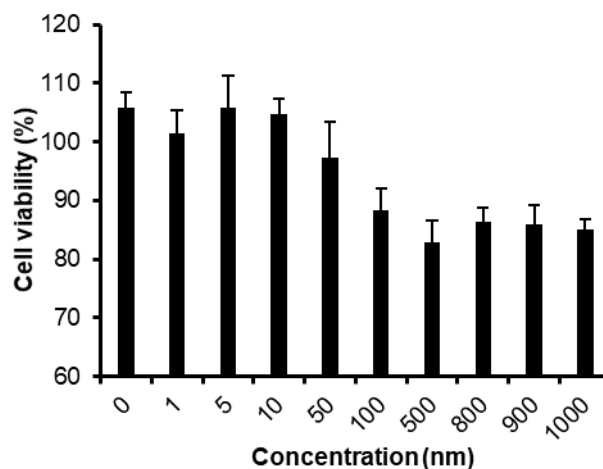
Figure 2.10. Cell viability studies to determine the Cu(II) citrate concentration to perform cell supplementation studies against lung carcinoma cell line model A549.

After the $[Cu_2(Citrate)_2OH]^{3-}$ concentration was chosen, a cell supplementation experiment was performed to observe the dependency of the cancer cells to Cu(II) in survival requirements. A549 cells were treated with and without $[Ti(Deferasirox)_2]^{2-}$ in the presence and absence of $[Cu_2(Citrate)_2OH]^{3-}$. After 72 h

of treatment, live-cell percentages were observed in cells treated with Cu(II); even in media-treated cells, a proliferation over the 100 % control was obtained. These results indicate a close correlation between cancer cell survival and the bioavailable Cu(II) (**Fig 2.11**).
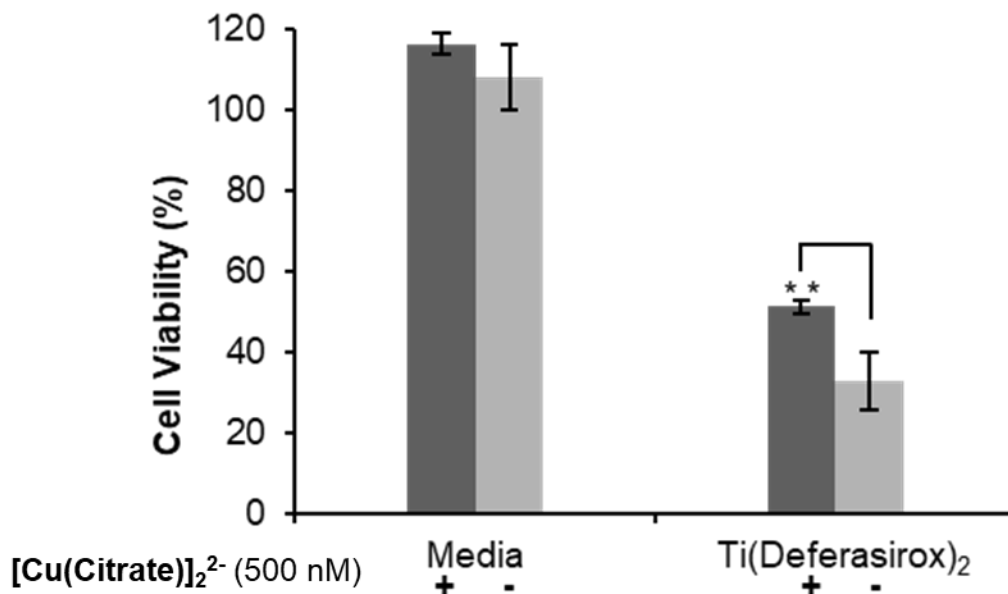
Figure 2.11. Cell supplementation studies using a Cu(II) citrate as a source of Cu(II) to observe the dependency of cancer cells (A549 cell line) on this metal.

The transmetalation process has shown that it can produce redox-active intermediates.[13] By transmetalation, it is a possibility that cell death can occur by a ROS generation pathway. [Ti(Deferasirox)$_2$]$^{2-}$ was tested against A549 cells to detect any ROS increase. A significant generation of ROS was detected in cells treated with [Ti(Deferasirox)$_2$]$^{2-}$ compared to the positive control (H_2O_2), the ligand, and a non-cytotoxic compound such as Titanium(IV) Citrate (**Fig 2.12**). Interestingly, even when titanium-based complexes are not a redox-active compound but by transmetallation of Ti(IV) and Fe(III) (and possibly Cu(II)) inside the cell allows [Ti(Deferasirox)$_2$]$^{2-}$ (an inactive redox compound) to be transformed to redox-active intermediates such as [Fe(Deferasirox)(Citrate)]$^{4-}$ (an active redox compound).[13]
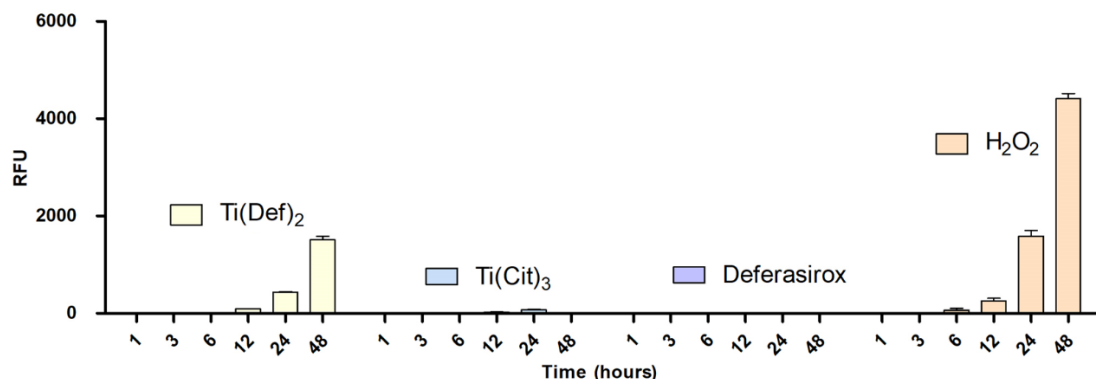
Figure 2.12. Time-dependent effect of Deferasirox, $[Ti(Deferasirox)_2]^{2-}$, Titanium(IV) citrate and the positive control (H_2O_2) on reactive oxygen species generation in A549 cells. Results are expressed in relative fluorescence units (RFU) six times (1, 3, 6, 12, 24, and 48 hours).

To explore whether $[Ti(Deferasirox)_2]^{2-}$ can transform intracellular labile Fe(III) into a cytotoxic species, in solution reactions were performed in the presence and absence of an antioxidant such as glutathione (GSH) (**Fig 2.13**). The reactions in which both $[Ti(Deferasirox)_2]^{2-}$ and $Fe(Citrate)_2$ showed the highest response, which confirms that the Fe-induced transmetalation could be part of the intracellular ROS increase. $[Ti(Deferasirox)_2]^{2-}$ the mechanism is still under study, and the increase by the compound itself should be further studied as part of how this compound works. Deferasirox did not show a detectable ROS formation. On the other hand, GSH could quench the positive control ROS generation, but this did not happen with the reaction that involved Fe and Ti. GSH is the principal antioxidant in our body and maintains the balance of ROS formation to avoid tissue damage. GSH can react with Fe(III) to reduce it to Fe(II), releasing electrons that can produce ROS. The effect of ROS production is higher in these reactions due to the presence of GSH, allowing a higher formation of ROS.
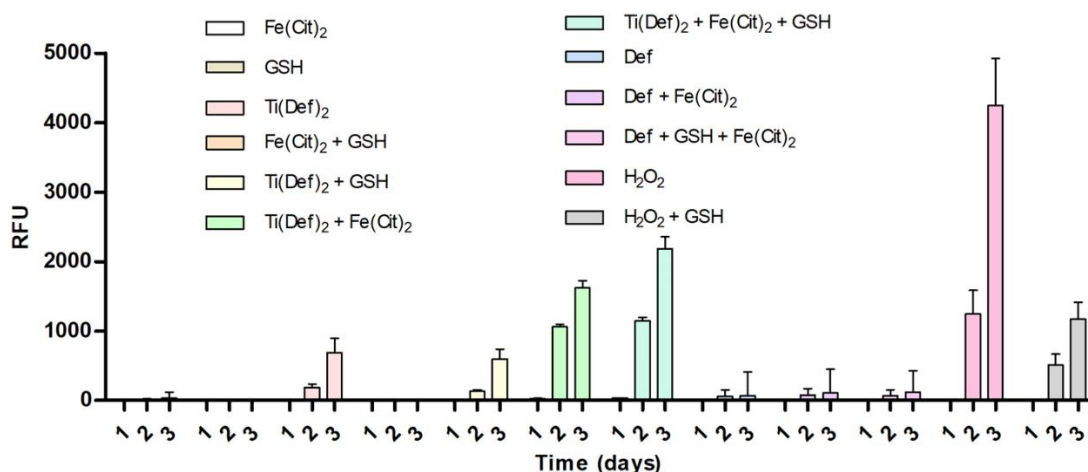
Figure 2.13. Time-dependent effect of $[Ti(Deferasirox)_2]^{2-}$, Titanium(IV) citrate and the positive control (H_2O_2) on reactive oxygen species generation in solution reactions. Results are expressed in relative fluorescence units (RFU) three times (1, 2, and 3 days).

To know where the ROS increase is coming from, mitochondrial ROS production was tested, and data suggest that Deferasirox and $[Ti(Deferasirox)_2]^{2-}$ can induce an imbalance in the mitochondrial ROS homeostasis by increasing the amount of ROS produced compared to the controls (**Fig 2.14**). A dose-dependent behavior was observed. The non-cytotoxic compound $Ti(Citrate)_3$ did not show mitochondrial production at any tested concentration. Deferasirox results could be related to the affinity with different metals leading to intracellular reactions that can affect the ROS production in the mitochondria. Intracellular ROS production observed in previous studies can be attributed to increased mitochondrial ROS production.
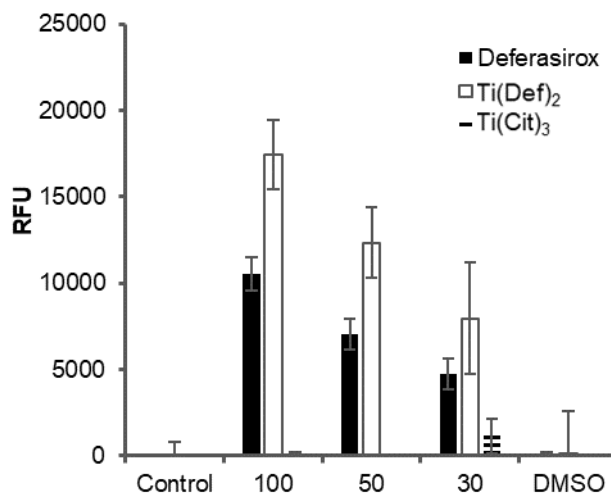
Figure 2.14. Mitochondrial ROS generation of $[Ti(Deferasirox)_2]^{2-}$, Titanium(IV) citrate and the positive control (H_2O_2) in A549 cells. Results are expressed in relative fluorescence units (RFU).

2. 4   DISCUSSION

As in the human body's normal biological processes, essential metals play important roles in cancer.[2] Until now, the Fe-induce transmetalation of $[Ti(Deferasirox)_2]^{2-}$ on physiologically relevant conditions has been studied and supports this compound's feasibility to affect the Fe-depending processes.[14, 23] Recently, its impact on the DNA synthesis process has been proven to be part of its mechanism of action.[13] Cu is an essential metal associated with cancer survival and angiogenesis.[11, 24] These findings have led researchers to decrease intracellular Cu as an anticancer strategy.[25-26]

Previous studies on Cu(II) deferasirox structure were performed, and a mononuclear species were obtained and analyzed by single-crystal X-ray.[20] But the Cu(II) Deferasirox speciation seems to be more complex. After synthesis and characterization, we found that the compound met the criteria to be a mononuclear specie based on the IR, elemental analysis, and UV-vis data. But, after the compound, precipitates were insoluble in most common solvents except when a basic pH was reached. Then, we chose pyridine and solvent, and using water as a precipitation inducer, we obtained suitable crystals for a single crystal X-ray. V(V) Deferasirox complexes have been characterized as dinuclear complexes.[19] Then, we hypothesized that Cu(II) Deferasirox can undergo a dimerization or a polymerization process that forms an insoluble precipitate. By single-crystal X-ray analysis, we confirm the presence of a dinuclear complex that could explain the solubility changes in the complex.

Interestingly, in transmetalation and pH titration experiments, the dimer was present in the solution, which could mean that the dimer is stable at a low concentration. In the presence of pyridine, this solvent induces a steric hindrance,

not allowing the water molecules to be in contact with the metal center and maintaining the compound in solution at higher concentrations. In summary, the Cu(II) Deferasirox concentration-based speciation model will present the aquated Cu(II) Deferasirox complex, [Cu(Deferasirox)(H_2O)]⁻ soluble in low concentration under 5 µM, detected by ESI-QTOF MS, the missing water molecule could be the result of the technique, but the elemental analysis data support its presence. The aquated dimer formation and subsequent precipitation were observed in concentrations higher than 5 µM and were detected in the MALDI TOF pH titration experiments. For the complex in the presence of pyridine as in the single crystal structure, higher concentrations (<10 mM) can be reached as a mononuclear specie detected by EPR. The dimer formation and precipitation are again observed by adding water to the Cu(II) Deferasirox pyridine solution over 10 mM concentration (**Fig 2.15**).
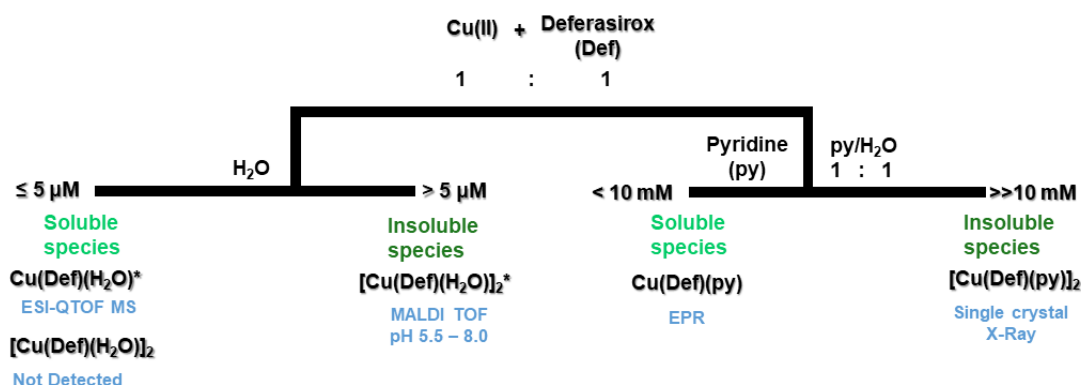
Figure 2.15. Cu(II) Deferasirox concentration-based speciation model.

Transmetalation experiments support the feasibility of [Ti(Deferasirox)$_2$]$^{2-}$ to interchange its metal center with the bioavailable Cu(II). Cu(II)-induced transmetalation occurs at as low Cu(II) equivalents as 0.5 molars. The reaction is favorable over Fe-induced transmetalation, not showing any metal interchange once the Cu(II) Deferasirox complex is formed. This transmetalation-approach mechanism can be activated intracellularly, binding both the bioavailable Fe and Cu and delivering Ti(IV) in a three-metal anticancer therapy approach and contributing to the previous reported [Ti(Deferasirox)$_2$]$^{2-}$ mechanism of action.[13-14] Even more interesting, the transmetalation product of [Ti(Deferasirox)$_2$]$^{2-}$-Cu(II) is cytotoxic to cancer cells, having a lower IC$_{50}$ than the initial compound in a pro-drug like mechanism.

The ability of [Ti(Deferasirox)$_2$]$^{2-}$ to generate ROS increase was also tested, resulting in a significant signal increase compared to the positive control. In solution reactions involving Ti and Fe, higher ROS production and mitochondrial ROS imbalance are also induced by the [Ti(Deferasirox)$_2$]$^{2-}$ complex. [Ti(Deferasirox)$_2$]$^{2-}$ is a non-redox active complex,[13] but in the presence of labile intracellular labile Fe(III), an active redox intermediate can be formed

[Fe(Deferasirox)(Citrate)]$^{4-}$.[13], Which can be responsible for activating apoptosis cascades by ROS increase.[27]

2.5 CONCLUSIONS

Cu(II) Deferasirox synthesis and characterization were achieved. Studies in the concentration-dependent species of this compound were done to understand the chemical behavior in different conditions. Several techniques such as mass spectrometry and EPR were used to determine the present species. Transmetalation experiments were conducted and analyzed to understand the speciation of Cu(II) Deferasirox in physiological conditions. Cell experiments were performed to evaluate the behavior of the compound in an intracellular environment regulated by the presence of labile sources of Fe and Cu. These two metals trigger the transmetalation process when they contact [Ti(Deferasirox)$_2$]$^{2-}$. These two processes activate the inhibition of different features in cancer survival. The Fe-transmetalation process will form a redox-active intermediate that increases the ROS production and generates an imbalance that leads to mitochondrial disruption and activates the apoptotic cascades and, ultimately, cell death. On the other side, Cu-induced transmetalation product Cu(II) Deferasirox is more cytotoxic than the initial compound, [Ti(Deferasirox)$_2$]$^{2-}$. Cu(II) Deferasirox results in a more biologically active specie intracellularly, and together by releasing Ti(IV), act in a synergistic action against cancer cells.

Fe and Cu bioavailability disruption disturb various biological processes that involve DNA synthesis and replication, angiogenesis, metastasis, and ending in cancer cell death. These cell death mechanisms are part of the multi-focused [Ti(Deferasirox)$_2$]$^{2-}$ intracellular mechanism of action. Additional studies have also shown the capability of [Ti(Deferasirox)$_2$]$^{2-}$ to have some antimicrobial activity, possibly affecting the metal homeostasis (**See appendix 7**).

2. 6 REFERENCES

1.   The "Accidental" Cure—Platinum-based Treatment for Cancer: The Discovery of Cisplatin. https://www.cancer.gov/research/progress/discovery/cisplatin.

2.   Zoroddu, M. A.; Aaseth, J.; Crisponi, G.; Medici, S.; Peana, M.; Nurchi, V. M., *J. Inorg. Biochem.* **2019,** *195*, 120-129.

3.   Lipinski, C. A., *Drug discovery today: Technologies* **2004,** *1* (4), 337-341.

4.   Hachey, A. C.; Havrylyuk, D.; Glazer, E. C., *Curr. Opin. Chem. Biol.* **2021,** *61*, 191-202.

5.   Fernández-Vega, L.; Ruiz Silva, V. A.; Domínguez-González, T. M.; Claudio-Betancourt, S.; Toro-Maldonado, R. E.; Capre Maso, L. C.; Sanabria Ortiz, K.; Pérez-Verdejo, J. A.; Román González, J.; Rosado-Fraticelli, G. T.; Pagán Meléndez, F.; Betancourt Santiago, F. M.; Rivera-Rivera, D. A.; Martínez Navarro, C.; Bruno Chardón, A. C.; Vera, A. O.; Tinoco, A. D., *Inorganics* **2020,** *8* (2), 10.

6.   Arredondo, M.; Núñez, M. T., *Mol. Asp. Med.* **2005,** *26* (4–5), 313-327.

7.   Vulpe, C. D.; Kuo, Y.-M.; Murphy, T. L.; Cowley, L.; Askwith, C.; Libina, N.; Gitschier, J.; Anderson, G. J., *Nat. Genet.* **1999,** *21* (2), 195-199.

8.   Chen, H.; Attieh, Z. K.; Syed, B. A.; Kuo, Y. M.; Stevens, V.; Fuqua, B. K.; Andersen, H. S.; Naylor, C. E.; Evans, R. W.; Gambling, L., *J. Nutr.* **2010,** *140* (10), 1728-1735.

9.   Mou, Y.; Wang, J.; Wu, J.; He, D.; Zhang, C.; Duan, C.; Li, B., *J. Hematol. Oncol.* **2019,** *12* (1), 34.

10.   Garrick, M. D.; Singleton, S. T.; Vargas, F.; Kuo, H.-C.; Zhao, L.; Knoppel, M.; Davidson, T.; Costa, M.; Prasad, P.; Roth, J. A.; Garrick, L. M., *Biol. Res.* **2006,** *39* (1), 79-85.

11.   Gaur, K.; Vázquez-Salgado, A. M.; Duran-Camacho, G.; Dominguez-Martinez, I.; Benjamín-Rivera, J. A.; Fernández-Vega, L.; Carmona Sarabia, L.; Cruz García, A.; Pérez-Deliz, F.; Méndez Román, J. A.; Vega-Cartagena, M.; Loza-Rosas, S. A.; Rodriguez Acevedo, X.; Tinoco, A. D., *Inorganics* **2018,** *6* (4), 126.

12.   Crisponi, G.; Nurchi, V. M.; Fanni, D.; Gerosa, C.; Nemolato, S.; Faa, G., *Coord. Chem. Rev.* **2010,** *254* (7–8), 876-889.

13.   Gaur, K.; Pérez Otero, S. C.; Benjamín-Rivera, J. A.; Rodríguez, I.; Loza-Rosas, S. A.; Vázquez Salgado, A. M.; Akam, E. A.; Hernández-Matias, L.; Sharma, R. K.; Alicea, N.; Kowaleff, M.; Washington, A. V.; Astashkin, A. V.; Tomat, E.; Tinoco, A. D., *JACS Au* **2021**.

14.   Loza-Rosas, S. A.; Vazquez, A. M.; Rivero, K. I.; L.J., N.; Delgado, Y.; Benjamin-Rivera, J. A.; Vazquez-Maldonado, A. L.; Parks, T. B.; Munet-Colon, C.; Tinoco, A. D., *Inorg. Chem.* **2017,** *56*, 7788-7802.

15.   *CrysAlis PRO, CrysAlis CCD, and CrysAlis RED*, Rigaku Oxford Diffraction: Oxfordshire, England, 2016.

16.   Sheldrick, G., Acta Crystallogr. *section c* **2015,** *71* (1), 3-8.

17.   Sheldrick, G., Acta Crystallogr. *section a* **2015,** *71* (1), 3-8.

18.   Dolomanov, O. V.; Bourhis, L. J.; Gildea, R. J.; Howard, J. A. K.; Puschmann, H., *J. Appl. Crystallogr.* **2009,** *42* (2), 339-341.

19.	Maurya, M. R.; Sarkar, B.; Avecilla, F.; Tariq, S.; Azam, A.; Correia, I., *ur. J. Inorg. Chem.* **2016,** (9), 1430-1441.

20.	Zandvakili, T.; Fatemi, S. J.; Ebrahimipour, S. Y.; Ebrahimnejad, H.; Castro, J.; Dusek, M.; Eigner, V., *J. Mol. Struct.* **2022,** *1249*, 131525.

21.	Steinhauser, S.; Heinz, U.; Bartholomä, M.; Weyhermüller, T.; Nick, H.; Hegetschweiler, K., *Eur. J. Inorg. Chem.* **2004,** *2004* (21), 4177-4192.

22.	Peisach, J.; Blumberg, W., *Arch. Biochem. Biophys.* **1974,** *165* (2), 691-708.

23.	Parks, T. B.; Cruz, Y. M.; Tinoco, A. D., *Inorg. Chem.* **2014,** *53* (3), 1743-1749.

24.	Blockhuys, S.; Wittung-Stafshede, P., *Biochem. Biophys. Res. Commun.* **2017,** *483* (1), 301-304.

25.	Brewer, G. J., *Curr. Cancer Drug Targets* **2005,** *5* (3), 195-202.

26.	Denoyer, D.; Pearson, H. B.; Clatworthy, S. A.; Smith, Z. M.; Francis, P. S.; Llanos, R. M.; Volitakis, I.; Phillips, W. A.; Meggyesy, P. M.; Masaldan, S., *Oncotarget* **2016,** *7* (24), 37064.

27.	Bonello, S.; Zähringer, C.; BelAiba, R. S.; Djordjevic, T.; Hess, J.; Michiels, C.; Kietzmann, T.; Görlach, A., *Arterioscler. Thromb. Vasc. Biol.* **2007,** *27* (4), 755-761.

Chapter 3

Evaluation of Drug Delivery Systems (DDS) as a mechanism to improve the specificity of Ti(IV) delivery to cancer cells

Over the years, cancer treatments have not changed much. Radiotherapy, chemotherapy, and surgery are still the most used treatments today. These treatments are often aggressive, with remarkable side effects and a decrease in the patient's quality of life.[1-5] Chemotherapy treatments are being improved, and new drugs are being developed to minimize the side effect and improve the drugs' outcomes.[1-5] Drug delivery systems (DDS) represent an alternative to current chemotherapy agents that show toxicity effects in patients.[6-8]

DDS are engineered to improve the delivery and specificity of drugs and are presented in various materials, structures, and functionalities. The most common are dendrimers, carbon nanotubes, micelles, liposomes, metallic nanoparticles, layered materials, and polymeric nanoparticles.[9] Nature also offers other DDSs platforms, such as proteins, peptides, and antibodies, which give advantages because of their biocompatibility. DDS are designed to control the therapeutic agent's release, allowing it to act longer and decrease side effects.[9]

Zirconium phosphate (ZrP) is a layered material that allows the intercalation of neutral and positively charged molecules and ions. ZrP does not represent any harm to the human body as it is a biocompatible material. This material has shown stability under physiological conditions. Once it reaches the more acidic environment in cancer cells, liposomes, or peroxisomes, it releases the cargo.[7, 10] Under the extreme acidic conditions such as in liposomes and peroxisomes, ZrP will dissociate in phosphate ions and a non-toxic Zr salt. The pH-dependant cargo release feature of ZrP gives this material the requirements to be used as a DDS for anticancer treatments.[7, 10-11] Compared to ZrP, proteins and peptides are also used as DDS. Serum albumin, a human protein, is used as a nanocarrier to protect the cargo, especially from ozonolysis. Peptides, proteins building blocks, are often used as an easier DDS due to their easier way to synthesize and purify.[8]

Recent in vivo studies have shown low Ti(IV) tumor accumulation.[12] Ti(IV)-based complexes have shown aqueous stability limitations, leading to failure to deliver Ti(IV) efficiently to cancer cells. Either because of the formation of TiO_2 precipitate or compounds can interact with healthy tissue, leading to an absence of activity or toxicity effects, respectively.[13-15] Another limitation of these compounds lies in the lack of knowledge about the intracellular mechanism of Ti(IV). In chapter 2, new cell death pathways were explored, expanding the understanding of how Ti(IV) compounds work. This chapter was developed in collaboration with Dra. Bárbara Casañas alumni from Dr. Colón's lab from the Department of Chemistry at UPR-RP. This work aimed to increase the Ti(IV) delivered to cells implementing different DDSs and compare the specificity of each of them. The bioconjugated

compound HAIYPRHK (P7) conjugated to $[Ti(Deferasirox)_2]^{2-}$ complex has been submitted for a provisional patent (**see appendix 6**).

3. 1 Materials and methods

3.1.1 Materials

Titanocene dichloride (Cp_2TiCl_2), DMSO, and zirconyl chloride octahydrate ($ZrOCl_2 \cdot 8H_2O$, 98%) were obtained from Sigma Aldrich. Acetonitrile and phosphoric acid (H_3PO_4, 85% v/v) were obtained from Fisher Scientific. Bovine serum albumin (BSA) was obtained from Amresco. Bradford assay reagent was purchased from VWR technologies. Deuterated NMR solvents were 99.9% D purity grade and were purchased from Cambridge isotope laboratories (CIL) or Sigma. All aqueous solutions were prepared with autoclaved (121°C and 18 PSI) nanopure-quality water (18.2 MΩ·cm resistivity; model Thermo scientific Easypure Rodi; Barnstead). Aminoacids were obtained from the Calbiochem brand by Sigma. All other reagents were standard and purchased commercially. Unless otherwise specified, all of the reagents were used as received without further purification. All solutions were prepared using nanopure water.

3.1.2 Instruments

All UV-Vis analyses were performed using NanoDrop 2000 (Thermo Scientific) and UV-2501PC (Shimadzu). ^1H NMR spectra were obtained on Bruker 500 MHz Fourier transform NMR spectrometer at the University of Puerto Rico NMR facility with the residual proton resonances of the deuterated solvents serving as internal references. Data were analyzed using the Origin software V7.083 (Origin Lab Corporation, Northampton, MA). Dynamic light scattering (DLS) experiments were performed at 25 °C using a Wyatt Dynapro Titan instrument (Wyatt Technology Corporation, Santa Barbara, CA). X-ray powder diffraction (XRPD) experiments were performed from 2 to 40° (in the 2θ axis) using a Rigaku Smart Lab X-ray diffractometer with Cu K_α radiation (λ = 1.5406 Å) with a filtered flat LiF secondary beam monochromator. Bragg's law ($n\lambda = 2d_{hkl} \sin \theta$) was used for the determination of the interlayer distance in the ZrP layers from the first-order diffraction peak, where λ is the wavelength of the X-ray source, d_{hkl} is the interlaminar distance between planes in the unit cell, and θ is the diffraction angle. X-ray photoelectron spectroscopy was carried out with a Physical electronics PHI 5600 ESCA system, with an X-ray of Mg polychromatic-400 W and pass energy 93 900 eV. The binding energy has been calibrated by taking the carbon 1s peak (284.6 eV) as reference. Vibrational spectroscopy data was obtained using a Bruker-Tensor 27 FT-IR spectrometer with the OPUS Data Collection Program for analysis.

Qualitative elemental analysis by energy-dispersive X-ray spectroscopy (EDS) using a JEOL 6480LV scanning electron microscope (SEM) with low vacuum and X-ray fluorescence (EDAX) capabilities was performed at the Materials Characterization Center (MCC). The average nanoparticle sizes of $Cp_2TiCl_2@ZrP$ and ZrP were determined by dynamic light scattering using a Zeta sizer model: nano ZS Malvern Instrument at Dr. Eduardo Nicolau's laboratory at the Molecular

Sciences Research Center. The Cp$_2$TiCl$_2$@ZrP sample was dispersed in water using 0.1% Triton X-100 as a micelle. Peptide synthesis and conjugation were performed in a Liberty blue (LB2081) coupled with a CEM microwave to control the reaction temperature. Mass spectra were collected on a MALDI TOF/TOF AB SCIEX 4800 Analyzer. Peptide purification was performed either in an Agilent Technologies HPLC or a Sykam HPLC. Multiwell plate absorbance was measured in a Tecan Infinite M200 PRO plate reader. Cells were grown in a Revco Elite III RCO5000T-5-ABC incubator. Cell counting and culture viability monitoring were performed using a Nikon Eclipse TS-100 microscope. ICP-OES data was collected in an Optima 8000 (Perkin-Elmer).

3.1.3 Methods
3.1.3.1   Preparation of Bovine Serum Albumin (BSA) solutions.

All the solutions in this study were prepared using a previously prepared HEPES buffer (pH 7.4). BSA was dissolved in the buffer and dialyzed using Spectra/Por dialysis tubing or Amicon Centriprep centrifugal filters (10 kDa molecular mass cut-off). A Cp$_2$TiCl$_2$ stock solution was freshly prepared in DMSO and used immediately.

3.1.3.2   Ti(IV) bound BSA solution stability studies using colorimetric techniques

Cp$_2$TiCl$_2$ stock solution in DMSO (40 mM) was added to the BSA solution (100 µM) to a final concentration of Cp$_2$TiCl$_2$ to be 2 mM (DMSO was kept below 5%). Then the BSA samples were incubated at 37 °C for 148 h. The solution's Ti(IV) concentration was measured calorimetrically by chelation with 2,3-dihydroxynaphthalene-6-sulfonate and using a standard addition method.[16-17] Ti(IV) concentration was determined using the solution absorbances at 370 nm (ε = 40,000 M^{-1}cm^{-1}).[18] To maintain consistency and observe how many equivalents of Cp$_2$TiCl$_2$ were being stabilized by the BSA, all the reactions were performed at constant BSA concentration (100 µM). Cp$_2$TiCl$_2$ concentration was increased up to 20 equivalents (200 µM). Experiments were conducted with four replicates (n=4).

3.1.3.3   Characterizing BSA-Cp$_2$TiCl$_2$ compound properties through Dynamic Light Scattering (DLS)

The hydrodynamic radius of BSA and the impact of adding two different molar excess (10 and 20) of Cp$_2$TiCl$_2$ on BSA size was determined by dynamic light scattering using a DynaProTitan instrument (Wyatt Technology, CA). A 20µM BSA solution in buffer was used for these experiments. Before the measurements, all the BSA samples were centrifuged at 15,000 g for 5 min.

3.1.3.4   Protein Digestion experiment

A549 cells were seeded in a 225 cm^3 culture flask and grown in a 5% CO$_2$ humidified atmosphere. At least three passages were done to ensure the integrity of the cells. When cells reached the 95% confluence, cells were washed with 1X PBS and detached with trypsin. Cells were carefully pelleted by centrifuging at

2,000 rpm for 5 min at 25°C. The supernatant was discarded, and the cells were washed twice with HEPES buffer followed by two cycles of centrifugation. Finally, the cell pellet was re-suspended in HEPES buffer. The pellet was lysed using a glass-on-glass Dounce homogenizer with a fitted pestle and homogenized for 5 minutes. To remove the cell membrane, the mixture was centrifuged at 6,000 rpm for 10 min at 10 °C, and the supernatant that contained protein fraction was carefully collected. Protein concentration was determined with a Bradford assay. Cell extracted protein was added to the samples to have albumin concentration from 10 to 100 µM and 2000 µM Cp_2TiCl_2 (1:20) in 500 µL HEPES buffer and incubated at 37 °C for 48h.

3.1.3.5   Synthesis of θ–ZrP

A 0.05 M $ZrOCl_2 \cdot 8H_2O$ aqueous solution (120 mL) was added dropwise to a preheated 6 M H_3PO_4 solution (85 mL) at 94 °C with constant stirring. The resulting solution was stirred at 94 °C for 48 hours. The solid formed in the reaction was collected by filtration and washed thoroughly with nanopure water. Using Bragg's law, the wet solid, characterized by XRPD, showed an intense peak at low angles (2θ = 8.6°) corresponding to an interlayer distance of 10.3 Å for this phase.

3.1.3.6   Intercalation of Cp_2TiCl_2 into ZrP

Before starting the intercalation, the θ-phase was quickly filtered and placed in the reaction solvent while still wet. A similar amount of the solid was dried at 75 ºC for 24 h to determine the weight and adjust the Cp_2TiCl_2: ZrP ratio. The intercalation reaction was performed by suspending θ–ZrP into a Cp_2TiCl_2 solution in acetonitrile at a 0.5:1 (Cp_2TiCl_2: ZrP) concentration ratio. The suspension was stirred constantly at room temperature for 5 days. The reaction mixture was filtered using 0.22 µm filters (Millipore), washed with acetonitrile, and the solid dried overnight at room temperature. An X-Ray powder diffraction (XRPD) analysis was performed to determine if the intercalation occurred. X-ray powder diffraction (XRPD) measurements were performed from 2 to 40˚ (in the 2θ axis). The concentration of the Cp_2TiCl_2 in the solution was calculated by UV-Vis absorption. Measurements were taken before and after the intercalation reaction. By difference, the loading % inside the layers of ZrP was calculated.

$$Loading\ Efficiency\ \% = (1 - [final]/[initial]) \times 100$$

The absorbance was recorded at 254 nm for Cp_2TiCl_2 in acetonitrile. A calibration curve was made for Cp_2TiCl_2, and with the obtained line equation, the concentration was calculated. Each experiment was repeated twice, leading to similar results. The average loading of Cp_2TiCl_2@ZrP is 29% ± 11.

3.1.3.7   Determining cell metal uptake in the presence of Ti(IV) bound delivery vehicles

Cp_2TiCl_2 samples (100 µM), ZrP, and formulate (Cp_2TiCl_2@ZrP) were prepared in HEPES buffer. A549 and MRC5 cells were cultured as previously described for A549 cells. After 24 h incubation, cells were treated and continued incubation for

another 3 h. Cell media was removed, washed twice with PBS, and then detached the cells with trypsin. The mixture was then transferred into 15 mL Falcon tubes. The cells were carefully pelleted by centrifuging at 2,000 rpm for 5 min at 25°C. The supernatant was discarded, and the cells were washed twice with 1X PBS followed by two cycles of centrifugation. Cells were finally re-suspended in 500 µL of 1X PBS. 50 µL of the suspended cells were used for cell counting using trypan blue. The cells were lysed with 6.5% HNO_3 (50 µL) and stored at -80 °C.

3.1.3.8 Determination of Ti(IV) uptake concentration by ICP-OES

Ti(IV) and Zr standards were prepared together from 100-500 ppb in 2% HNO_3. Based on the expected Ti(IV) concentration in cells, 200 µL of the cell lysates were diluted to a final volume of 5 mL in 2% HNO_3. Samples were analyzed for Ti at 334.940 nm and Zr at 343.823. All the samples were tested two times independently with three replicates for each, and the mean value was recorded. Data were processed with the WinLab32 software version 5.4 (Perkin-Elmer).

3.1.3.9 Determining cell viability in the presence of Ti(IV) bound delivery vehicles

A cell viability assay was performed using the MTS reagent [[3-(4,5-dimethylthiazol-2-yl)-5-(3-carboxymethoxyphenyl)-2-(4-sulfophenyl)-2H-tetrazolium, CellTiter 96® AQueous] (Promega Corp., Madison, WI). Cells were seeded in 96-well plates (100 µL) at 5×10^4 cells/well and cultivated as previously described. At 24 h after seeding, the media was replaced with FBS-free DMEM and incubated again for 3 h. Cells were treated with 100 µL of 100 µM compounds (dissolved in 20 mM HEPES buffer, DMSO less than 2%). Controls were treated with the background solution. Cells were incubated for another 24h, and 20 µL of MTS reagent was added. The plates were incubated for another 1h, and the absorbance was measured at 490 nm. MTS assay was repeated 3 times with an n=6, and mean values were recorded.

3.1.3.10 Peptide conjugate synthesis

The peptide conjugated ligands, Deferasirox-P7 (DP7) and Deferasirox-Substance P (DSP), were synthesized by attaching the peptides with Deferasirox. For DSP, the Deferasirox ligand was attached at the end of the peptide chain next to arginine. The approach to couple deferasirox to HAIYPRH transferrin receptor peptide was to add a lysine residue with an unprotected side chain at the end of each sequence, making the final sequence HAIYPRHK (P7). The uncapped side-chain allowed us to couple the carboxylic moiety of deferasirox to the amine group of lysine, forming DP7. Following the solid phase peptide synthesis strategy: 1-[Bis(dimethylamino)methylene]-1H-1,2,3-triazolo[4,5-b]pyridinium-3-oxid-hexafluoro-phosphate (HATU) was used as carboxylic acid terminus activator and N,N-diisopropyletylamine (DIPEA) as FMOC group remover. The products were cleaved from the resin by incubating the resin-product mixture with a cleavage cocktail consisting of 95% trifluoroacetic acid (TFA), 2.5% water, and 2.5% triisopropylsilane (TIPS) for 30 minutes. The resulting mixture was filtered and cleaned with TFA, and the supernatant was collected. Coldwater was used to

precipitate the product. Solid was obtained by centrifugation and lyophilized to remove the solvent. Mass spectrum obtained for the DP7 and DSP conjugates by MALDI TOF/TOF (positive ion mode) were $C_{68}H_{87}N_{20}O_{12} + H^+$, m/z = 1377.57 and $C_{42}H_{24}N_6O_8 + H^+$, m/z = 1703.82, respectively. Reverse-phase HPLC was used for purification of the crude (C_{18} column, ACN + 0.1 % TFA / water + 0.1 % TFA). The Ti(IV)-bioconjugated complexes were prepared by adding 1 equivalent of metal dissolved in DMF to 2 equivalent of the peptide-conjugated ligand. Charaterization of the $[Ti(Deferasirox)_2]^{2-}$ (TD)-P7 and, TDSP were performed by MALDI TOF/TOF (positive ion mode) were $C_{68}H_{89}N_{20}O_{15}Ti + H^+$, m/z = 1474.45 and $C_{168}H_{218}N_{42}O_{32}S_2Ti + H^+$, m/z = 1703.82, respectively. UV–vis (PBS, DMF 1%): λ_{max} 264 nm, ε = 22,767 M^{-1} cm^{-1}, λ_{max} 314 nm, ε = 17,933 M^{-1} cm^{-1}, λ_{max} = 373 nm, ε = 11,005 $M^{-1}cm^{-1}$.

3.1.3.11 Cell viability of the bioconjugate at low micromolar concentrations

To evaluate the biological activity of the peptide conjugated compounds at low concentrations, A549 ($1x10^5$ cells/well) and MRC5 ($1x10^5$ cells/well) cell lines were treated with 1 and 5 µM of the peptide conjugate compounds in 96-well plates. The experiment was run for 72 h, cells were cultured and incubated as previously described, and an MTT (3-(4,5-dimethylthiazol-2-yl)-2,5-diphenyltetrazolium bromide) assay was used to measure the viable cells after treatment.

3.1.3.12 Iron supplementation experiment

Iron supplementation was performed to observe the impact of Fe(III) in the behavior of our conjugated ligand and conjugated Ti(IV) complex. Compounds were prepared to be at the final concentration of 40 µM. Iron citrate $[Fe(Citrate)_2]^{5-}$ was prepared at 10X the desired concentration (1000 µM), and 10 µL were added to previously seeded 90 µL of cells at $1x10^5$ cell/mL/well. Then, compounds were prepared at twice the desired concentration, and 100 µL was added. Cells were incubated in the previously described conditions. The experiment was run for 72 h.

3.1.3.13 Peptide-conjugate metal uptake experiment

A549 and MRC5 cell lines were cultured as previously described. Cells were grown in 125 cm^2 flasks and suspended in cell media. The cell solution was distributed in 25 (100 mm x 20 mm) Petri dishes and incubated for 24 h for each cell line. Stock solutions ($[Ti(Deferasirox)_2]^{2-}$ (TD), TDP7, and TDSP) were prepared at 2 µM in 1X PBS (2 % DMF). Solutions were prepared to be 50:50 PBS: DMEM to reach the final concentration for the treatment. 10 mL of the stock solutions were added to each plate (n=4). The cell control plate was established as 1X PBS (2 % DMF) and mixed 50:50 with cell media. All the samples and controls were incubated for 3h at 37 °C, 5% CO_2 in a humidified atmosphere. After 3h treatment, cell media was removed from the plates and treated with HNO_3 (142 µL) and 30 % TCA (60 µL) and heated for 1 h at 70 °C, sonicated, and

centrifugated. The supernatant was separated into new falcon tubes, and solutions were brought to volume (5 mL) to measure the amount of Ti(IV) in an ICP OES instrument (OPTIMA 8000).

3. 2   RESULTS AND DISCUSSIONS
3.2.1   BSA as DDS stabilize the Ti(IV) metal ion

Ti(IV)-based compounds are aqueous unstable. Ti(IV) is a hard acid and, in contact with water, goes rapidly under hydrolysis and subsequent precipitacion.[19] BSA is proposed to bind and stabilize the metal ion.[20] To observe how many Ti(IV) equivalents can be stabilized by BSA, Cp_2TiCl_2 was incubated with BSA (100 µM) at 37 °C. After 48 h, the Ti(IV) concentration stabilized, reached the maximum, and slightly decreased after this time. However, even after 148 h, approximately 80 % of the initial concentration of Cp_2TiCl_2 was still stabilized (**Fig 3.1 A**). The reaction was performed at a different concentration from 200-2000 µM, obtaining the same result. For the control experiments in the absence of BSA, the precipitate was observed after 1h and increase until 24 h. As a result Ti(IV) concentration in solution was decreased (**Fig 3.1 B**). This results indicate the ability of BSA to stabilize the Ti(IV) metal ion and possibly delivering more to the cells.
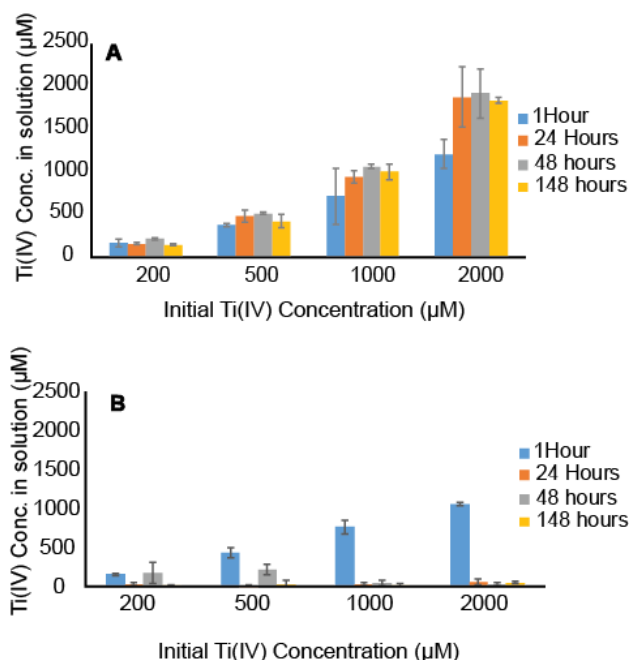
Fig 3.1. Ti(IV) concentration in solution was measured colorimetrically as a function of time for the samples after Cp_2TiCl_2 was dissolved in HEPES buffer in the presence **(A)** and absence **(B)** of BSA and incubated at 37 °C.

Metal-based chemotherapeutics can be affected by the high content of HSA in blood, decreasing its specificity. Understanding the ability of metal complexes to bind to HSA and its role in transport and distribution becomes crucial in developing new chemotherapeutics.[21] Recently, other perspectives using HSA as a drug carrier instead of combating its effects have been increasing.[22-25]

HSA (20 µM) was treated with 0.4, 2, and 4 µM of lysate to observe the influence of the intracellular environment on Ti(IV) liberation. Samples were incubated for 22 h, and a decrease in Ti(IV) concentration was observed proportional to the lysate concentration added. Almost 30 % of the relative Ti(IV) concentration was decreased (**Fig 3.2**). Some precipitation was observed during the experiment, and a gel electrophoresis experiment (SDS-PAGE gel) was performed to understand if the protein was fragmented. No precipitation was observed in control samples. Results show that HSA fragments are formed when the protein is in contact with the cell lysate (Fig 3.3). Ti(IV) concentration decrease can mean the formation of TiO_2 after the metal is liberated from the protein. Other bands in the gel could be attributed to the proteins from the cell lysate. These results show the capability of HSA to stabilize Ti(IV) in an aqueous solution but still, when the metal reaches the intracellular environment; precipitation can still occur.
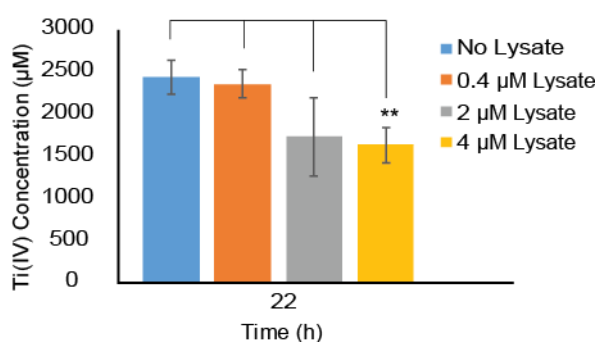
Figure 3.2. Ti(IV) concentration was measured using a UV-Vis spectrophotometer as a function of time. Cp_2TiCl_2 was dissolved in HEPES buffer in the presence of 20 µM BSA with different lysate concentrations and incubated at 37 °C for 22 hours. Student's t-test, **, p-value <0.01.
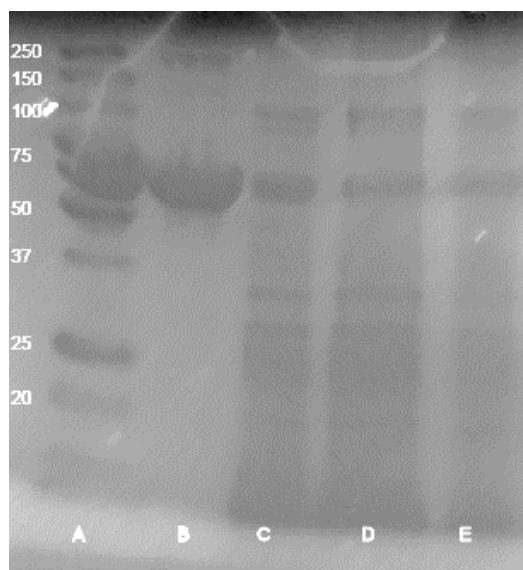
Figure 3.3. Precipitates were collected after incubation of Cp_2TiCl_2-BSA in the presence of lysis at 37 °C and were eluted on an SDS-PAGE gel. **(A)** Bio-Rad Precision Plus All Blue protein marker; **(B)** Reaction solution of BSA with 20

equivalents of Cp_2TiCl_2 alone; **(C)** Solid collected from lysis reaction after 24 h incubation of BSA with Cp_2TiCl_2 in the presence of lysis protein collected from A549 cells; **(D)** The solid obtained from the lysis reaction was washed with a copious amount of water; **(E)** The water obtained from the wash of the solid obtained from lysis reaction was evaporated.

3.2.2 The θ-ZrP phase interlayer material can intercalate Cp_2TiCl_2

The θ-ZrP phase was synthesized by the protocol previously described. The 002-pane reflection of ZrP corresponding to the interlayer distance confirms the obtention of the θ-ZrP (**Fig 3.4**) with an interlayer distance of 10.3 Å. When the solid was completely dried, the obtention of the α-ZrP phase was achieved with an interlayer distance of 7.6 Å. For intercalation purposes, the θ-ZrP phase will be used due to the broader interlayer distance.

The direct intercalation of Cp_2TiCl_2 was achieved by the batch method, where Cp_2TiCl_2 was added to a suspension of θ-ZrP at a Cp_2TiCl_2: ZrP loading level of 0.5:1, using acetonitrile as solvent. After the intercalation reaction was stopped, the resulting solid was filtered, washed with acetonitrile, dried, and pulverized before XRPD analysis. The XRPD patterns for Cp_2TiCl_2 intercalated in ZrP (Cp_2TiCl_2@ZrP) (**Fig 3.5**) confirmed successful intercalation. The ZrP solid produced a pure expanded phase evidenced by the diffraction peak observed at 11.0 Å and the absence of the 7.6 Å peak of α-ZrP. In addition, the diffraction patterns show that the Cp_2TiCl_2@ZrP crystallinity is low. Broad diffraction peaks of low intensities, characteristic of a heterogeneous distribution of the intercalated species within the system creating disorder, were obtained.

Furthermore, as a consequence of the low crystallinity, the diffraction peaks for the (020) and (31-2) reflections at 33.8° and 34.2° (2θ) generated confirmed that the ZrP layers remained intact.
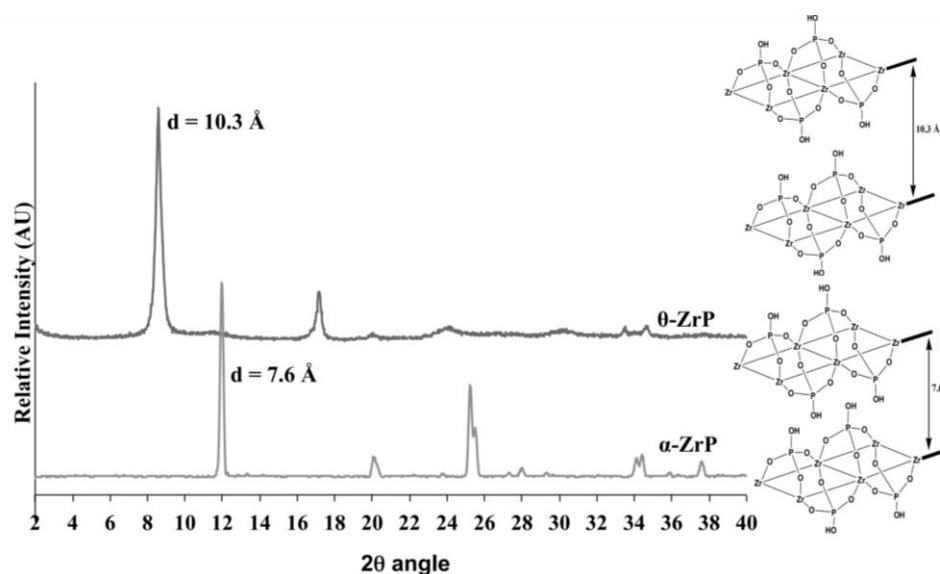
Figure 3.4. XRPD patterns of α-ZrP and θ-ZrP phases.

53
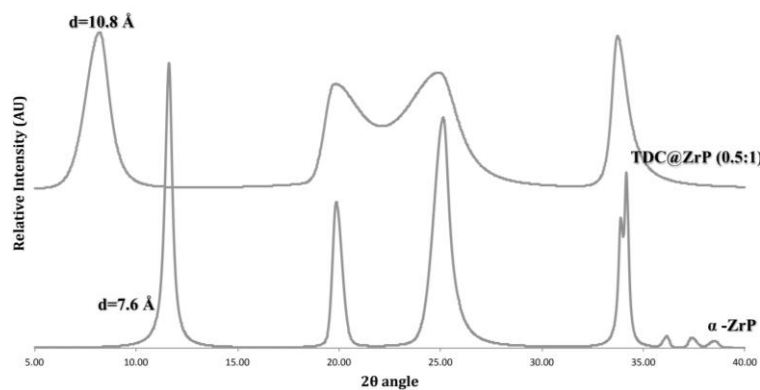
Figure 3.5. XRPD patterns of $Cp_2TiCl_2@ZrP$ intercalation procedure.

EDX spectrum for the optimized $Cp_2TiCl_2@ZrP$ intercalated product shows the characteristic peaks that indicate the presence of Ti, Zr, P, O, and C, but no Cl peak is observed (**Fig 3.6**). The absence of the chloride peak in the EDX spectrum confirms the substitution of the chloride ligands in the intercalated material.
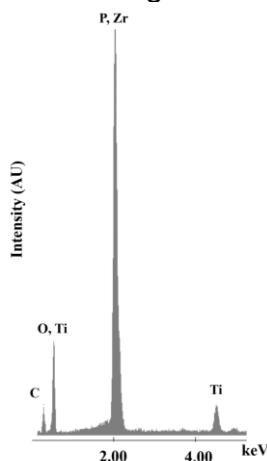
Figure 3.6. SEM-EDX spectrum of the $Cp_2TiCl_2@ZrP$ intercalation product.

DLS measurements were performed to obtain the surface charge and average diameter of $Cp_2TiCl_2@ZrP$ nanoparticles. To decrease the aggregation in the intercalated product of Cp_2TiCl_2, Triton 10x was added to the suspension to a 0.1 % concentration. The size of ZrP appeared to have a diameter of 237.8 ± 2.1 nm (**Fig 3.7**). For $Cp_2TiCl_2@ZrP$ particles using Triton X-100, the diameter size appeared to be around 289.3 ± 15.3 nm (**Fig 3.7**). The additional peak at 7.5 nm in the $Cp_2TiCl_2@ZrP$ sample is the characteristic average diameter for the Triton X-100 micelle.
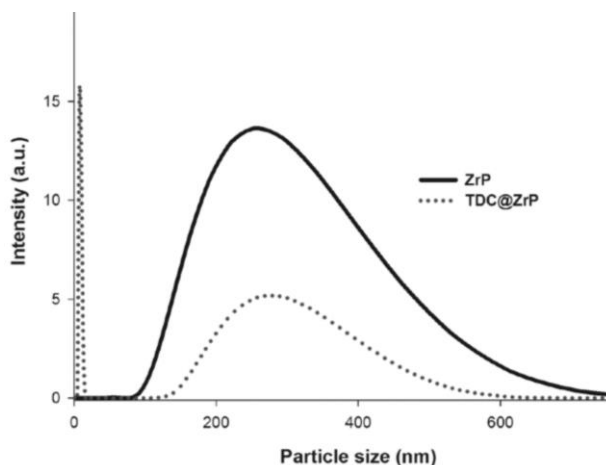
Figure 3.7. Particle size distribution of ZrP and *Cp$_2$TiCl$_2$*@ZrP.

The IR spectrum of the Cp$_2$TiCl$_2$@ZrP material should be comparable to the signals obtained for the spectra of the ZrP and Cp$_2$TiCl$_2$ together. But if Cp$_2$TiCl$_2$ or ZrP suffer any chemical change after intercalation, the bands could be displaced, change, or disappear. The IR spectrum of the Cp$_2$TiCl$_2$@ZrP sample (**Fig 3.8**) shows a decrease in intensity of the ZrP lattice water bands (from water molecules in the crystal lattice) that appear in the 3580-3200 cm^{-1} and 1630-1600 cm^{-1} regions in the unintercalated ZrP IR spectrum. A decrease in the intensity of the lattice water vibrational bands is characteristic of intercalated materials, resulting here from the displacement of interlayer water by the metallocene derivative upon intercalation. Two peaks corresponding to the metallocene Cp rings (at 1440 cm^{-1} for the vC=C bands and 820 cm^{-1} characteristics of the vibrational band of the C-H bond in the Cp rings) are observed in the spectrum of the pure Cp$_2$TiCl$_2$ compound are also observed in the Cp$_2$TiCl$_2$@ZrP IR spectrum. The IR results strongly suggest that the intercalation of the Cp$_2$TiCl$_2$ was successfully achieved without any significant chemical change of the Cp rings in the intercalated molecules.
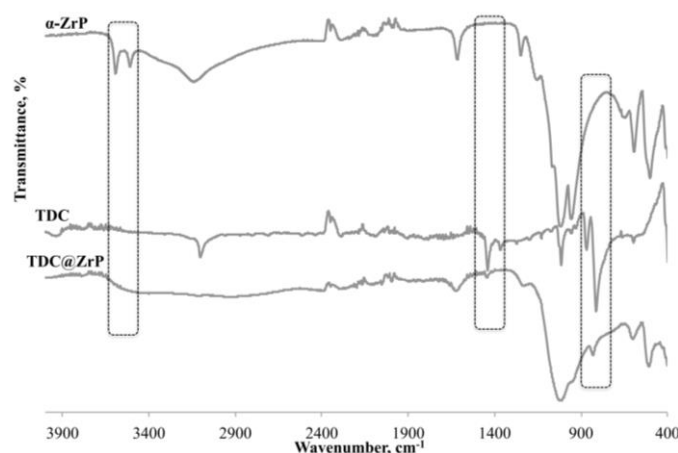
Figure 3.8. FT-IR spectra of ZrP, Cp$_2$TiCl$_2$, and Cp$_2$TiCl$_2$@ZrP. The rectangles highlight the ZrP lattice water bands at 3580-3200 cm^{-1} and the metallocene Cp rings bands at 1440, 1370, and 820 cm^{-1} regions.

3.2.3 Transferrin receptor peptides to deliver Ti(IV) to cancer cells

The peptide conjugated ligands DP7 and DSP were synthesized (**Fig 3.9**) and their in situ Ti(IV) complex. A mass spectrum obtained confirmed the presence of the compounds by comparing them with the expected theoretical isotopic distribution (**Fig 3.10**). The peptide synthesis was performed in a resin (rink amide) by the solid phase peptide synthesis (SPPS) technique which allows to attach each aminoacid and perform washes to avoid the majority of side products. By this method, purification is straightforward and reaches high synthesis yields. Peptides were attached to a ligand, Deferasirox, an FDA-approved iron chelator that has been proven to bind and stabilize the Ti(IV) ion in aqueous environments.[26] Conjugation with transferrin receptor peptides will improve the uptake of the compound by cancer cells, taking advantage of the peptides to a specific receptor that is overexpressed in cancer cells.[27-29]
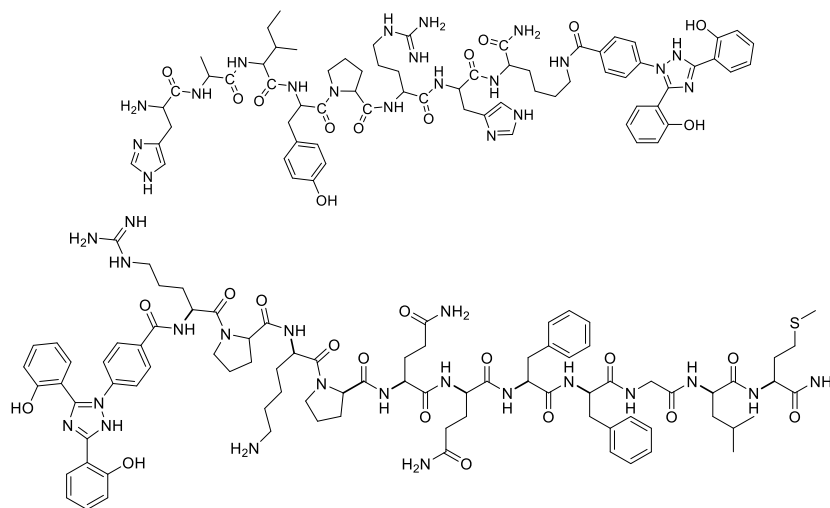
Figure 3.9. DP7 chemical structure (up) and DSP chemical structure (down).

Deferasirox ligand can mimick the tranferrin protein binding site, which gives this ligand the ability to bind Fe and Ti, metals with similar chemical characteristics.[30-32] UV-vis data confirmed the Ti(IV) coordination by the obtained of extinction coefficient similar to the TD complex[26] to the ones obtained for the bioconjugates λ_{max} 264 nm, $\varepsilon = 22,767$ M^{-1} cm^{-1}, λ_{max} 314 nm, $\varepsilon = 17,933$ M^{-1} cm^{-1}, $\lambda_{max} = 373$ nm, $\varepsilon = 11,005$ $M^{-1}cm^{-1}$.
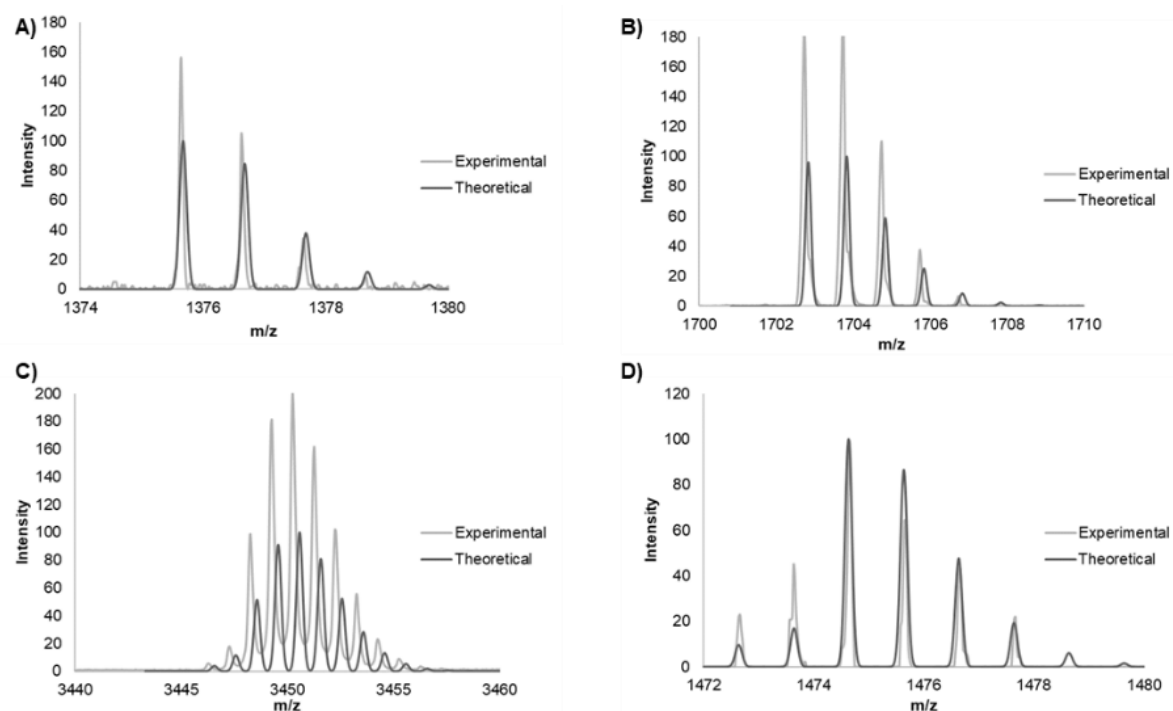
Figure 3.10. MALDI TOF spectrum of the peptide conjugated ligands and its Ti(IV) complexes. **(A)** DP7, **(B)** DSP, **(C)** TDSP, **(D)** TDP7.

Reverse-phase HPLC was used for purification of the peptide conjugated ligands (**Fig 3.11**) (C_{18} column, ACN + 0.1 % TFA / water + 0.1 % TFA). DP7 compound was found at the retention time of 11.32 min, and DSP was found at 46.5 min (**Fig 3.11**). After purification, both ligands were to a > 98% purity.
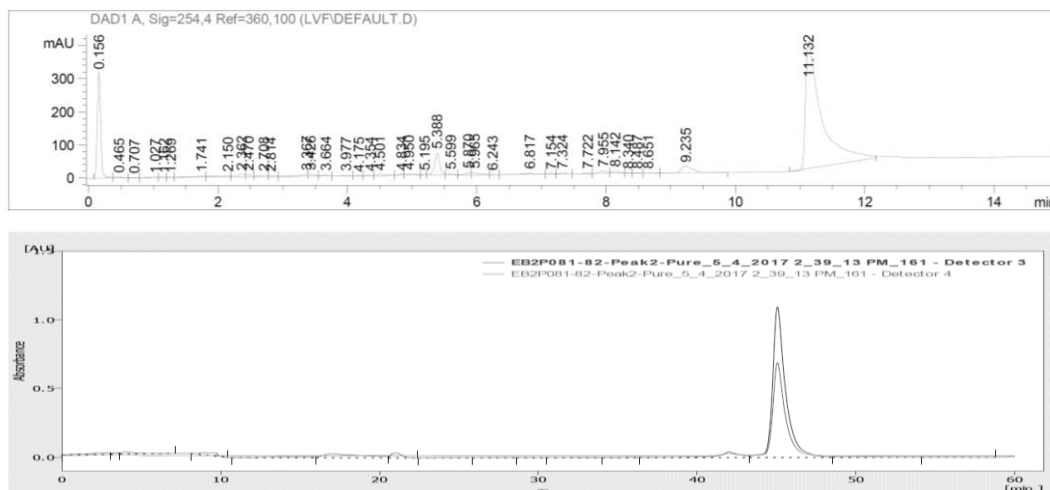
Figure 3.11. Chromatogram of purification of Def-P7 (Up). Chromatogram of the purification of Def-SP (Down).

In situ Ti(IV) coordination with a labile Ti source (TiCl$_4$ dissolved in DMF) was performed, taking advantage of the previously proved TD coordination affinity.[26]
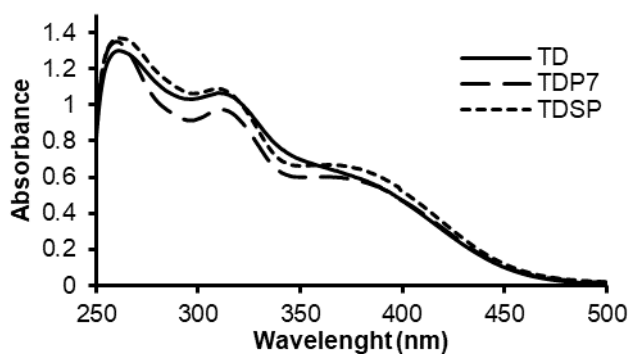
Figure 3.12. UV-Vis spectrum of the TD complex and the peptide conjugated Ti(IV) complexes.

3.2.4 Ti(IV) intracellular accumulation does not mean more anticancer specificity

Cellular uptake studies for Cp$_2$TiCl$_2$-BSA, Cp$_2$TiCl$_2$ formulated with ZrP nanoparticles (Cp$_2$TiCl$_2$@ZrP), and the bioconjugated compounds were performed in both MRC5 and A549 cell lines. Data suggest that more Ti(IV) entered into the cells by the bioconjugates compounds than by the formulated Cp$_2$TiCl$_2$@ZrP and the BSA samples (**Fig 3.13**). Almost 100-fold Ti(IV) uptake was observed comparing the BSA- Cp$_2$TiCl$_2$ sample and Cp$_2$TiCl$_2$@ZrP formulate. The amount of Ti(IV) uptake by the cells treated with the conjugates was 500-fold the amount uptake by the formulated Cp$_2$TiCl$_2$@ZrP for A549 cells. Interestingly, the Ti(IV) concentration in MRC5 was much lower, around 5-fold times the concentration in A549 cells, indicating a relative selectivity expected by the overexpression of transferrin receptor in A549 cells than in non-cancer cells such as MRC5 (**Fig 3.13 C**).[33-34]

For the control samples, for which the cells were just treated with ZrP only, there was more Zr observed in non-cancer cells (**Fig 3.13 B**). When the formulate is compared, the Zr uptake was higher, reflected in the amount of Ti uptake by the same samples (**Fig 3.13 A**). ZrP was uptake by the cells containing the Cp_2TiCl_2 in the interlayer space, which means that Ti(IV) was successfully delivered intracellularly.

Previous studies have proven that BSA stabilizes ti (IV) in solution, but low uptake was observed in the presence of 10 % FBS media containing.[35] In our studies, no significant increase of intracellular Ti(IV) was observed in the presence and absence of BSA. Even the stabilized metal ion did not reach the intracellular environment intact. Previously described protein digestion studies showed that a precipitate is observed in contact with the intracellular content. This effect could be affecting the Ti(IV) delivery due to interactions of the BSA- Cp_2TiCl_2 sample with cellular media that also include a mixture of proteins. This result was similar to what was observed for titanocene Y, with minimal uptake in the presence of serum compared to the serum-free media in HT-29 cells.[36]

Thermal denaturation is one of the characteristic properties of a protein. To understand what are the factors affecting Ti(IV) uptake in the presence of BSA, the differential scanning calorimetric (DSC) technique was used to know the stability of the Ti(IV) bound BSA. Thermal denaturation of a 1.3 mg/mL (20 µM) BSA solution in HEPES buffer, pH at 7.4, was measured at a scan rate of 60 °C/h. The thermal denaturation of native BSA was observed at 59.8 ± 0.5 °C (**Fig 3.14**), which is consistent with the reported data in sodium phosphate buffer.[37] However, the addition of different Ti(IV) concentrations did not significantly influence the temperature of the transition maximum (*T*m). With increasing Ti(IV) concentration in the protein solution, for example, when 20 equivalents of Cp_2TiCl_2 were added, the thermal transitions become narrower. A stabilization effect of Ti(IV) ions can be considered as such behavior was observed for Zn(II) ions in an aqueous solution.[38]
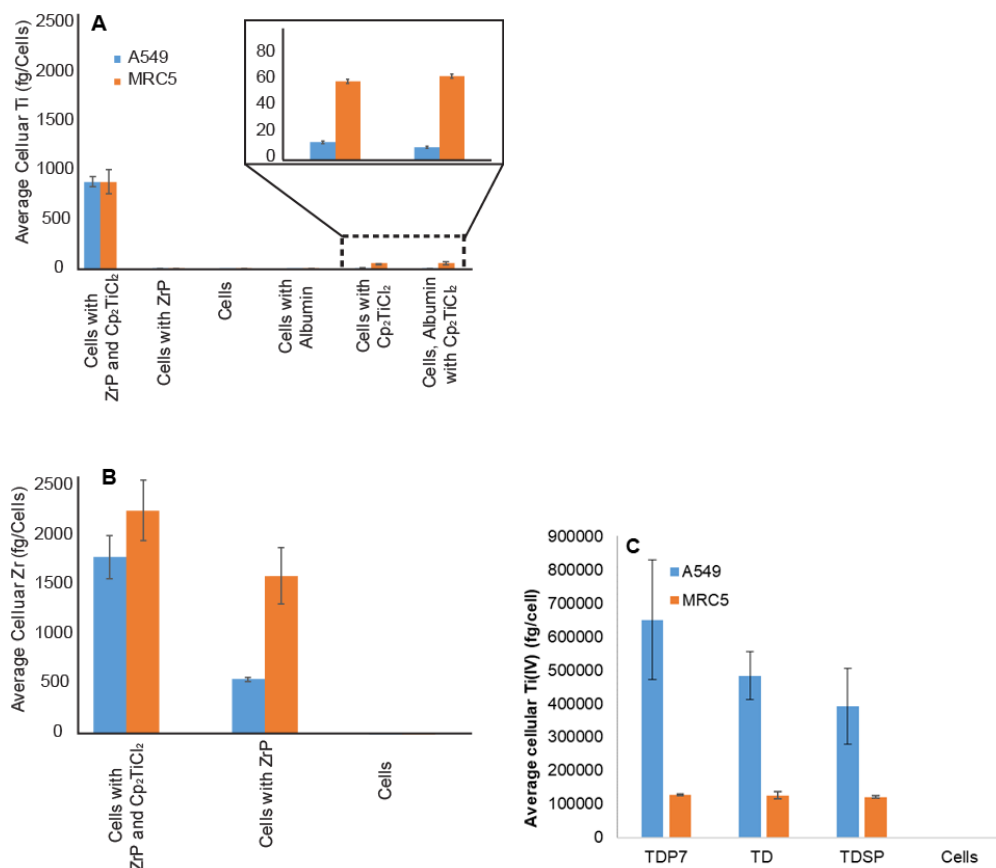
Figure 3.13. Average cellular uptake of Ti(IV) and ZrP were measured using ICP-OES and reported in femtogram/Cells. **A)** Cellular uptake studies for Cp_2TiCl_2 in both A549 and MRC5 cells in the presence of albumin and ZrP nanoparticles. **B)** Cellular uptake measured for ZrP alone in both A549 and MRC5 cells. **C)** Cellular uptake studies for TDP7, TDSP and TD in A549 and MRC5 cells.
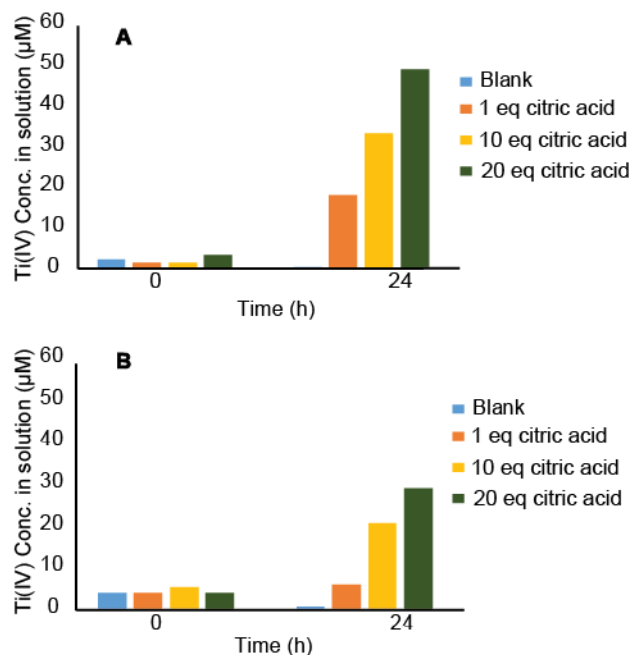
Figure 3.14. Ti(IV) release for the $Cp_2TiCl_2@ZrP$ was determined calorimetrically after adding citric acid to the sample containing $Cp_2TiCl_2@ZrP$ in Acetate buffer (A) and Hepes buffer (B) and incubated at 37 °C for 24 hours.

To test the specificity of the DDS to deliver Ti(IV) to cancer cells effectively and to potentiate the biological action of Ti(IV)-based complexes by metal stabilization, intercalation, or receptor-mediated delivery, cell viability in cancer and non-cancer cell lines were tested. The cytotoxic/antiproliferative effect for Cp_2TiCl_2-BSA and the intercalated product ($Cp_2TiCl_2@ZrP$) was evaluated in A549 and MRC5 cell lines using an MTS assay (**Table 3.1**). No biological activity was observed by the BSA- Cp_2TiCl_2 and for $Cp_2TiCl_2@ZrP$ samples. Cells were treated with high concentration, as high as 100 µM, and the lower cell viability value was over 80 % viability, which means the IC_{50} value of both samples are over this concentration. Today, many IC_{50} values are presented at low micromolar even nanomolar concentrations.[39-42] BSA-Cp_2TiCl_2 sample did not show high Ti(IV) intracellular accumulation, which explains the lack of activity. Perhaps, in the case of the $Cp_2TiCl_2@ZrP$, the uptake Ti(IV) is not being released from the ZrP layers, not allowing the metal to perform any activity in the cells. Another possibility is that even if it's released, it can be precipitating once it gets in contact with the intracellular environment. To know whether the Ti(IV) was being released from the ZrP layers, the formulate was taken in acidic (acetate buffer pH 5.2) and neutral buffer (HEPES buffer pH 7.4) and treated with citric acid. The experimental data showed that the Ti(IV) was released in neutral and acidic conditions (**Fig3.14**). Therefore, the first reason may be ruled out because the tumor's microenvironment is more acidic than the physiological conditions,[43] which may facilitate Ti(IV) release in the cancer cells. However, Cp rings on released titanocene complex could have been dissociated at acidic pH as Cp rings' dissociation was observed for Cp_2TiCl_2 at pH ~5.5 and above.[44] As a result, presumably inactive TiO_2 precipitated.

Table 3.1. The Average cell viability was measured using an MTS assay for A549 and MRC5 cells with different compounds at 100µM concentration. $Cp_2TiCl_2@ZrP$ (Cp_2TiCl_2 intercalated with ZrP).

	A549	MRC5
	% Viability	% Viability
Control	100.0 ± 8.4	100.0 ±7.9
100 µM Cp_2TiCl_2	81.4 ±24.9	83.3 ±19.7
100 µM $Cp_2TiCl_2@ZrP$	103.1 ±15.1	99.3 ±17.3
ZrP only	122.1 ±13.7	126.2 ±20.4
100µM BSA-Cp_2TiCl_2	88.3 ±17.1	89.2 ±17.8

The peptide conjugated Ti(IV) complexes TDP7 and TDSP had very different results at low concentrations (1 -20 µM). TDSP did not show activity with cell viability values over 80 % at 10 and 20 µM. On the other side, TDP7 improved the action of the parent compound TD by between 40 -60 % of improvement in both tested concentrations and had more selectivity towards A549 cells than MRC5 cells (**Fig 3.15 A and B**). Two factors can explain these results, i) A549 cells have a higher transferrin receptor expression than non-cancer cells,[45] allowing more uptake of the compound and producing more cell death. Metal uptake data showed more intracellular Ti(IV) in A549 cells than MRC5 cells (**Fig 3.13**), and ii) Substance P is a neuropeptide, and its selectivity could then be directed to neuronal cells. But, it is also known that this peptide could induce proliferation, causing the contrary effect in cancer cells which is observed by high cell viability percentages in A549 cells (**Fig 3.15 C**).
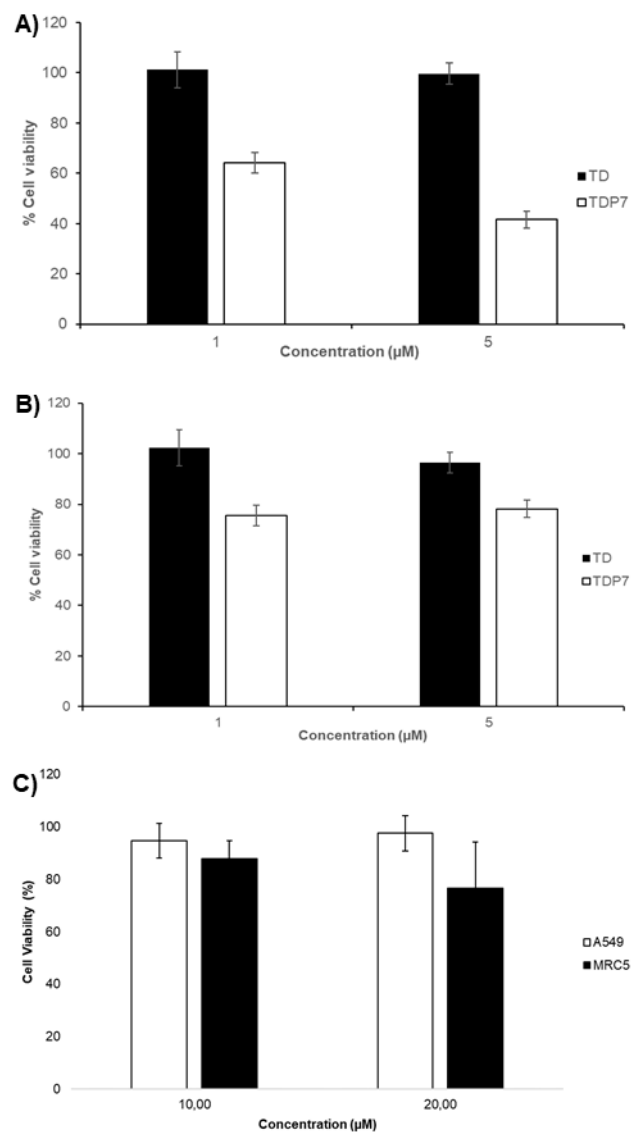
Figure 3.15. Cell viability assays on the peptide-conjugated complexes in MRC5 y A549 cell lines. **(A)** TD and TDP7 against A549 cells, **(B)** TD and TDP7 against MRC5 cells, and **(C)** TDSP against A549 and MRC5 cells.

3. 3 CONCLUSIONS

Recently, DDS has become a mechanism to improve the performance of anticancer drugs. Experiments demonstrate that metal accumulation does not always mean more activity. The Cp_2TiCl_2-BSA conjugated improved the metal ion instability in an aqueous environment. But, in contact with the lysate cell product, it loses the activity by precipitation of the protein and hence produces precipitation of the metal ion as TiO_2. These results were supported with no intracellular Ti(IV) accumulation and no-anticancer activity against lung cancer cells.

In the formulated Cp_2TiCl_2@ZrP and the TDSP bioconjugate results, a significant increase in Ti(IV) uptake was observed, but no cellular activity improvement. For Cp_2TiCl_2@ZrP, it is probable that once the Ti(IV) is released from the interlayer space of ZrP, it precipitates, losing its activity. For the TDSP, as previously described, more factors are observed playing against the compound's activity. SP peptide can increase viable cancer cells. On the other side, the peptide-directed DDS by the P7 peptide seems to be more efficient in delivering the Ti(IV) ion and releasing it intracellularly as a still stable compound. Previous studies confirm the stability and activity of TD against cancer cells, but no selectivity was observed.[26] The bioactive peptide TDP7 increases the intracellular Ti(IV) and improves the specificity against cancer cells.

3. 4   REFERENCES

1.   The "Accidental" Cure—Platinum-based Treatment for Cancer: The Discovery of Cisplatin. https://www.cancer.gov/research/progress/discovery/cisplatin.
2.   Brewer, G. J.; Dick, R. D.; Grover, D. K.; LeClaire, V.; Tseng, M.; Wicha, M.; Pienta, K.; Redman, B. G.; Jahan, T.; Sondak, V. K.,   *Clin. Cancer Res.* **2000,** *6* (1), 1-10.
3.   Corcé, V.; Gouin, S. G.; Renaud, S.; Gaboriau, F.; Deniaud, D., *Bioorg. Med. Chem. Lett.* **2016,** *26* (2), 251-256.
4.   Melendez, E., *Crit. Rev. Oncol. Hematol.* **2002,** *42* (3), 309-315.
5.   Zugazagoitia, J.; Guedes, C.; Ponce, S.; Ferrer, I.; Molina-Pinelo, S.; Paz-Ares, L., *Clin. Ther.* **2016,** *38* (7), 1551-1566.
6.   Tesauro, D.; Accardo, A.; Diaferia, C.; Milano, V.; Guillon, J.; Ronga, L.; Rossi, F., *Molecules* **2019,** *24* (2), 351.
7.   Diaz, A.; Saxena, V.; Gonzalez, J.; David, A.; Casanas, B.; Carpenter, C.; Batteas, J. D.; Colon, J. L.; Clearfield, A.; Hussain, M. D., *ChemComm* **2012,** *48* (12), 1754-1756.
8.   Kratz, F., *J. Control. Release* **2008,** *132* (3), 171-183.
9.   Vargason, A. M.; Anselmo, A. C.; Mitragotri, S., *Nat. Biomed. Eng.* **2021,** *5* (9), 951-967.
10.   Gonzalez, M. L.; Ortiz, M.; Hernandez, C.; Caban, J.; Rodriguez, A.; Colon, J. L.; Baez, A., *J. Nanosci. Nanotechnol.* **2016,** *16* (1), 117-129.
11.   Gonzalez-Villegas, J.; Kan, Y. W.; Bakhmutov, V. I.; Garcia-Vargas, A.; Martinez, M.; Clearfield, A.; Colon, J. L., *Inorganica Chim. Acta* **2017,** *468*, 270-279.
12.   Severin, G. W.; Nielsen, C. H.; Jensen, A. I.; Fonslet, J.; Kjær, A.; Zhuravlev, F., *Journal of medicinal chemistry* **2015,** *58* (18), 7591-7595.
13.   Caruso, F.; Rossi, M., *Mini Rev. Med. Chem.* **2004,** *4* (1), 49-60.
14.   Tshuva, E. Y.; Ashenhurst, J. A., *Eur. J. Inorg. Chem.* **2009,** *2009* (15), 2203-2218.
15.   Tshuva, E. Y.; Peri, D., *Coord. Chem. Rev.* **2009,** *253* (15–16), 2098-2115.
16.   Tinoco, A. D.; Incarvito, C. D.; Valentine, A. M., *JACS* **2007,** *129* (11), 3444-3454.
17.   Tinoco, A. D.; Saxena, M.; Sharma, S.; Noinaj, N.; Delgado, Y.; Gonzalez, E. P. Q.; Conklin, S. E.; Zambrana, N.; Loza-Rosas, S. A.; Parks, T. B., *JACS* **2016,** *138* (17), 5659-5665.
18.   Tinoco, A. D.; Eames, E. V.; Incarvito, C. D.; Valentine, A. M., *Inorg. Chem.* **2008,** *47* (18), 8380-8390.
19.   Christodoulou, C. V.; Eliopoulos, A. G.; Young, L. S.; Hodgkins, L.; Ferry, D. R.; Kerr, D. J., *Br. J. Cancer* **1998,** *77* (12), 2088-2097.
20.   Parodi, A.; Miao, J.; Soond, S. M.; Rudzińska, M.; Zamyatnin, A. A., Jr., *Biomolecules* **2019,** *9* (6), 218.
21.   Topală, T.; Bodoki, A.; Oprean, L.; Oprean, R., *Clujul Med.* **2014,** *87* (4), 215.
22.   Bal, W.; Sokołowska, M.; Kurowska, E.; Faller, P., *Biochim. Biophys. Acta Gen. Subj.* **2013,** *1830* (12), 5444-5455.
23.   Costa Pessoa, J.; Tomaz, I., *Curr. Med. Chem.* **2010,** *17* (31), 3701-3738.
24.   Desai, N. P.; Trieu, V.; Hwang, L. Y.; Wu, R.; Soon-Shiong, P.; Gradishar, W. J., *Anticancer Drugs* **2008,** *19* (9), 899-909.
25.   Frei, E., *Diabetol. metab. syndr.* **2011,** *3* (1), 11.
26.   Loza-Rosas, S. A.; Vazquez, A. M.; Rivero, K. I.; L.J., N.; Delgado, Y.; Benjamin-Rivera, J. A.; Vazquez-Maldonado, A. L.; Parks, T. B.; Munet-Colon, C.; Tinoco, A. D., *Inorg. Chem.* **2017,** *56*, 7788-7802.

27.   Rizk, S. S.; Misiura, A.; Paduch, M.; Kossiakoff, A. A., *Bioconjug. Chem.* **2012,** *23* (1), 42-46.

28.   Anabousi, S.; Bakowsky, U.; Schneider, M.; Huwer, H.; Lehr, C. M.; Ehrhardt, C., *Eur. J. Pharm. Sci.* **2006,** *29* (5), 367-374.

29.   Daniels, T. R.; Delgado, T.; Rodriguez, J. A.; Helguera, G.; Penichet, M. L., *J. Clin. Immunol.* **2006,** *121* (2), 144-58.

30.   Benjamín-Rivera, J. A.; Cardona-Rivera, A. E.; Vázquez-Maldonado, Á. L.; Dones-Lassalle, C. Y.; Pabón-Colon, H. L.; Rodríguez-Rivera, H. M.; Rodríguez, I.; González-Espiet, J. C.; Pazol, J.; Pérez-Ríos, J. D.; Catala-Torres, J. F.; Carrasquillo Rivera, M.; De Jesus-Soto, M. G.; Cordero-Virella, N. A.; Cruz-Maldonado, P. M.; González-Pagan, P.; Hernández-Ríos, R.; Gaur, K.; Loza-Rosas, S. A.; Tinoco, A. D., *Inorganics* **2020,** *8* (9), 48.

31.   Gaur, K.; Vázquez-Salgado, A. M.; Duran-Camacho, G.; Dominguez-Martinez, I.; Benjamín-Rivera, J. A.; Fernández-Vega, L.; Carmona Sarabia, L.; Cruz García, A.; Pérez-Deliz, F.; Méndez Román, J. A.; Vega-Cartagena, M.; Loza-Rosas, S. A.; Rodriguez Acevedo, X.; Tinoco, A. D., *Inorganics* **2018,** *6* (4), 126.

32.   Loza-Rosas, S. A.; Saxena, M.; Delgado, Y.; Gaur, K.; Pandrala, M.; Tinoco, A. D., *Metallomics* **2017,** *9* (4), 346-356.

33.   Prades, R.; Guerrero, S.; Araya, E.; Molina, C.; Salas, E.; Zurita, E.; Selva, J.; Egea, G.; Lopez-Iglesias, C.; Teixido, M.; Kogan, M. J.; Giralt, E., *Biomaterials* **2012,** *33* (29), 7194-7205.

34.   Xie, Y. R.; Killinger, B.; Moszczynska, A.; Merkel, O. M., *Molecules* **2016,** *21* (10).

35.   Lindl, T., *Zell-und Gewebekultur*. Spektrum Akademischer Verlag: 2002.

36.   Schur, J.; Manna, C. M.; Deally, A.; Köster, R. W.; Tacke, M.; Tshuva, E. Y.; Ott, I., *ChemComm.* **2013,** *49* (42), 4785-4787.

37.   Borzova, V. A.; Markossian, K. A.; Chebotareva, N. A.; Kleymenov, S. Y.; Poliansky, N. B.; Muranov, K. O.; Stein-Margolina, V. A.; Shubin, V. V.; Markov, D. I.; Kurganov, B. I., *PloS One* **2016,** *11* (4), e0153495.

38.   Ostojić, S.; Dragutinović, V.; Kićanović, M.; Simonović, B. R., *J. Serb. Chem. Soc.* **2007,** *72* (4), 331-337.

39.   Sommerwerk, S.; Heller, L.; Kerzig, C.; Kramell, A. E.; Csuk, R., *Eur. J. Med. Chem.* **2017,** *127*, 1-9.

40.   Loughlin, W. A.; Jenkins, I. D.; Karis, N. D.; Healy, P. C., *Eur. J. Med. Chem.* **2017,** *127*, 341-356.

41.   Durcik, M.; Lovison, D.; Skok, Ž.; Cruz, C. D.; Tammela, P.; Tomašič, T.; Tiz, D. B.; Draskovits, G.; Nyerges, Á.; Pál, C., *Eur. J. Med. Chem.* **2018,** *154*, 117-132.

42.   Wu, W. W.; Phue, J.-N.; Lee, C.-T.; Lin, C.; Xu, L.; Wang, R.; Zhang, Y.; Shen, R.-F., *BMC Genet.* **2018,** *19* (1), 1-10.

43.   Yamagata, M.; Tannock, I., *British journal of cancer* **1996,** *73* (11), 1328.

44.   Toney, J. H.; Marks, T. J., *JACS* **1985,** *107* (4), 947-953.

45.   Lee, J. H.; Engler, J. A.; Collawn, J. F.; Moore, B. A., *Eur. J. Biochem.* **2001,** *268* (7), 2004-2012.

Chapter 4

Research development into the design of bimetallic complexes as new generation anticancer drugs

Behind the empirical search of new chemotherapeutics, tremendous potential in developing new generations of more successful anticancer treatments is kept. Coordination chemistry is crucial when metal-based drugs are being designed. Metals dictate which ligands would be compatible based on the hard-soft acid-base (HSAB) theory. At the same time, ligands' chemistry will play an essential role in compounds' stability.[1] Then, the choice of the ligand is not a trivial decision.

Titanocene dichloride (Cp_2TiCl_2), a Titanium(IV) (Ti(IV)) complex, was the second metal-based drug to reach clinical trials. Cp_2TiCl_2 quickly fails due to aqueous instability issues. Derivatives have been prepared over the years, modifying the ligands to improve the stability and, hence, the drug's performance.[2-4] The chemistry behind how ligands change the aqueous stability, mechanism of action, and even its biological activity is fascinating. Choosing a ligand could mean targeting a different biological aim or no activity at all.

Contel et al. designed bimetallic complexes as the next generation of anticancer drugs. Her studies demonstrate that two fused drugs work better than the drugs combined. She focused on fusing Cp_2TiCl_2 with other metallic complexes such as auranofin. But Cp_2TiCl_2 is not the best example of an effective drug because, as it was mentioned before, it failed the clinical trials due to instability issues. Auranofin (AF), on the other hand, is a repurposed drug usually used to treat rheumatoid arthritis (AR) and has shown good potential as a cancer drug. AF can use different mechanistic pathways, which is crucial in developing bimetallic drugs.[5-8]

Ti(IV) drugs have been evolving, and up today, there are more stable and effective compounds that can display their biological properties against cancer cells. Previous work in our lab has shown that Deferasirox, a chemical transferrin mimetic (cTfm) ligand, has improved the aqueous stability of the metal ion and demonstrated good biological activity against different cancer cells lines.[9] The mechanistic insights studied in chapter two showed how this compound might work intracellularly. Affecting Cu(II) and Fe(III), essential metals in cancer progression and their transmetallation ability trigger a lethal increase in ROS production, activating cancer cell death pathways. All this research that has been done could be lead to a new generation of more effective and potent bimetallic Ti(IV) drugs.

Ti(IV) Deferasirox has been shown to work well with other anticancer drugs such as cisplatin.[10] From what is understood, both drugs use different mechanistic pathways to induce cell death and explain why there is a synergistic effect between them. Then, fusing a platinum drug with Ti(IV) Deferasirox could work even better, as Contel's work established. Following that thought, heterometallic Ti(IV) Deferasirox drugs will take advantage of the different mechanisms metals and ligands perform intracellularly. The carboxylic group in the ligand deferasirox allows for different chemistry reactions to conjugated compounds. For example, in chapter 3, the carboxylic group was used to add peptides by an amide bond formation. Thus, there are broad possibilities for designing new, more potent, and more effective multicentered heterometallic Ti(IV) complexes.

This work was co-directed by Lauren Fernández-Vega and published in Inorganics, an Open Access Journal from MDPI (See appendix 8 for thesis publication permission).[11] Participants in this work are as follows: Valeria A. Ruiz Silva, Tania M. Domínguez-González, Sebastián Claudio-Betancourt, Rafael E. Toro-Maldonado, Luisa C. Capre Maso, Karina Sanabria Ortiz, Jean A. Pérez-Verdejo, Janeishly Román González, Grecia T. Rosado-Fraticelli, Fabiola Pagán Meléndez, Fabiola M. Betancourt Santiago, Daniel A. Rivera-Rivera, Carlos Martínez Navarro, Andrea C. Bruno Chardón, Axel O. Vera and Arthur D. Tinoco.

Review
Evaluating Ligand Modifications of the Titanocene and Auranofin Moieties for the Development of More Potent Anticancer Drugs

4.1. Introduction

Cancer is the second main cause of death throughout the world, claiming 9.56 million lives in 2017 [12]. In 2019, the American Cancer Society estimated that there would be 1,735,350 new cases of cancer and 606,880 deaths in the United States alone [13]. Chemotherapy, the use of chemical agents to treat cancer, remains one of the most effective anticancer strategies, with the platinum(II)-based compounds cisplatin, carboplatin, and oxaliplatin being widely used globally. Three others, nedaplatin, lobaplatin, and heptaplatin are used in specific countries but have not received FDA approval in the United States [14]. Cisplatin (Figure 4.1) was the first metal-based chemotherapeutic agent, which was discovered serendipitously by Barnett Rosenberg in 1965 [15]. Today, Pt(II) compounds are used to treat 40% to 80% of cancer patients [16-17]. However, as with other chemo drugs, their efficacy is hindered by clinical failures, including acquired resistance, a limited spectrum of activity, and high toxicity due to negative side effects [18]. A major source of the side effects associated with Pt-based drugs is the lack of exclusivity for cancer cells, resulting in unwanted biomolecular interactions with Pt(II). The formation of Pt(II)-DNA adducts in cancer cells is an intended target of the Pt(II) drugs as the adducts lead to suppressed DNA replication, but these adducts can also form in healthy tissue [19]. Even if the Pt(II) drugs could be selective for cancer cells, another issue is that the DNA reparation mechanism of the cells can attenuate the antiproliferative behavior of the metal. An overexpression of the multidrug

resistance receptors (MDR) leads to a heightened efflux of the metal from the cell, significantly reducing the total metal content within cells [20].

Efforts are being made to improve the efficacy and cancer specificity of Pt compounds and to subsequently minimize their toxicity. In academia, the profound evolution of such compounds for anticancer treatment has been dictated by a better understanding of their antiproliferative and associated apoptotic mechanisms of action. It is now understood, for instance, that DNA is not the sole cellular target of Pt(II) (only about 1% of Pt(II) from cisplatin reaches DNA [21]), although it is certainly one of the more important ones [21]. Key to the knowledge development of the drug design of Pt compounds has been the recognition of the importance of the ligands to the activity of the compounds. Taking advantage of the coordination properties of the metal ion, cytotoxic ligands with a distinct mechanism of effect have been attached to the metal to increase the potency of the compounds [22-23]. Other ligands have been explored to develop anticancer *trans*-Pt(II) compounds [24] and even Pt(IV) compounds. Cellular reduction of the Pt(IV) ion to Pt(II) serves as an effective strategy to release cytotoxic agents bound to the metal center. Covalently conjugating certain drug delivery vectors onto the ligands has allowed increasing cellular uptake of Pt [25] and likely minimized the attenuation of the MDR system.
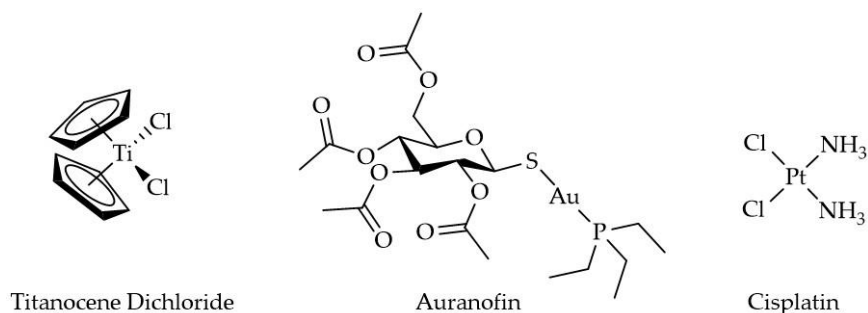
Figure 4.1. The chemical structures for titanocene dichloride, auranofin, and cisplatin.

The discovery of the therapeutic properties of Pt revolutionized the drug field, reshaping the thinking behind drug design by demonstrating that a nonorganic species could impact human health and lead to a scientific renaissance to discover other metals for medical applications. Initially, the search was rather primitive and centered on empirically testing the therapeutic potential of different coordination compounds rather than a targeted approach. From this effort, titanium and gold, amongst other metals, emerged as very promising anticancer agents. In this review we will examine titanium(IV) and gold(I) in the anticancer field because their very different coordination chemistry yield distinct mechanisms of cellular effect, different even from the Pt(II) compounds. We will specifically focus on the titanocene (Cp_2Ti^{2+}) and auranofin (AF) families of compounds (Figure 4.1) to evaluate how understanding their mechanisms of effect, the aqueous chemistry and speciation of the metal ions, and the functional role of the ligands, have led to important evolution of the ligands, producing a new generation of anticancer agents with the potential to enter the drug market.

4.2. Titanocene Dichloride and its Ligand Evaluation

4.2.1. Biologically Relevant Ti(IV) Coordination Chemistry

The most stable and common oxidation state of titanium is +4; however, compounds in a range of lower oxidation states, −1, 0, +2, +3, are also known [26]. Nevertheless, these lower oxidation states are readily oxidized to Ti(IV) by air, water, or other reagents. In our aerobic atmosphere, particularly near neutral pH, Ti(IV) is favored, and most of the Ti in the environment is oxidized [26-27]. Even within the reducing environment of cells, Ti is expected to exist in the +4 state due to the absence of strong biological reducing agents [28]. The most prevalent coordination number of Ti(IV) is six, although four-, five-, seven-, and eight-coordinate compounds are known [26, 29]. As a d^0 metal ion, Ti(IV) coordination compounds are diamagnetic and do not have crystal field stabilization energy (CFSE). The lack of CFSE should make these compounds ligand exchange labile, but the high metal oxidation state decreases this lability [30].

The biological coordination chemistry of Ti(IV) is dictated by it being a very strong Brønsted-Lowry acid and a Hard Lewis Acid. The Brønsted-Lowry property is observed in the extensive hydrolysis that water molecules bound to Ti(IV) undergo [30]. Standard Ti(IV) salts are difficult to prepare from aqueous solutions, as they often yield hydrolyzed species, and at weakly acidic, neutral, or basic pH, will precipitate from the solution [29, 31-32]. Due to its propensity for hydrolysis, well-characterized compounds of Ti(IV) that are prepared or stabilized in an aqueous solution are somewhat rare. There are examples of stable Ti(IV) complexes containing chelating ligands that exhibit partial hydrolysis in the form of the titanyl unit (TiO^{2+}) [33-34] or oxo bridges [35]. As a Hard Lewis Acid, Ti(IV) is predominantly coordinated by biological chelators that contain oxygen-rich binding moieties, although binding by nitrogen-containing chelators has also been observed (Figures 4.2 and 4.3). The bioinorganic coordination chemistry of Ti(IV) largely mimics that of Fe(III) and is the subject of a recent review of ours [28].
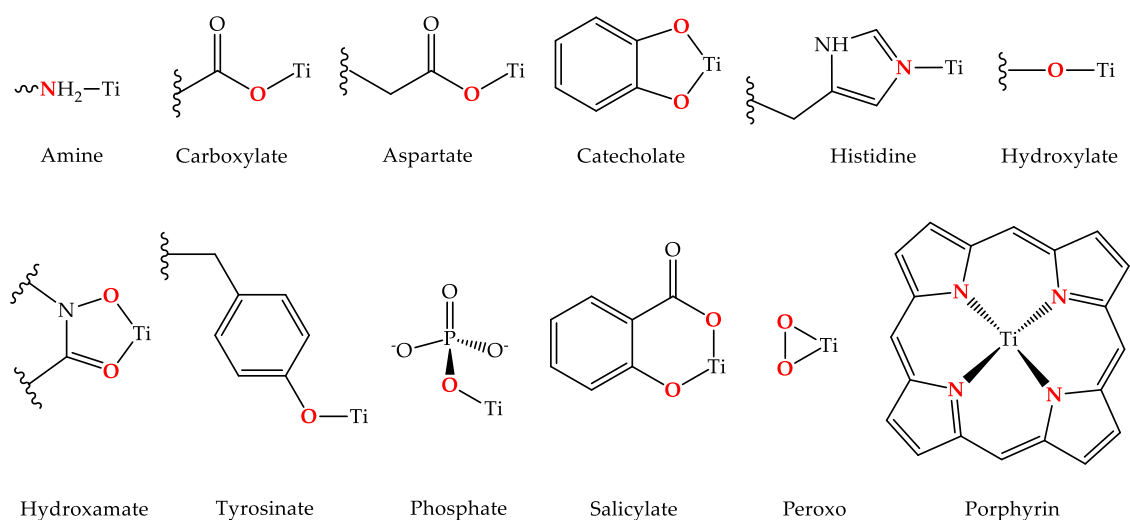
Figure 4.2. Typical Ti(IV) binding moieties of endogenous ligands with some representative coordination modalities. Reprinted from Coordination Chemistry
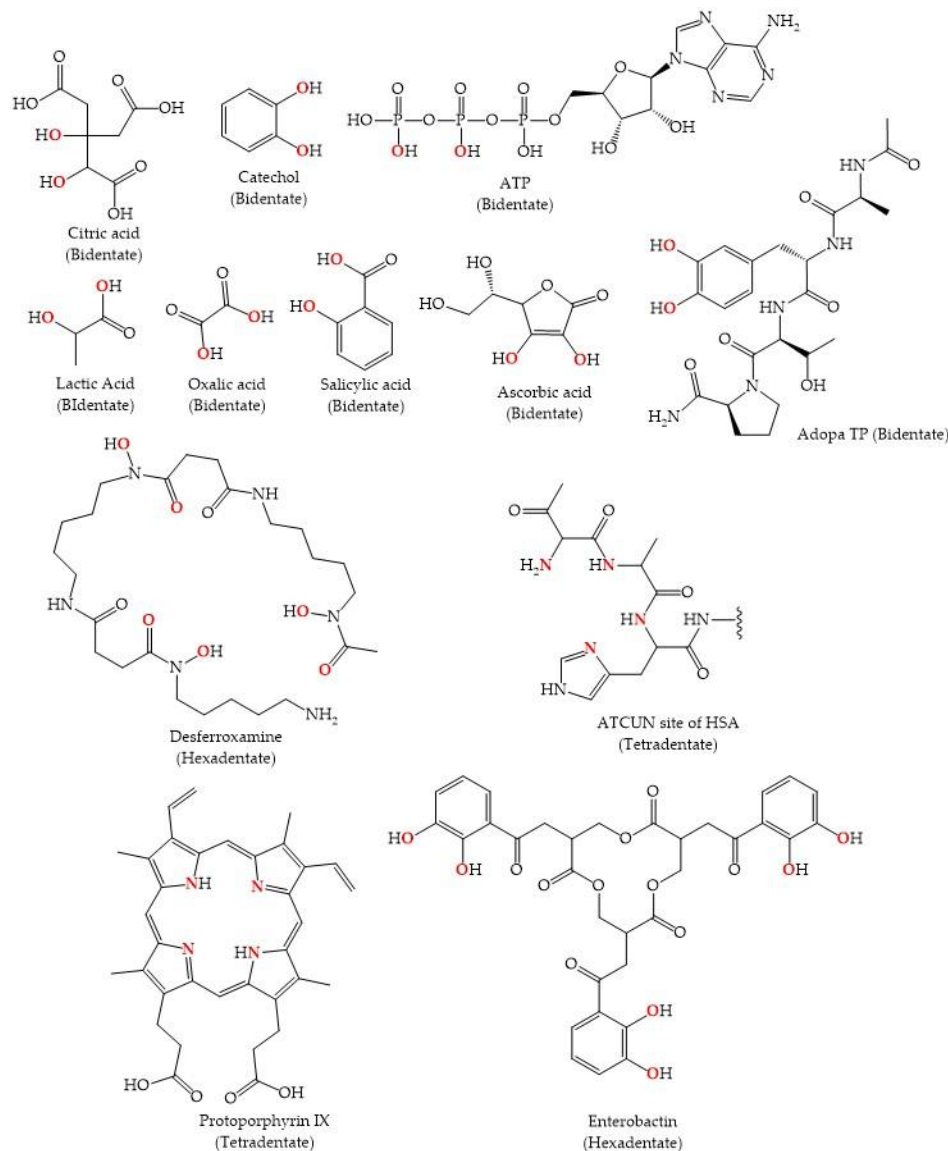
Figure 4.3. Some endogenous (or proposed) biological Ti(IV) chelators. Typical Ti(IV) binding moieties of endogenous ligands with some representative coordination modalities. Reprinted from Coordination Chemistry Reviews, 363, M. Saxena, S. A. Loza-Rosas, K. Gaur, S. Sharma, S. C. Pérez Otero, A. D. Tinoco, Exploring titanium(IV) chemical proximity to iron(III) to elucidate a function for Ti(IV) in the human body, 109–125, Copyright (2018), with permission from Elsevier.

4.2.2. History of Ti(IV) in Anticancer Research

Soon after the discovery of cisplatin, the search was on for other anticancer complexes with different central metals. The problem was that there was no established structure-activity relationships for metals other than Pt to help guide this mission [36]. The search was initially empirically driven, basically becoming the hunt for the next cisplatin-like compound. Ti(IV) was one of the first metals to be explored in the form of titanocene dichloride (Cp_2TiCl_2). In their initial work with the compound, Köpf and Köpf-Maier wrote, "We expected (Cp_2TiCl_2) to possibly show such an activity, since it contains a *cis*-dichlorometal moiety in the neutral complex, like the well-known antitumor agent (cisplatin)" [37]. Cp_2TiCl_2 very superficially resembles cisplatin. Its tetrahedral geometry (Figure 4.1) is unlike the square planar geometry of cisplatin. A second Ti(IV) compound, budotitane, belonging to the class of bis(β-diketonato) metal complexes, also caught the interest of researchers because of the cis arrangement of its ethoxide ligands. Fortunately, both Cp_2TiCl_2 and budotitane exhibited potent antiproliferative behavior against a variety of cell lines. We will focus exclusively on Cp_2TiCl_2 because it was the compound to advance the furthest from benchtop work to clinical testing and continues to be explored in modified forms today.

Cp_2TiCl_2 was initially tested against Ehrlich ascites tumor cells (murine mammary cancer) implanted in mice. The results were extremely promising because the compound had a cure rate in the therapeutic range of 80% [37]. Other studies demonstrated that it could be effective against Lewis lung carcinoma, colon B adenocarcinoma, B16 melanoma, and several other cancer types [38-39]. Cp_2TiCl_2 was also quite effective against cisplatin resistant cancer cell lines both in vitro and in vivo, which was an early clue that it operated via a different mechanism of action [40].

The cytotoxicity of Cp_2TiCl_2 is predicated on the rapid hydrolysis of the compound in aqueous solution (Figure 4.4). The compound is poorly soluble in water, but once introduced into water with the help of a co-solvent such as DMSO, the chloro ligands are quick to dissociate. At pH 3.0, the first chloro ligand dissociates within seconds and the second chloro ligand dissociates with a half-life of fifty minutes [41]. These dissociation events are accompanied by aquation and hydrolysis. The cyclopentadienyl rings dissociate at a half-life of 57 h. Above pH 6.0, in the absence of any metal coordinating anion, Cp_2TiCl_2 undergoes virtually complete dissociation within seconds, yielding insoluble white precipitates that largely consists of titanium dioxide (TiO_2) and polymeric hydrolyzed species containing substoichiometric equivalents of the Cp ligand [41]. It is believed that Cp_2TiCl_2 is a prodrug that once introduced into blood, requires facile delivery of Ti(IV) to the protein serum transferrin (sTf) for effective delivery into cells. STf is a bilobal glycoprotein present at ~30 µM in blood and is the primary transporter of iron(III) into all mammalian cells via endocytosis. Each of its lobes contains a metal binding site with identical coordinating amino acid moieties; Fe(III) is bound by two tyrosines, a histidine, an aspartate, and a carbonate anion that serves as a bidentate synergistic ligand. The protein is only 30% Fe(III) saturated [42] and thus can participate in the delivery of nonferric ions into cells [43-45].
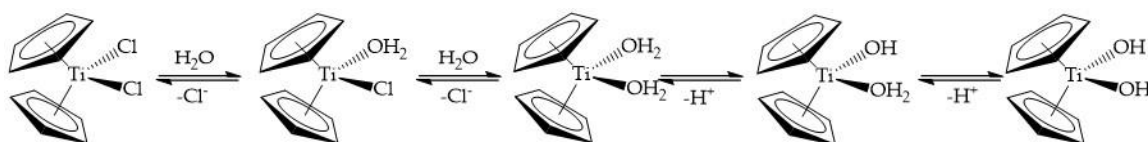
Figure 4.4. The hydrolysis of titanocene dichloride under acidic conditions focusing only on the dissociation of the chloro ligands.

The discovery of Ti(IV) binding by STf [46-48] was very exciting because sTf is an excellent target for enhanced delivery of a drug to cancer cells versus normal cells. Due to their higher requirement for Fe(III), cancer cells overexpress the transferrin receptor, which is the protein responsible for the endocytotic uptake of metal-bound sTf into cells [49]. Although Ti(IV) can bind to sTf directly from Cp_2TiCl_2 as a hydrolyzed metal ion, it appears more likely to first be rapidly coordinated by the small anion citrate, which is present in blood at 100 µM, forming a Ti(IV) citrate complex (possibly Ti(citrate)$_3{}^{8-}$) that then delivers the metal ion to sTf (Figure 4.5) [50]. In this pathway, Ti(IV) is bound by sTf in a manner similar, but not identical to Fe(III). It is coordinated by the two tyrosines of the binding site and carbonate, and by one citrate molecule serving as an additional bidentate synergistic ligand. This interaction constitutes a ternary complex (Ti-citrate)$_2$-sTf [50]. The citrate taking the place of the histidine and aspartate is likely a consequence of the Harder Lewis Acidity of Ti(IV). Presumably, in the absence of the citrate, an oxo or hydroxo moiety would take its place [28]. Once Ti(IV) is within the endosomes in cells, ATP is proposed to scavenge it from STf and transport it into the cytosol [48]. Ultimately, Ti(IV) accumulates in the nucleus and within cytosolic lysosomes (site of protein degradation). An electron-spectroscopic imaging (ESI) study of human stomach, colon, and lung adenocarcinoma cells, isolated from xenografted mice following Cp_2TiCl_2 treatment, demonstrated that within the nucleus and lysosomes, Ti(IV) colocalizes with phosphorus [51]. This colocalization is probably in the form of biomolecular phosphate coordination of the metal ion. Ti(IV) can bind to the phosphodiester backbone of DNA [52-53] and to phosphoproteins [54], and these interactions are key to its induction of apoptosis. Ti(IV) has the capacity to cleave phosphodiester bonds. Under acidic conditions, Ti(IV) can cleave ATP and produce inorganic phosphate [48]. However, it has been conclusively shown that Ti(IV) binding to DNA is incapable of cleaving the phosphodiester bonds and cause strand breaks [53]. Instead, the Ti(IV) binding causes detrimental structural changes that results in cell cycle arrest in the late S/early G2 phase and induces apoptosis at any phase of the cell cycle [55]. The apoptotic event results in the observed DNA breaks and a correlated increase in p53 levels, a protein that participates in DNA damage repair mechanisms [55]. Less clear is the potential interaction of Ti(IV) with phosphoproteins. Perhaps Ti(IV) binding to specific phosphoproteins could inhibit their functionality. Ti(IV) could also play a role in protein phosphorylation [28] and could thus significantly alter phosphorylation levels within cells [56]. Ti(IV) is also capable of blocking human topoisomerase interaction with DNA either by possible direct coordination to DNA or the topoisomerase [57], or by means of an indirect secondary effect [40]. This inhibition prevents the normal

process of DNA replication. The exact biomolecular pathway leading to apoptosis remains elusive (Figure 4.5).
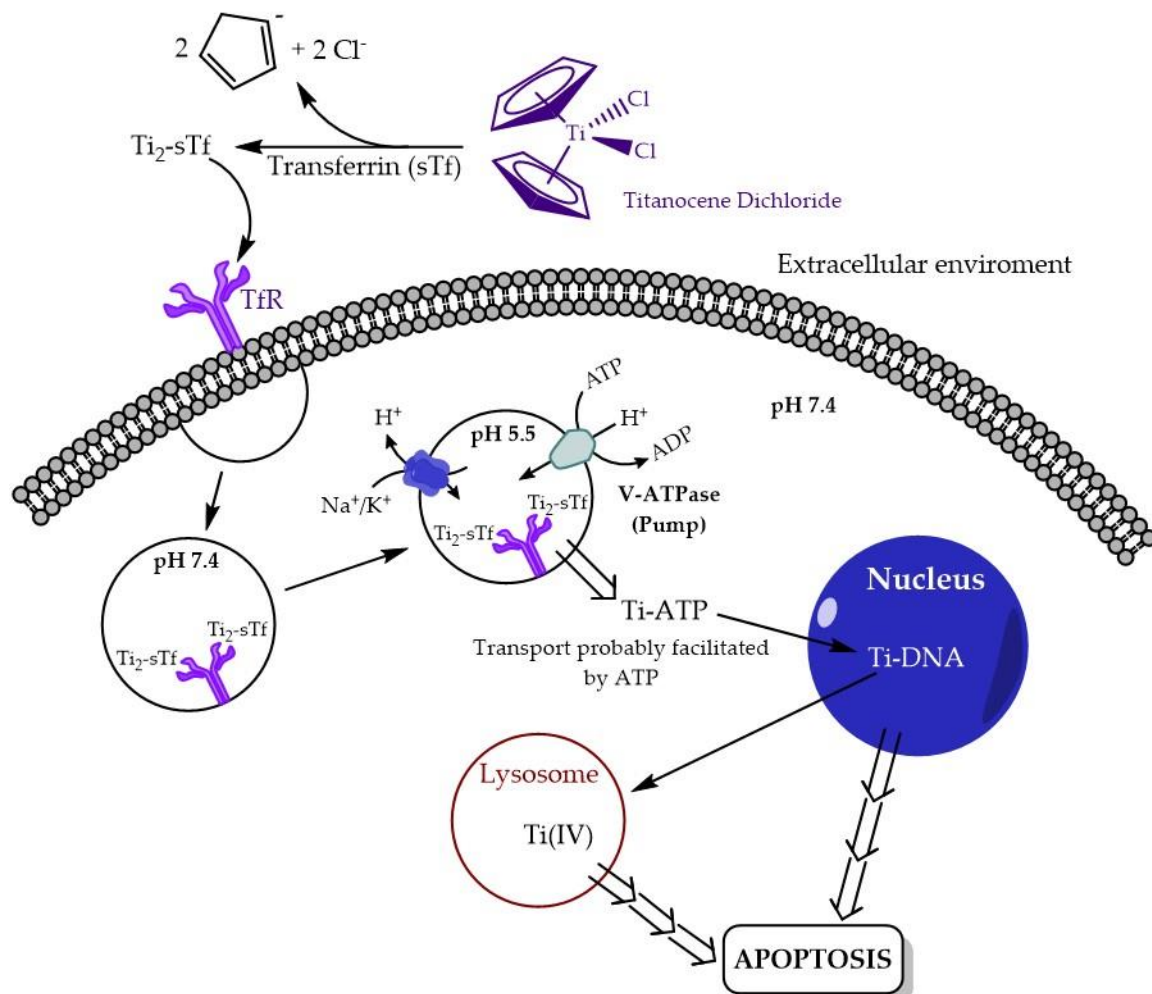
Figure 4.5. Proposed cytotoxic mechanism of action of Cp_2TiCl_2.

A less explored contribution to the mechanism of action of Cp_2TiCl_2 is the role that human serum albumin (HSA) may play. HSA is the most abundant serum protein (~600 μM). It possesses numerous binding sites capable of binding a variety of species, including metal ions, hydrophobic molecules, charged aromatic molecules, and drugs [58-60]. HSA binding of fatty acids causes protein conformational changes that enhances its binding of different species. The protein plays important functions in the pharmacodynamics of a drug in the human body, either increasing its lifespan in blood or sequestering it and helping to clear it from the system. It can also play a cellular transport function [58-60]. When Cp_2TiCl_2 was mixed at equimolar levels with HSA (1 mM), ^1H NMR revealed that the Cp_2Ti^{2+} moiety appears to bind to HSA (at an unidentified site) and remain stably bound for an indefinite amount of time. HSA, like sTf, provides a source of selectivity towards cancer cells because the accelerated metabolism of cancer cells causes them to catabolize albumin as a nutrient source much more than normal cells do

and this results in a greater interaction with and possible uptake of albumin [61]. HSA binding of the Cp_2Ti^{2+} moiety could thus provide a pathway for it to enter intact into cells. Alternatively, HSA could facilitate a direct contact of this lipophilic moiety with the cell membrane and enable entry via passive diffusion. It is uncertain, however, how long the moiety could remain intact within the aqueous environment of the cytosol (which is pH 7.4) and whether it could reach DNA intact. Nonetheless, the presence of the Cp ring could help to stabilize Ti(IV) coordination to DNA and more effectively damage it structurally.

4.2.3. Ti(IV) in Anticancer Clinical Trials

Budotitane was the first Ti(IV) compound to reach clinical trials. Two phase 1 trials were administered on cancer patients who were not responsive to other treatments. In the first trial, the dose limiting toxicity was nephrotoxicity (accompanied by nausea, vomiting, weakness, and malaise) [62], and in the second was cardiac arrhythmia [63]. In both studies, some patients experienced an impairment of their sense of taste. A tumor response to budotitane was not observed in either study, and the compound was not considered for further testing.

A total of five clinical trials were conducted to examine Cp_2TiCl_2. Three phase I trials involved patients with advanced solid tumors and evaluated the dose limiting toxicity of the compound. Christodoulou et al. identified 140 mg/m^2 as the maximum tolerated dose (MTD) [64] whereas Korfel et al. recommended 315 mg/m^2 [65] and Mross et al. recommended 240 mg/m^2 [66]. The differences in recommendation had to do with the frequency of administration. The toxicities observed for Cp_2TiCl_2 treatment were comparable to those of budotitane. Additional reported toxicities included hepatic toxicity, blurred vision, hypertension, anorexia, and insomnia.

Cp_2TiCl_2 advanced to phase II testing. Lümmen et al. administered a dose of 270 mg/m^2 every three weeks for six weeks to renal-cell carcinoma patients ($n = 14$), in which 78.6% of the patients received two cycles [67]. Patients showed signs of tumor progression and high toxicity while undergoing treatment. Kröger et al. also administered the same dosage to patients with metastatic breast cancer, but the compound failed to show significant antitumor activity against this population [68]. This study was halted due to several reasons (i.e., progression, toxicity), and the recommended dosage was lowered to 240 mg/m^2 for future clinical trials. Despite promising *invitro* data, none of the admitted patients in the phase II trials achieved a complete or partial response to Cp_2TiCl_2 therapy. Failure in the phase II trials resulted in the compound being removed from further testing.

4.2.4. Titanocene Dichloride Therapeutic Limitation due to Its Formulation and Speciation in the Body

The hydrolytic instability of Cp_2TiCl_2 can be a major deterrent to its therapeutic potential. The compound is simply too reactive and can readily transform under different solution conditions into different Ti(IV) species. For clinical trial testing, Cp_2TiCl_2 was prepared in was what termed a soluble, water stable formulation called MKT4, in which the compound was combined with the sugar alcohol mannitol. Buettner et al. propose that the mannitol can coordinate to the Cp_2Ti^{2+}

moiety in a doubly deprotonated fashion forming a neutral $Cp_2Ti(mannitol)$ compound that is far more stable than Cp_2TiCl_2 [69]. The MKT4 formulated Cp_2TiCl_2 exhibits cytotoxic behavior against several cancer cell lines about on par with the parent compound [69]. Solutions of Cp_2TiCl_2 prepared in methanol or ethanol and left to equilibrate after some time will transform into Ti(IV) species with bound Cp and alcohol ligands such as $[Cp_2Ti(OMe)]^+$ and $[CpTi(H_2O)(OH)]^+$ as detected by Electrospray Ionization Mass Spectrometry (ESI-MS) [70]. These species formed by aging in the alcohols exhibit far stronger cytotoxic potency against HCT116 (human adenocarcinoma) cells than freshly prepared Cp_2TiCl_2. They also result in elevated metal uptake in the cells. Ravera et al. suggest that these relatively more stable species may permit the Ti to exist in a lipophilic cell permeable form that could result in higher accumulation within cells [70].

The problem still remains that titanocenyl mannitol or alcohol byproducts are quasi-stable. In the environment of blood, they are likely to be biotransformed (transiently) by citrate into a Ti(IV) citrate complex and then ultimately converted into the ternary complex $(Ti\text{-}citrate)_2\text{-}sTf$ [50]. This ternary complex does not display cytotoxic behavior at low µM concentration [34]. Citrate and sTf have been shown to be able to work synergistically to attenuate the cytotoxicity of anticancer Ti(IV) complexes by inducing their dissociation [50]. This is not to say that Ti(IV)-bound STf is incapable of being cytotoxic. The issue is a matter of concentration. At a very high concentration, and nearing mM amounts, the complex displays antiproliferative behavior [71], implying that a certain concentration threshold needs to be met in order for cellular Ti(IV) levels to reach a high enough level to detrimentally impact cells. Even if the Cp_2Ti^{2+} could bind to SA, the Cp_2Ti–SA 1:1 complex also requires very high concentration (near mM) for antiproliferative behavior [34, 71], which could account for why Cp_2TiCl_2 exhibits high µM IC_{50} values against numerous cell lines [55]. Cell media is typically supplemented with 10% fetal bovine serum, which contains citrate and biologically active serum proteins capable of interacting with the titanocene moiety. In their seminal work to unlock the mechanism of action of Cp_2TiCl_2, Christodoulou et al. did not detect any apoptotic behavior until examining the compound at mid to high µM concentrations [55].

4.2.5. Titanocenyl Modification and Encapsulation to Alter Method of Transport for Improved Cytotoxic Potency

Extensive studies have been performed to substitute the chloro groups and modify the substituents of the cyclopentadienyl rings of Cp_2TiCl_2 to improve solubility, aqueous stability, and cytotoxicity of the family of titanocene compounds. These efforts have achieved varying degrees of success, and this catalog of work has been the subject of excellent reviews by Harding et al., Caruso et al., Hamilton et al., De la Cueva-Alique et al., and Santiago et al. [39-40, 72-75]. Rather than revisiting these assessments, we will instead focus on select studies in which efforts were made to modify the ligand platform to prepare titanocenyl derivatives that may exploit alternative transport mechanistic routes for cellular uptake.

Top et al. sought to vectorize titanocene by appending a tamoxifen-like moiety as an alkylated substituent of one of the Cp rings (Figure 4.6) [76]. Tamoxifen is a selective estrogen receptor modulator (SERM) and the objective was to examine whether a tamoxifen-like modification of Cp_2TiCl_2 would enhance its specificity and activity against the hormone dependent breast cancer cell MCF7. Surprisingly, the tamoxifen derivative produced a proliferative effect, as did the parent Cp_2TiCl_2 compound itself, both within nM to low µM concentration range. It was concluded that one of the hydrolysis products of Cp_2Ti^{2+} including fully Cp dissociated Ti(IV) must exert an estrogenic effect and that the incorporation of a tamoxifen-like modification of one of the Cp rings was not enough to overcome this hydrolytic behavior. It is important to note that at high concentrations, Cp_2TiCl_2 is antiproliferative against MCF7 (IC$_{50}$ = 570 µM). Interestingly, the titanocene derivative titanocene Y (Figure 4.6) featuring alkylated derivatives of aromatic groups on both Cp rings, in the vein of the type of modification achieved with tamoxifen, does not exhibit a proliferative effect on MCF7 cells [77]. Titanocene Y is a far more hydrolytically stable complex, which could account for this difference in behavior.
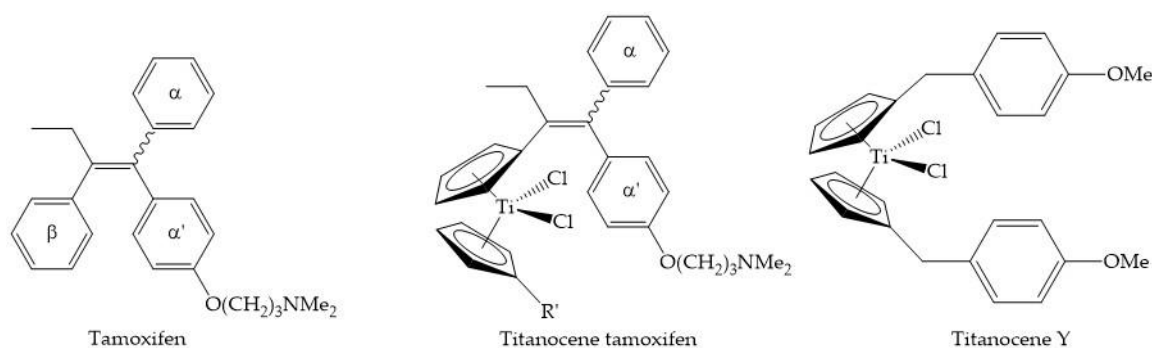
Figure 4.6. The chemical structures for tamoxifen, titanocene tamoxifen, and Titanocene Y.

In a strategy similar to Top et al. [76], Gao et al. synthesized steroid-functionalized titanocenes, with modification of one of the two Cp rings, and determined their activity against MCF7 and colon cancer HT29 cells following 72 h of incubation [78]. The calculated IC$_{50}$ values for the titanocenyl compounds of clionasterol, pregnenolone, dihydrocholesterol, dehydroepiandrosterone, epiandrosterone, androsterone, and cholesterol (Figure 4.7) ranged from 16.2–200 µM against HT29 cells and 13–200 µM against MCF7 cells. These values are much lower than the IC$_{50}$ values determined for Cp_2TiCl_2 against HT29 (413 µM) and MCF7 (570 µM). No proliferative behavior, however, was observed at the low µM concentration range like Top et al. observed in tamoxifen-like modification of Cp_2TiCl_2 [76]. Cholesterol-functionalized titanocenes (clionasterol, dihydrocholesterol, and cholesterol derivatives) exhibited much lower activities (IC$_{50}$ > 200 µM) than the activities of sex steroid-functionalized titanocenes (IC$_{50}$ < 50 µM). This significant and selective increase in activity suggests that the steroid functionalities are facilitating cellular uptake. Gao et al. demonstrated with computational methods that steroid-functionalized titanocenes could bind the

estrogen receptor alpha (ERα; PDB 1A52) [79]. They showed that the steroids on their own docked the protein analogously to the steroid hormone β-estradiol, surrounded by the amino acid residues Glu-353, Arg-394, His-524, Leu-387, and Met-388. However, the steroids conjugated to the titanocenes docked the protein via hydrophobic interactions in a fashion different from β-estradiol. While this result was a very promising finding, Gao et al. report that the steroid-functionalized titanocenes partially decompose in water after a few hours. Nonetheless, even after dissociation, the steroids appear to be able to interact with the titanocenyl moiety and still enable ERα binding of this group [78]. This study reveals a route for titanocenyl uptake through a plasma membrane estrogen receptor.
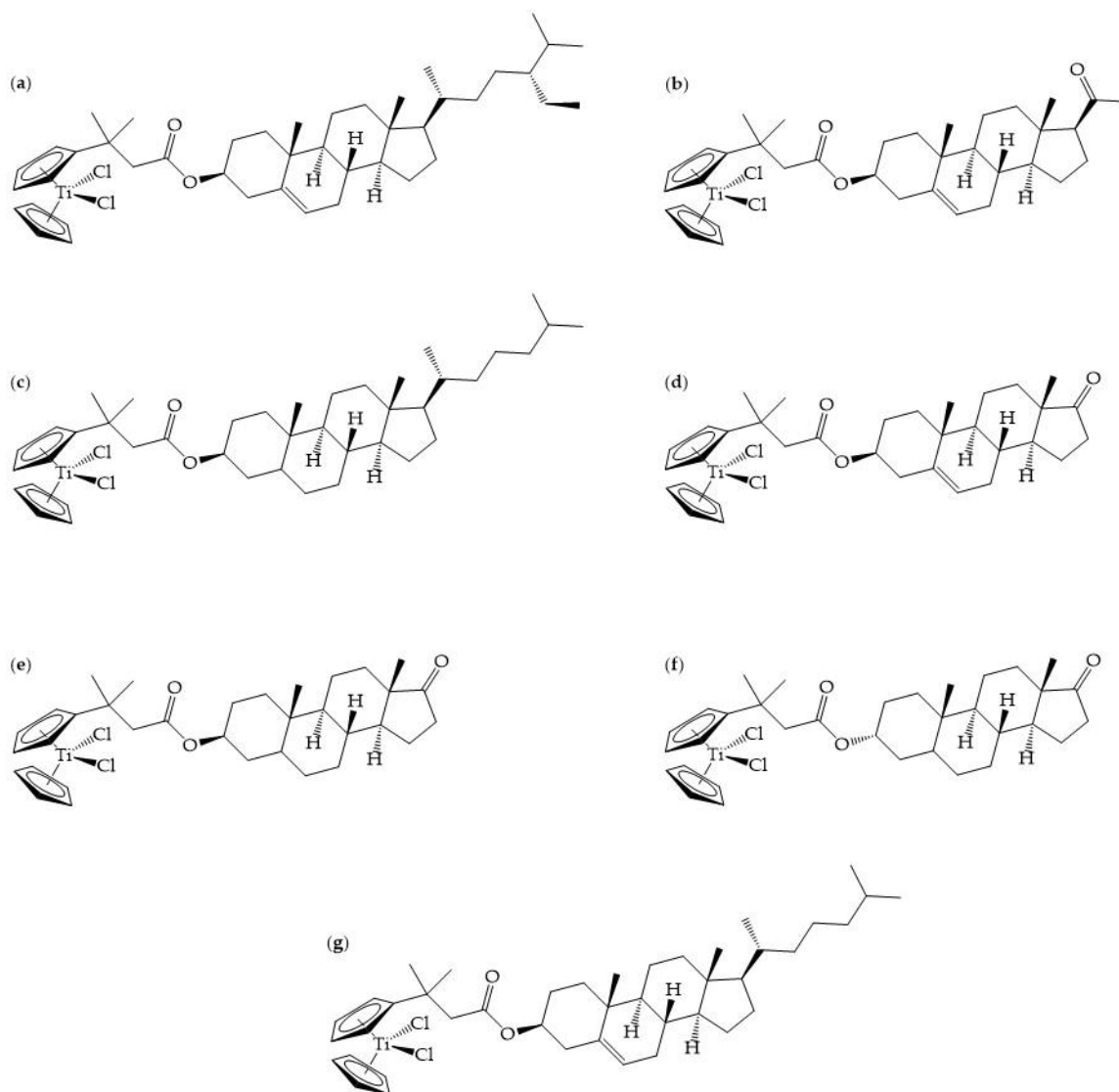
Figure 4.7. The chemical structures for titanocenyl clionasterol (**a**), pregnenolone (**b**), dihydrocholesterol (**c**), dehydroepiandrosterone (**d**), epiandrosterone (**e**), androsterone (**f**), and cholesterol (**g**) [78].

In a series of studies, a different approach was taken to functionalize the titanocene moiety to not only stabilize the compound and enhance its cellular

uptake but to also apply it to specific cancers [80-83]. Titanocene and select derivatives were grafted onto the surface of ceramic materials, including mesoporous silicas, alumina, and hydroxyapatite, that can be used as components of synthetic hard tissues, such as bone fillers or prosthetics (Figure 4.8). The objective is to be able to apply these materials for the treatment of bone tumors and for any remaining surface-bound metallodrugs to prevent reappearance of these tumors. This extensive work has been recently reviewed [74, 84] but we wish to highlight a few key findings. The cytotoxicity of the ceramic materials and their titanocenyl grafted counterparts are measured in terms of M_{50} values, the quantity of material in μg/mL necessary to reduce the cell population's growth by 50%. The ceramic materials alone exhibit very weak antiproliferative behavior, whereas the titanocene grafted material are moderately to strongly antiproliferative [80-83]. Ceballos-Torres et al. conducted a study of titanocenes grafted onto the mesoporous silica-based material KIT-6 [85]. In this work they acknowledged that the relative proportion of titanocene is not identical in all nanostructured materials. They calculated the cytotoxic activity of all of the functionalized materials in terms of Ti M_{50} index, the quantity of anchored Ti needed to inhibit normal cell growth by 50% [85]. Using this approach, they were able to determine a set of these functionalized materials that were highly selective toward cancer cells and displayed potent cytotoxicity. They then characterized their mechanism of cytotoxicity. It was observed that these materials are more strongly apoptotic than their "free" titanocenyl counterparts. The most promising ones are able to stimulate Bax-α proapoptotic expression and decrease Bcl-cl anti-apoptotic expression, and moderately inhibit the activity of PARP-1, a protein that participates in DNA damage repair, through cleavage [85]. They also observed that as in previous studies [81-82], the titanocenyl groups do not dissociate from the materials to interact with DNA. Instead there appears to be a direct interaction between the functionalized materials and DNA through electrostatic interactions. Also of significance, titanocenyl functionalized materials are able to increase the cellular uptake of Ti from about 0.4 to 4.6% of total available Ti (from free titanocenyl moiety) to 4 to 23% [85].

The addition of a vector on the titanocenyl framework may not be a necessity to facilitate enhanced cytotoxicity as can be observed with titanocene Y (Figure 4.6), one of the most active second generation non-vectorized titanocenes. A number of studies have been conducted to evaluate its mechanism of action against different cell lines. Cuffe et al. found that it can cause double-strand breaks and induce apoptosis in the human prostate cancer cell lines PwR-1E, 22Rv1, DU145, and PC3 [86] although likely not via Ti(IV) induced cleavage of the phosphodiester bond of the DNA backbone [53]. They treated PwR-1E and PC-3 cells with titanocene Y for 6, 12, 24, and 48 h and noted no significant effect on the ratio of G_1, S, or G_2 phases of the cell cycle [53]. Bannon et al. examined the effect of titanocene Y on A431 cells (epidermoid carcinoma) and saw a different behavior in terms of effecting the cell cycle [87]. Titanocene Y caused an accumulation of cells in the G_2/M phase and a decrease of cells in the G_1 phase at 24 h before the appearance of a pre-G_1 peak at 48 h. They also found that titanocene Y (50 μM) induces caspase-3 and -7 activation of apoptosis in these cells. Treatment of

A431 xenograft mice with titanocene Y (40 mg·kg⁻¹day⁻¹) for five consecutive days caused a 40% inhibition in mean tumor volume [87].
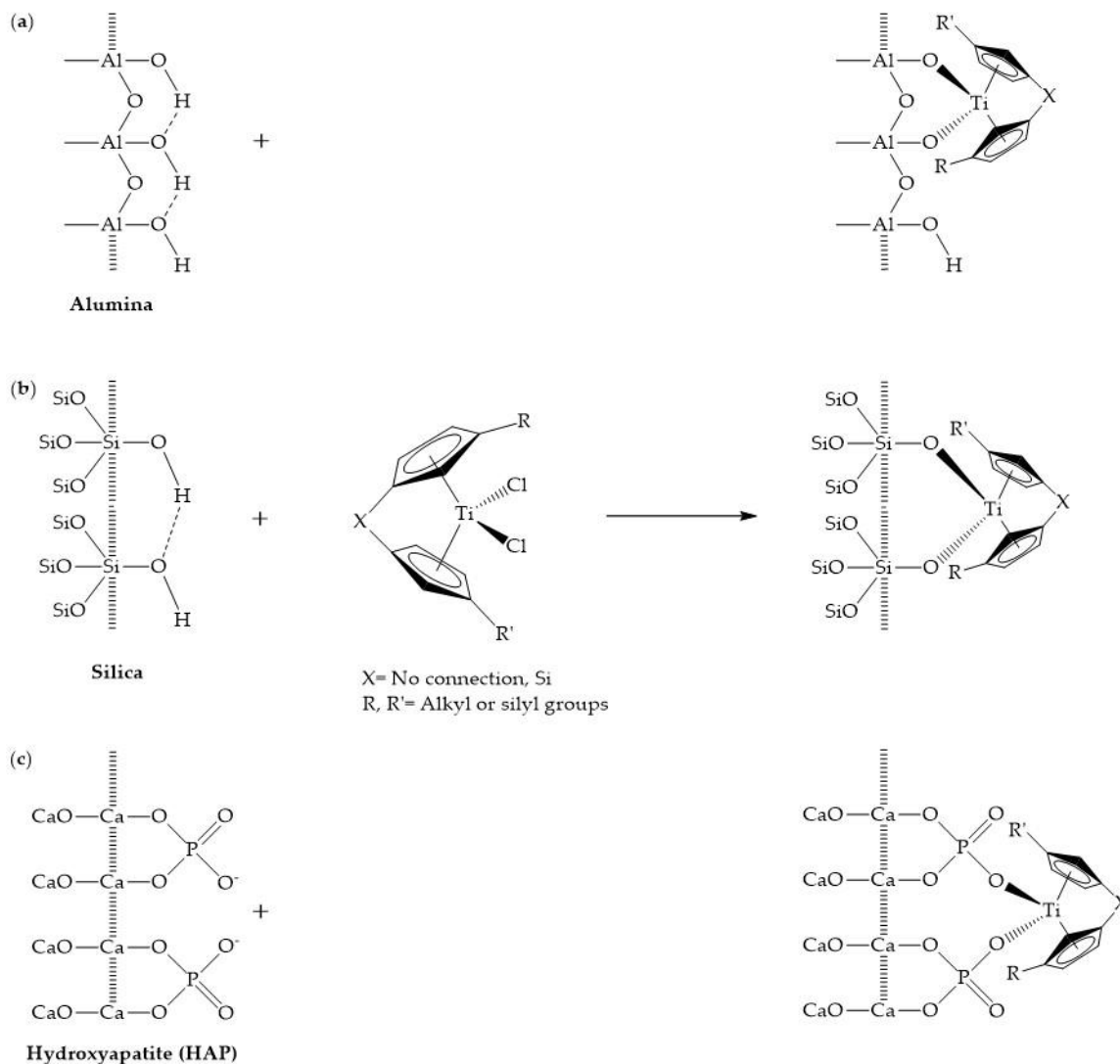
Figure 4.8. The titanocenyl moiety coordinating onto alumina (**a**), mesoporous silica (**b**), and dehydroxylated hydroxyapatite (HAP) (**c**).

Although the identity of the active form of titanocene Y is not yet known, Tacke et al. proposed that the titanocenyl moiety may be able to bind directly to the DNA phosphate backbone. A calculated structure of the DNA-Titanocene Y adduct shows Ti(IV) coordinated bidentate to a phospho group. The titanocenyl moiety is stabilized via a Na⁺ salt bridge interaction between the methoxy groups of the aromatic pendants of the Cp rings and two phospho groups on adjacent sides of the phospho group binding the Ti(IV) (Figure 4.9) [53]. This potentially strong interaction could facilitate greater structural damage to DNA than merely free Ti(IV) binding or even Cp_2Ti^{2+} binding. This strong interaction could impede topoisomerase interaction and thus inhibit DNA replication [57]. HSA binding of the titanocenyl moiety of titanocene Y may be imperative to its cytotoxicity in some

cells. Titanocene Y demonstrates antiproliferative activity against MCF7 cells at low µM only in the presence of albumin [77]. Schur et al. studied the effect of serum proteins on titanocene Y transport into cells [88], which elucidates insight into the active form of the compound. Titanocene Y is much more antiproliferative against MCF7 (IC_{50} = 4.1 µM) and HT29 (IC_{50} = 5.9 µM) cancer cells than titanocene (IC_{50} > 500 µM in both cases). These cell viability experiments were performed using serum containing cell media. Using high-resolution continuum source atomic absorption spectrometry (HR-CS AAS), they determined that titanocene Y binds DNA (290 pmol Ti/µg DNA) and albumin (76% bound) although to a lower extent than titanocene (320 pmol Ti/µg DNA, 98% bound) [88]. When cell culture media contained serum, intracellular titanium in cells incubated with titanocene Y (10 µM) increased 20 times after 27 h but remained below 1 nmol Ti/mg cellular protein. Cells incubated with Cp_2TiCl_2 (10 µM) in the presence of serum exhibited virtually no detectable titanium uptake. Cells incubated with titanocene Y (10 µM) without serum exhibited a significant increase in intracellular titanium after 27 h (4 nmol Ti/mg protein). This finding supports what we have already established that Ti(IV) from Cp_2TiCl_2 and titanocene Y binds strongly to serum transport proteins. For titanocene, sTf and HSA binding of either free Ti(IV) or the titanocenyl moiety, respectively, is likely to impact its cytotoxic potential. It is not clear why no Ti(IV) uptake could be detected except if uncontrolled hydrolysis of the compound occurred in this study resulting in a speciation that affects the nature of how these proteins interacted with the metal ion. For titanocene Y, lower Ti cellular uptake in the presence of serum may not necessarily impede its cytotoxic potential. Titanocene Y is highly stable in water with a half-life of more than a week [89] but its speciation at pH 7.4 has not been reported. In the absence of serum, it may transform into hydrolyzed species that can be taken up by cells but may not result in Ti(IV) in the form of the titanocenyl moiety binding to DNA. In the presence of serum, the titanocenyl group is likely stabilized by rapid and strong binding to albumin. The cellular delivery of this group from albumin appears to be kinetically slow but perhaps a larger % of the titanocenyl moiety is able to bind at DNA, resulting in a more effective cytotoxic behavior. This would explain why titanocene Y shows antiproliferative behavior against MCF7 cells only in the presence of albumin [77].
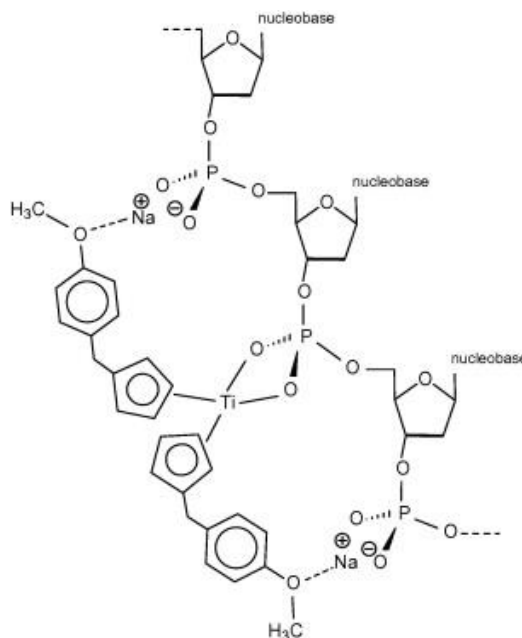
Figure 4.9. The calculated structure for the coordination of the $(\eta^5–C_5H_4–CH_2–C_6H_4–OCH_3)_2Ti^{2+}$ moiety to the phosphobackbone of DNA. Reprinted from Journal of Inorganic Biochemistry, 104, A. Erxleben, J. Claffey, M. Tacke, Binding and hydrolysis studies of antitumoural titanocene dichloride and Titanocene Y with phosphate diesters, 109–125, Copyright (2018), with permission from Elsevier.

Studies that have probed manipulating the titanocenyl ligand platform to deviate from the sTf model of Ti(IV) cellular uptake have led to development of more potent anticancer titanocene compounds. As demonstrated with the small molecule titanocene Y, simple modifications may me enough to make a more powerful and selective drug and is currently the most promising compound to advance Ti(IV), as a monometallic species, back to clinical trials.

4.3. Auranofin and its Ligand Evaluation

4.3.1. Biologically Relevant Au(I) Coordination Chemistry

Under biological conditions, gold (Au) can be found in an oxidation state of +1 and +3. In the reducing environment of cells, Au would predominantly exist in the +1 state [90]. For the purposes of this review, we will focus on pertinent Au(I) coordination chemistry. Au(I) has a completely filled outer electronic shell $([Xe]4f^{14}d^{10})$, is diamagnetic, and, like Ti(IV), has zero CFSE. Also like Ti(IV), the structure of Au(I) complexes are determined by steric effects of the ligands and simple electrostatic interactions that occur between ligands in the coordination environment of the metal ion. However, because Au(I) is a large cation with a low oxidation state, its outer electronic distribution is easily polarized, making it a Soft Lewis Acid, which prefers binding to Soft Lewis Bases. Due to electrostatic reasons, Au(I) has a higher stability in a linear two-coordinate geometry when its ligands are anionic. Au(I) can also form three-coordinate trigonal complexes and

four-coordinate tetrahedral complexes. The higher coordination number is achieved with neutral ligands. Au(I) complexes with monodentate ligands in solution are extremely labile. This lability can be fine-tuned with the use of chelators [91].

4.3.2. Brief History of the Medical Use of Gold

Evidence dating back to 3000 BC suggests that the Egyptians used gold in purifying tonics while the Chinese, as early as 2500 BC, used it in medicines and tinctures for healing [92]. The formal use of Au as a treatment for medical conditions may be credited to two professors at the University of Montpellier in the 19th century: Andre-Jean Chrestien and Pierre Figuier [93]. Together, they worked on the formulation and advocated for the use of Au compounds, such as Au sodium chromide for the treatment of tuberculosis (TB) [93]. In 1890, German bacteriologist Robert Koch found that Au cyanide $K[Au(CN)_2]$ stopped tubercle bacillus from reproducing [94]. Due to this discovery, Au compounds were then evaluated as a treatment for TB. Many TB patients developed rheumatoid arthritis (RA), and it appeared that the Au cyanide alleviated some of the symptoms. However, it was found that the compound was not an effective therapeutic for TB, but was indeed for RA.

In 1960, The Empire Rheumatism Council, now known as Versus Arthritis, confirmed Au salts were an effective treatment for RA. This treatment became known as chrysotherapy. In 1972, Sutton, McGusty, Walz, and DiMartino published a study characterizing a series of Au compounds with trialkylphosphine ligands [95]. These complexes exhibited antiarthritic activity after oral administration to adjuvant arthritic rats. The triethylphosphine Au complexes were found to be the most effective, of which auranofin (AF) was particularly active [95]. AF is a linear Au(I) compound, in which the Au(I) is coordinated to the aforementioned trialkylphosphines and an S-glycosyl group (2,3,4,6-tetra-O-acetyl-1-thio-β-D-glucopyranose) (Figure 4.1).

Finklestein et al. were the first to perform clinical studies with AF (labeled SK&FD-39162) in 1976 [96], evaluating eight patients over six months. AF was administered in the form of 3 mg capsules either twice or three times a day for the first three months and then were given placebo for the remaining three months. Clinical improvement was observed starting at the fifth week of treatment. At the beginning of the trial, there were a total of 60 swollen joints and by week 15, there were only 9 [96]. In this study, no negative effects were observed but the sample size was too small to draw any definite conclusions. Other clinical trials have provided insight into Au(I) side effects and the optimal method of its administration [97-99]. AF, delivered orally, and Au(I) sodium thiomalate (GST), injected intramuscularly, were tested on patients. Both compounds cause gastrointestinal side effects, including diarrhea. They also cause aphthous ulcers, skin rash and pruritis, conjunctivitis and alopecia [97]. Although AF and GST exhibit comparable efficacy, AF causes less side effects [99]. Both are FDA approved (AF was approved in 1985) and have been used clinically to treat RA. Today the use of Au(I) compounds for this purpose is not common especially because their long term use, which is

common due to their slow time for therapeutic effect, results in Au(I) itself triggering autoimmunity diseases [21].

4.3.3. Drug Repurposing of AF for Anticancer Application and an Evaluation of Its Mechanism of Action

At present, one of the mechanisms by which to expedite a promising compound to the drug market for a medical condition is to repurpose a known drug used for a different condition [100]. The benefits of this approach are numerous. Time, money, and human resources are decreased due to clinical trials already having been performed on the drug to examine its toxicity and to determine its safe dosage and optimal method of formulation and administration. AF is one such drug that is being repurposed for many different conditions [101-102]. Interest in AF for anticancer application stemmed from the finding that arthritic patients undergoing gold therapy had statistically lower incidences of cancer [21]. AF was found to be antiproliferative against many tumor cells in vitro [103]. In a study with 15 tumor models in mice, AF was found to be active against P388 leukemia and this was achieved via intraperitoneal administration [104]. A structure activity relationship study of 63 complexes of the general structural formula L–Au–X revealed that in vivo anticancer activity (especially against P388 leukemia) is generally optimized by ligation of Au(I) with a substituted phosphine (L) and thiosugar (X) [105].

Like Cp_2TiCl_2, AF is classified a prodrug. Although Au(I) is able to bind to similar ligands as Pt(II) due to its Soft Lewis Acid nature, the proposed anticancer mechanism of action of AF and related Au(I) complexes is quite distinct from the Pt(II) drugs. DNA is not the primary target of these complexes. Their cytotoxicity is mediated by their ability to alter mitochondrial function and inhibit key enzymes by Au(I) binding strongly to functionally important thiol- or seleno-containing residues. Most of the thiol-containing enzymes, such as thioredoxin reductase (TrxR), glutathione reductase (GR), and cysteine protease, are overexpressed in cancer cells, thus providing potential anticancer targets for Au(I)-based therapy. Thiol groups are important in regulating mitochondrial membrane permeability. A study was performed on mitochondria isolated from rat livers [106]. In the presence of Ca^{2+} ions, Au(I) at submicromolar concentrations was observed to induce mitochondrial permeability transition [106]. In other words, the mitochondrial membrane becomes very permeable. This process appears to be triggered, in part, by Au(I) interfering with the thioredoxin redox system. The thioredoxin redox system comprises thioredoxin (Trx) and thioredoxin reductase (TrxR), which help to maintain redox balance within cells. Trx is found to reduce and activate many transcription factors involved in the regulation of cell growth and survival. Both Trx and TrxR are expressed as isoforms for cytosolic (TrxR1, Trx1) and mitochondrial (TrxR2, Trx2) localization [107]. These enzymes interact with one another in a tightly regulated redox process involving the formation of disulfide bonds in Trx and a sulfide and selenide bond in TrxR (Figure 4.10). As Au(I) binds tightly to thiol and selenol groups, it behaves as a potent inhibitor of Trx and TrxR. TrxR inhibition is particularly high ($IC_{50} = 2.6$ nM for purified enzyme) [108]. AF provokes an alteration of the redox state of the cell, leading to an elevated production of reactive oxygen

species (ROS) beyond homeostatic control, which creates the conditions for apoptosis[107]. Apoptotic induction through a mitochondrion pathway is also observed with AF related complexes [109]. The inhibition of TrxR by these complexes can oxidize peroxiredoxin (Prx) enzymes. Peroxiredoxin 3 (Prx3) protects mitochondria from the ROS agent H_2O_2. This means that disturbance of Prxs can cause mitochondrial damage. High ROS levels disturbs the activity of cytosolic Prx1 and activates p38 MAPK, which can give a signal to the initiator caspase to trigger apoptotic events [107]. This trigger then leads to poly-ADP-ribose polymerase 1 degradation, DNA fragmentation, and finally, cell death. Due to the increased permeability of the mitochondrial membrane, the proapoptotic cytochrome c is released into the cytosol and contributes to signaling caspase-3 activation of apoptosis [108]. Despite DNA not being a direct target of Au(I), its replication can also be affected beyond fragmentation. AF can inhibit DNA polymerases essential for DNA replication if Au(I) binds to catalytically important sulfhydryl groups in these enzymes [102].

4.3.4. Auranofin Therapeutic Limitation due to Its Speciation in the Body

Various studies suggest that Au(I) from AF enters into cells via a sequential thiol exchange mechanism, where cell association of AF occurs from the shuttling of Au(I) between the sulfhydryl groups present on the cell resulting in the dissociation of the thioglucose moiety (Figure 4.9) [110-111]. The intracellular distribution of AF results from shuttling of membrane sulfhydryl bound gold-triethylphosphine to cytosolic sulfhydryl groups [111]. This would be a form of passive transport through the cell membrane. The triethylphosphine is believed to eventually dissociate in the process of Au(I) reaching its intracellular targets. Studies with a triple radioactively labeled auranofin, ^{195}Au, ^{35}S, and ^{32}P, show different rates of clearance from the body. The $t_{1/2}$ for urine excretion is $Et_3^{32}P = O$ (8 h), ^{35}S (16 h), and ^{195}Au (20 days) [112]. These results ultimately suggest that AF is a prodrug.
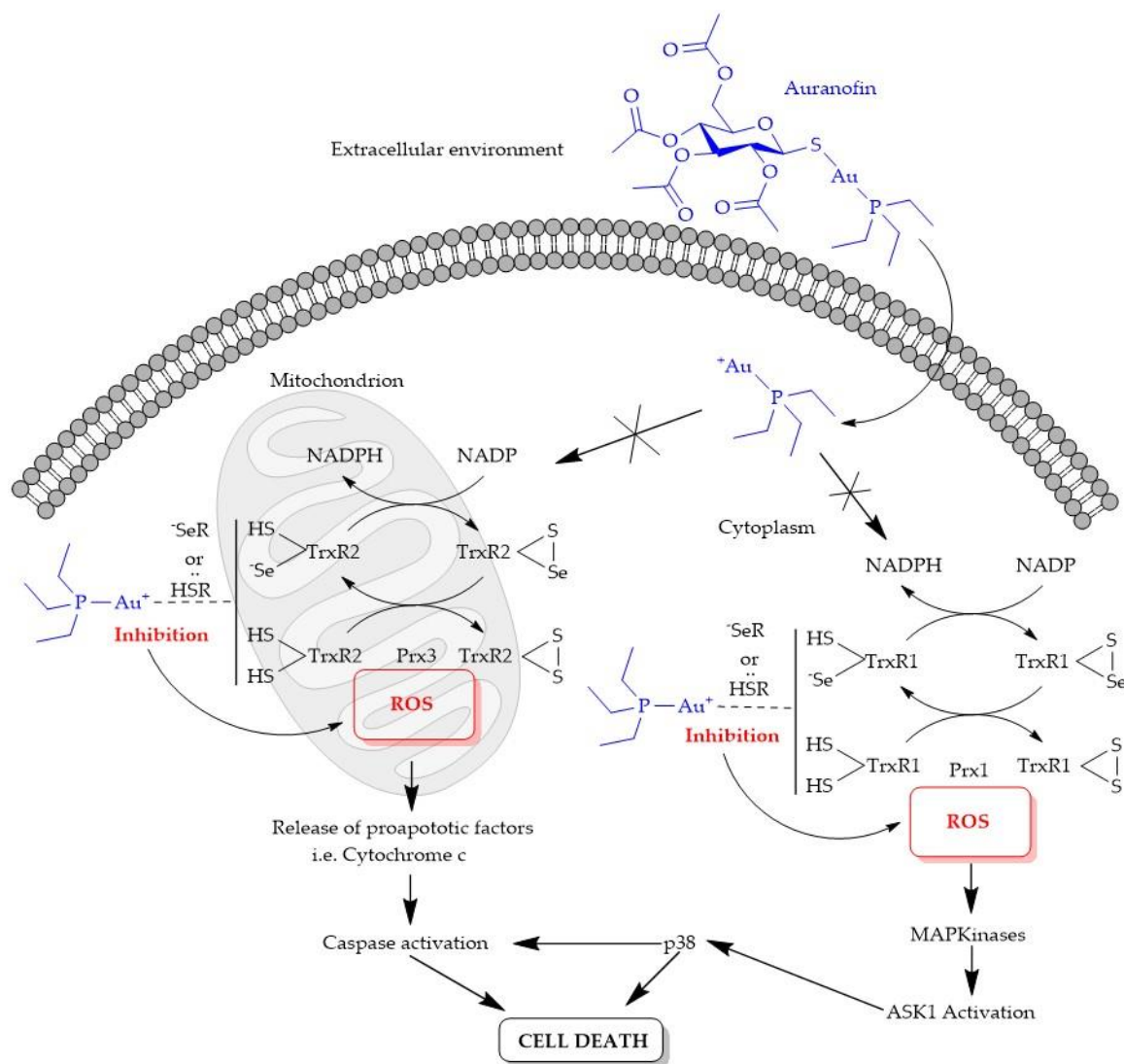
Figure 4.10. The proposed mechanism of cellular uptake and cytotoxicity of auranofin.

The differences in the biological fate of the different components of AF could be due to additional factors involving AF speciation in the body and biomolecular interactions. Although AF is delivered orally, AF is actually not very water soluble. In the acidic conditions of the stomach, AF would rapidly degrade, leading to the loss of the thiosugar [113], but its relative insolubility may help to partially circumvent this issue. It is estimated that 25% of orally administered AF is absorbed from the gastrointestinal tract for distribution throughout the body [114-115]. AF cellular uptake competes with its serum speciation and this competition decreases its antiproliferative behavior [104,99,100]. In blood, AF rapidly interacts with the free cysteine (Cys34) residue of HSA, which results in the dissociation of the thioglucose, yielding a HSA{CysS–Au–PEt₃}. It is not entirely clear whether HSA affinity for the [AuPEt₃]⁺ moiety, hinders Au(I) interaction with and uptake by cell membranes. However, once the PEt₃ ligand dissociates following HSA induced oxidation, forming Et₃PO, the cytotoxicity of Au(I) is believed to be completely

86

ablated. In the presence of the cyanide (CN⁻) ligand, Au(I) from AF quickly dissociates its phosphine and thiosugar ligands to form the highly stable [Au(CN)$_2$]⁻ complex, which can bind to an anionic site of HSA. Though the cyanide ligand exists at very low amounts in the body, it is thought to play a major role in the wide distribution of [Au(CN)$_2$]⁻ in the tissue of chrysotherapy patients [21] but likely serves to attenuate Au(I) cytotoxicity. Within cells, another biomolecular interaction can weaken the cytotoxic potential of AF. Glutathione (GSH), the cytosolic redox regulating small molecule, can strongly bind Au(I). GSH binding can induce the dissociation of the [Au-PEt$_3$]⁺ moiety that manages to enter cells and can deter Au(I) interaction with cellular targets, in a manner analogous to its inhibition of Pt(II)-induced antiproliferation of cells [90].

4.3.5. Modifying the Phosphine and Thiosugar Ligands of Auranofin to Understand Their Mechanistic Contribution

The extreme lability of the Au(I) center limits the therapeutic potential of the prodrug AF and related Au(I) complexes. HSA binding of Au(I) as a consequence of the dissociation of the thiosugar ligand is a pivotal event for the attenuation of its cytotoxicity. A series of structure activity relationship studies have been performed to better understand the importance of the phosphine and thiosugar ligands to the bioactivity of Au(I). These studies provide insight into AF modifications that can make it a less ligand-exchange labile compound and subsequently less able to facilitate Au(I) binding by HSA in order to enhance its cytotoxic potency.

A recent study by Garcia et al. reveals very important ligand structural details that regulate the cytotoxicity of AF derivative complexes [116]. Four two coordinate, nearly linear Au(I) complexes were synthesized in which the phosphine group was either the PEt$_3$ moiety or triphenylphosphine (PPh$_3$) and the thiosugar was replaced with the sulfur coordinating groups 5-adamantyl-1,3-thiazolidine-2-thione (ATT) and 3-methyladamantane-1,3,4-oxadiazle-2-thione (MOT) (Figure 4.11) [116]. Table 4.1 provides an overview of all the cell viability data collected for treatment of these compounds against the cancer cell lines B16-F10 (mouse metastatic melanoma), CT26-WT (murine colon), and 4T1 (mouse metastatic mammary adenocarcinoma) and the non-cancer cell line BHK21 (Baby Hamster Kidney) [116]. Quite apparent is that complete substitution of the thiosugar with a non-sulfur coordinating ligand as in AuPEt$_3$Cl and AuPPh$_3$Cl results in decreased cytotoxic potency by an average factor of 13 to 18 times. Garcia et al. rationalized that substitution of the thiosugar with the adamantyl containing ligands could increase the cytotoxicity because the adamantyl groups help the Au(I) complexes to bind at one of the two active sites of the TrxR enzyme, as shown by molecular docking, before direct Au(I) coordination occurs in the enzyme [116]. However, none of the four adamantyl-containing complexes demonstrated superior inhibitory effect toward TrxR than AF. Interestingly, AuPEt$_3$MOT, in spite of displaying cytotoxicity comparable to AF, is the most promising derivative of this study because it exhibits a superior selectivity index (S.I.) for targeting the cancer cells (S.I. for AuPEt$_3$MOT = 5.8 and S.I. for AF = 3.0). We calculated the selectivity index for each compound by dividing the IC$_{50}$ value for BHK21 cells by the

average IC_{50} value for the three cancer cell lines. The other three adamantyl-containing complexes exhibited inferior cytotoxicity and comparable S.I. to AF. There is no clear structure activity correlation with regards to the potential benefit of utilizing the adamantyl-containing ligands.
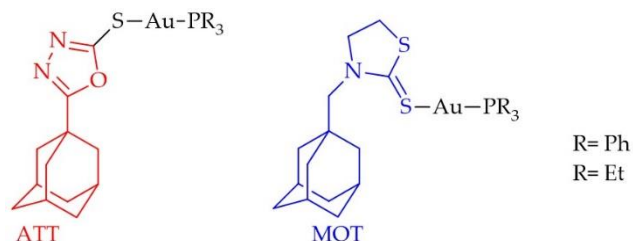
Figure 4.11. The Au(I) complexes with the sulfur coordinating groups 5-adamantyl-1,3-thiazolidine-2-thione (ATT) and 3-methyladamantane-1,3,4-oxadiazle-2-thione (MOT) and the phosphine ligands containing ethyl or phenyl substituents [116].

Table 4.1. Antiproliferative activities of Au(I) complexes against cancer cell lines and inhibition at 5 µM of TrxR activity [116].

Compounds	Cancer Cells IC_{50} (µM ± SD)				TrxR Inhibition (% ± SD)
	B16-F10 Melanoma	CT26-WT Colon	4T1 Breast	Non-Cancer Cell BHK21	
AuPPh₃ATT	5.7 ± 0.5	5.7 ± 0.9	6.6 ± 0.5	18.5 ± 2.9	40.7 ± 1.5
AuPEt₃ATT	1.2 ± 0.2	1.8 ± 0.8	1.6 ± 0.5	5.5 ± 0.1	51.6 ± 1.6
AuPPh₃MOT	1.8 ± 0.5	1.8 ± 0.3	3.0 ± 1.8	6.9 ± 0.8	57.3 ± 0.7
AuPEt₃MOT	1.0 ± 0.1	0.9 ± 0.1	1.1 ± 0.2	5.8 ± 0.1	60.2 ± 0.7
AuPPh₃Cl	6.6 ± 0.1	12.1 ± 2.8	10.3 ± 2.3	23.0 ± 0.3	-
AuPEt₃Cl	2.3 ± 0.5	9.0 ± 0.7	9.5 ± 1.1	22.5 ± 0.2	-
AF	0.5 ± 0.4	0.5 ± 0.4	0.6 ± 0.2	1.6 ± 0.5	59.7 ± 1.5

In the presence of 2 mg/mL of bovine serum albumin (BSA), which shares 80% sequence identity to HSA and can thus be viewed as nearly identical, almost all Au(I) complexes in Garcia et al.'s study exhibited anywhere from 10 to 100 times less cytotoxicity (as gauged by IC_{50} values) against the cancer and noncancer cell lines (Table 4.1) [116]. The decreased cytotoxicity effect was most pronounced for the noncancer cell line likely because, as previously mentioned, cancer cells catabolize albumin significantly more than normal cells [61]. Nonetheless, albumin debilitates the cytotoxicity of AF and related Au(I) complexes [61, 117].

Substitution of the ethyl groups of the phospine ligand to the bulky aromatic groups in Garcia et al.'s study resulted in a decrease in cytotoxicity (Table 4.1) [116]. This decrease in cytotoxicity due to the incorporation of aromatic groups in the phosphine was also observed by Chaves et al. with the very similar Au(I) complexes containing both forms of the phosphine and 3-benzyl-1,3-thiazolidine-2-thione and 5-phenyl-1,3,4-oxadiazole-2-thione as the S-coordinating ligands

[118]. A study by Dean et al. sheds some light as to why this substitution may be undesirable. In their work, they prepared Au(I) compounds with a series of thiourea molecules as the S-coordinating ligands and electron-rich diakyl-aryl phosphines (Figure 4.12) [119]. The hope was that the bulkier phosphine ligands would make them less labile to dissociation. In the presence of HSA, the S-coordinating ligands dissociate rapidly like the thiosugar of AF and the Au(I) phosphine moieties bind to HSA. Unexpectedly, the Au(I) diakyl-aryl phosphine moieties bind more extensively to HSA than $[AuPEt_3]^+$, which coordinates in a 1:1 protein:metal adduct, as monitored by electrospray ionization time of flight mass spectrometry (ESI-TOF MS) (Figure 4.13). The Au(I) complex with the 1,1′-biphenyl-2-yl-di-tert-butylphosphine (JohnPhos) ligand forms adducts with as many as three Au(I) phosphine moieties (Figure 4.13) [119]. This study suggests that the addition of bulky, aromatic groups on the phosphine can result in greater interactions with albumin and subsequently, less cellular uptake of Au(I) and lower cytotoxicity.
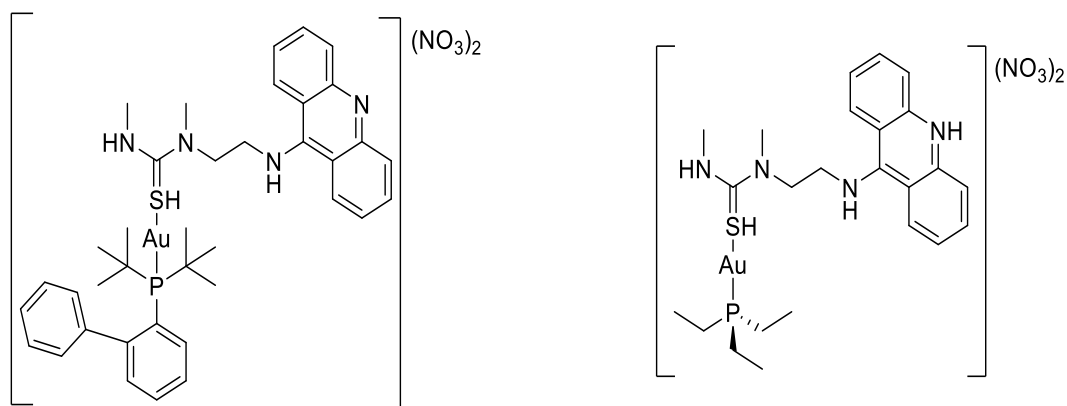
Figure 4.12. The chemical structures for a selection of AF derivatives containing the S-coordinating (1-[2-(acridin-9-ylamino)ethyl]-1,3-dimethylthiourea) (ACRAMTU) ligand and the 1,1′-biphenyl-2-yl]di-tert butylphosphine) (JohnPhos) (**a**) and triethylphosphine (**b**) [119].
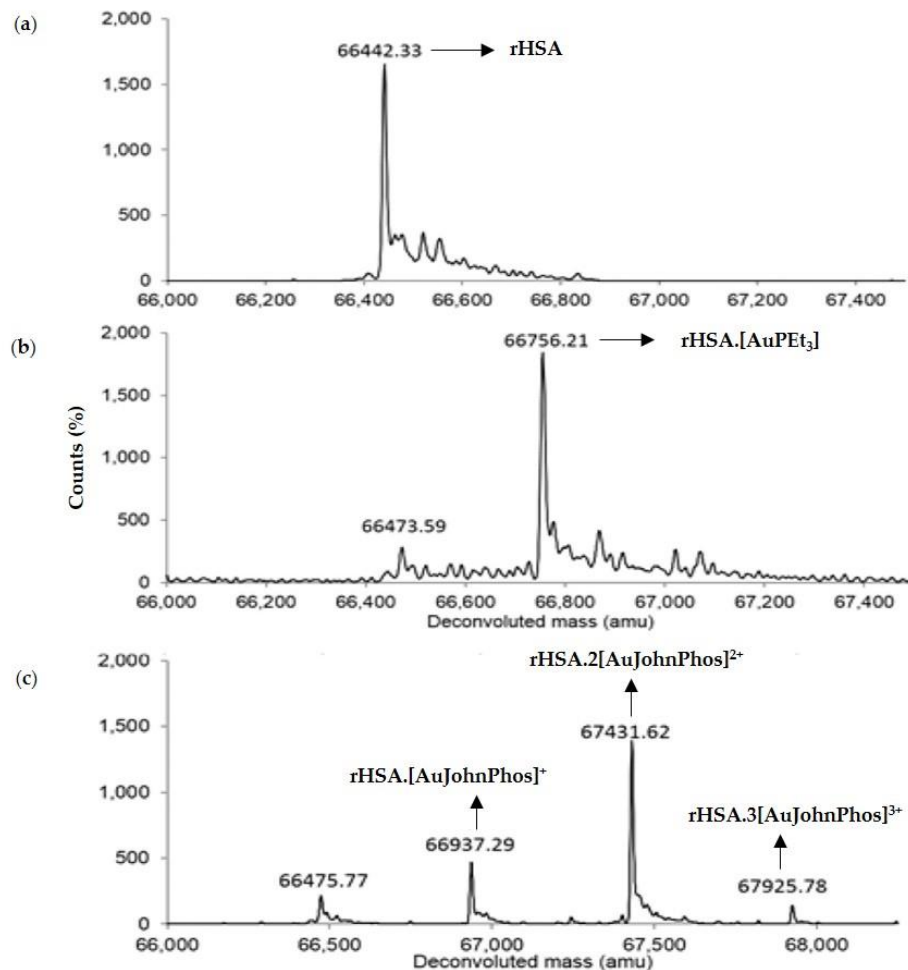
Figure 4.13. The ESI-TOF MS of free HSA (**a**) and HSA reacted with 1.33 equiv. of [AuPEt₃]⁺ (**b**) and 1.75 equiv of [Au(JohnPhos)] (**c**) [119]. Adapted with permission from Dean, T. C.; Yang, M.; Liu, M.; Grayson, J. M.; DeMartino, A. W.; Day, C. S.; Lee, J.; Furdui, C. M.; Bierbach, U. Human Serum Albumin delivered [AuPEt₃]⁺ is a potent inhibitor of T cell proliferation. *ACS Med. Chem. Lett.* **2017**, *8*, 572–576. Copyright (2017) American Chemical Society.

Several studies demonstrate that the thiosugar of AF plays a more significant role than simply enabling sulfyl group exchange transport of the lipophilic [AuPEt₃]⁺ moiety through the cellular membrane. Due to the high trans effect of the phosphine moiety of AF, the sulfur ligand, which is an excellent nucleophile, is more readily labile [30] than it would normally be. Modifying the nucleophilicity of the ligand trans to the phosphine can alter the ligand exchange reactivity of Au(I). Pratesi et al. conducted a study to examine how substitution of the thiosugar in AF with ligands of varying nucleophilicity would impact the interaction of Au(I) with BSA [120]. AuPEt₃X complexes were prepared with the X ligands CN^-, SCN^-, and N_3^-, written in the order of decreasing nucleophilicity [120]. These complexes and AF were incubated with BSA in a 3:1 metal to protein molar ratio at pH 6.8 for up to 72 h. Their interaction with BSA was monitored by ESI-MS by measuring the intact protein mass and accounting for any mass differences that could be due to

90

the formation of Au(I) adducts (Figure 4.14). It was observed that the AuPEt₃X complexes reacted more extensively with BSA as the nucleophilicity of X decreased. The AuPEt₃(CN) compound forms one adduct with BSA, the BSA{CysS34-Au-PEt₃} species, as a consequence of the dissociation of the CN⁻ ligand. A similar result is observed for AF. The ESI-MS data for both complexes show that some amount of free BSA remains present, suggesting that perhaps a significant amount of the complexes may remain intact especially when considering that they were reacted in excess of the protein. The AuPEt₃(SCN) compound forms both a mono [AuPEt₃]⁺ and bis[AuPEt₃]⁺ adduct (BSA{CysS34-Au-PEt₃+[AuPEt₃]⁺}) with BSA after 1 h. By 72 h (at equilibrium) only the mono [AuPEt₃]⁺ adduct is observed, consuming all of the free BSA. The AuPEt₃(N₃) compound only forms the bis[AuPEt₃]⁺ adduct with all of the available BSA.
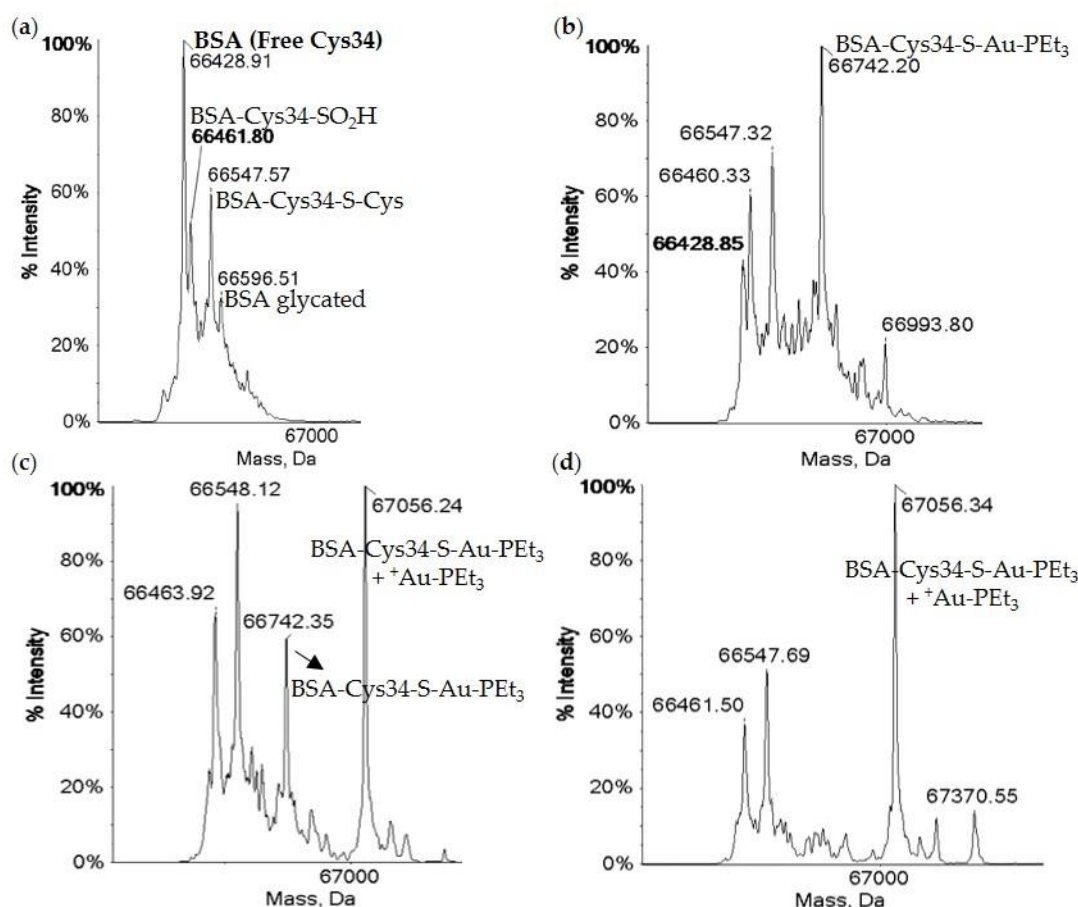
Figure 4.14. The ESI-MS of metal-free BSA (**a**) and BSA (100 µM) incubated with AuPEt₃(CN) (**b**), AuPEt₃(SCN) (**c**), AuPEt₃(N₃) (**d**) in a 3:1 metal to protein molar ratio after 1 h at pH 6.8 (20 mM NH₄ Acetate) and 37 °C [120]. Note that metal-free BSA consists of several post translational modifications (PTMs) and only the Cys34 with no PTM is able to coordinate directly to Au(I). Also note that the incubation with AF produces an MS spectrum virtually identical to (**b**). Adapted with permission from Pratesi, A.; Cirri, D.; Ciofi, L.; Messori, L. Reactions of auranofin and its pseudohalide derivatives with

serum albumin investigated through ESI-Q-TOF MS. *Inorg. Chem.* **2018**, *57*, 10507–10510. Copyright (2018) American Chemical Society.

In 2010, Hill et al. substituted the sulfur of the thioligand of AF with selenium because of the stronger affinity that Se has for Au(I) than S [121]. This substitution had an effect opposite of what was intended. Seleno-auranofin (SeAF; Et$_3$PAuSe-tagl) is extremely labile in aqueous solution, far more than AF, resulting in ligand scrambling and several species forming in solution as observed by ESI-MS (Figure 4.15) [121]. This lability is even more prevalent in the presence of albumin. ^{31}P NMR reveals that albumin degrades SeAF more rapidly than AF (Figure 4.16) [121]. After one hour, the intact SeAF complex no longer exists (a small signal for one of its ligand scrambled products is observed) whereas the intact AF does. There is significant buildup of dissociated Et$_3$PO in the SeAF reaction and little build up in the AF reaction, which suggests that the Se group accelerates the oxidation-induced release of the phosphine from Au(I) coordinated to the Cys34 site of BSA. By 24 h, the majority of the Et$_3$P group from SeAF has transformed into Et$_3$PO. In the case of AF, the majority of Et$_3$P exists as the AuPEt$_3^+$ moiety bound to BSA although there is still some intact AF [121]. These time course results demonstrate that AF is far more labile exchange inert than originally thought.
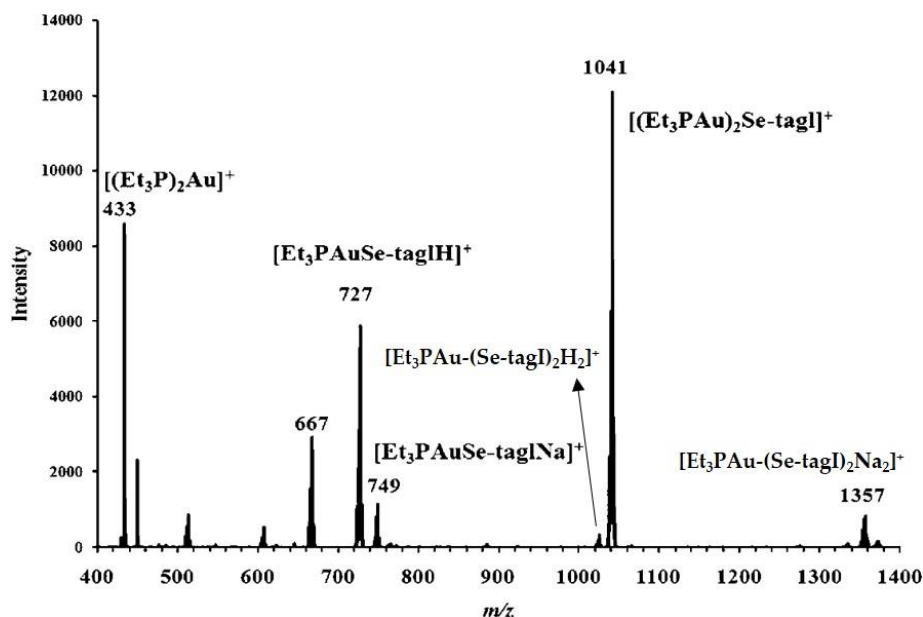
Figure 4.15. The ESI-MS spectra for the speciation of 10 mM SeAF (Et$_3$PAuSe-tagl) in a 1:1 MeOH:H$_2$O solution mixture [121]. Adapted with permission from Hill, D.T.; Isab, A.A.; Griswold, D.E.; DiMartino, M.J.; Matz, E.D.; Figueroa, A.L.; Wawro, J.E.; DeBrosse, C.; Reiff, W.M.; Elder, R.C.; Jones, B.; Webb, J.W.; Shaw, C.F. Seleno-auranofin (Et$_3$PAuSe-tagl): synthesis, spectroscopic (EXAFS, ^{197}Au Mossbauer, ^{31}P, ^{1}H, ^{13}C, and ^{77}Se NMR, ESI-MS) characterization, biological activity, and rapid serum albumin-induced triethylphosphine oxide generation. *Inorg. Chem.* **2010**, *49*, 7663–7675. Copyright (2010) American Chemical Society.
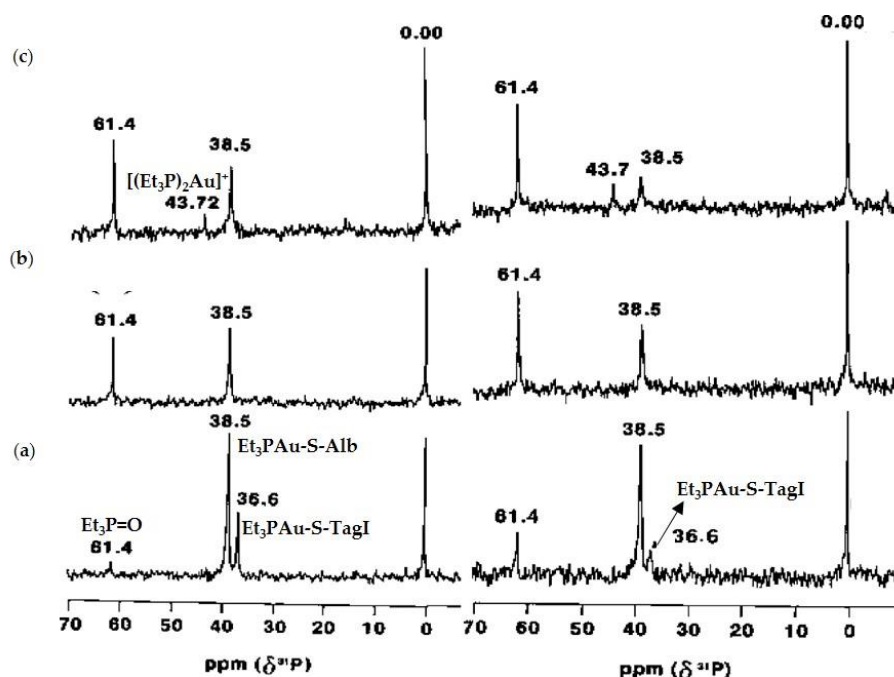
Figure 4.16. $^{31}P\{^1H\}$ NMR spectra of 4.3 mM BSA (containing ~50% free Cys34) incubated with Et$_3$PAuX (X = S-tagl, CN, Se-tagl) at 1:1 ratio with the free Cys34 and measured within 1 h (left) and after 24 h (right) at pH 7.9 in deuterated NH$_4$HCO$_3$ buffer; Et$_3$PAuS-tagl (**a**), Et$_3$PAuCN (**b**), and Et$_3$PAuSe-tagl (**c**) [121]. Adapted with permission from Hill, D.T.; Isab, A.A.; Griswold, D.E.; DiMartino, M.J.; Matz, E.D.; Figueroa, A.L.; Wawro, J.E.; DeBrosse, C.; Reiff, W.M.; Elder, R.C.; Jones, B.; Webb, J.W.; Shaw, C.F. Seleno-auranofin (Et$_3$PAuSe-tagl): synthesis, spectroscopic (EXAFS, ^{197}Au Mossbauer, ^{31}P, ^{1}H, ^{13}C, and ^{77}Se NMR, ESI-MS) characterization, biological activity, and rapid serum albumin-induced triethylphosphine oxide generation. *Inorg. Chem.* **2010**, *49*, 7663–7675. Copyright (2010) American Chemical Society.

Recent efforts have tried to determine whether the thioglucose ligand may be able to facilitate a receptor mediated delivery of AF. The Warburg effect is the experimental observation that cancer cells prefer metabolism via glycolysis, thus, their rapid growth and proliferation usually involves glucose transporter (GLUT) overexpression and increased glucose uptake. This gives promise to the design of metallodrugs with glucose-like or glycomimetic moieties as semi-targeted anticancer treatments [122]. Walther et al. synthesized and studied the in vitro and in vivo anticancer properties of an AF analogue (NHC*-AuSR), in which a 1,3-dibenzyl-4,5-diphenyl-imidazon-2-ylidene ligand (NHC*) replaces AF's triethylphosphine ligand (Figure 4.17). Nitrogen heterocyclic carbene (NHC) ligands have attracted much attention for the development of anticancer metallodrugs due to their high stability and ease of modification. The anticancer properties of the compound was compared to those of the chloro derivative (NHC*-AuCl) in order to determine if the thioglucose ligand enhances the compound's cellular uptake through glucose transporters. Their antiproliferative potency against 60 cancer cell lines (the NCI-60 cancer cell line panel), their *in*

vivo toxicity and tumor growth inhibition against a human renal cancer cell line (CAKi-1) tumor in a xenograft mouse model, and their TrxR inhibition were assessed. Also, computational molecular modelling was used to determine if the thioglucose analogue could be a glucose transporter ligand [123]. The results showed that both compounds exhibited very good cytotoxicity against a wide range of cancer cell lines, mostly at micromolar concentrations. In the tumor xenograft experiment, both compounds caused significant and almost identical tumor volume growth reductions while also being of low toxicity. Thirty-five days after tumor transplantation, the tumor volume of the Au(I) compound treated mice was <50% that of the control group. Significant TrxR inhibition by both compounds (IC_{50} = 1.5 ± 0.2 μM for NHC-AuCl and 3.1 ± 0.4 μM for NHC*-AuSR) occurred. However, this inhibition was weaker than AF (IC_{50} = 90 nM) [123]. Like AF, the two Au(I) compounds enhanced oxidative stress resulting in apoptotic cell death. The molecular modeling results suggested that the thioglucose analogue could be a potential ligand for glucose transporter 1 [123].
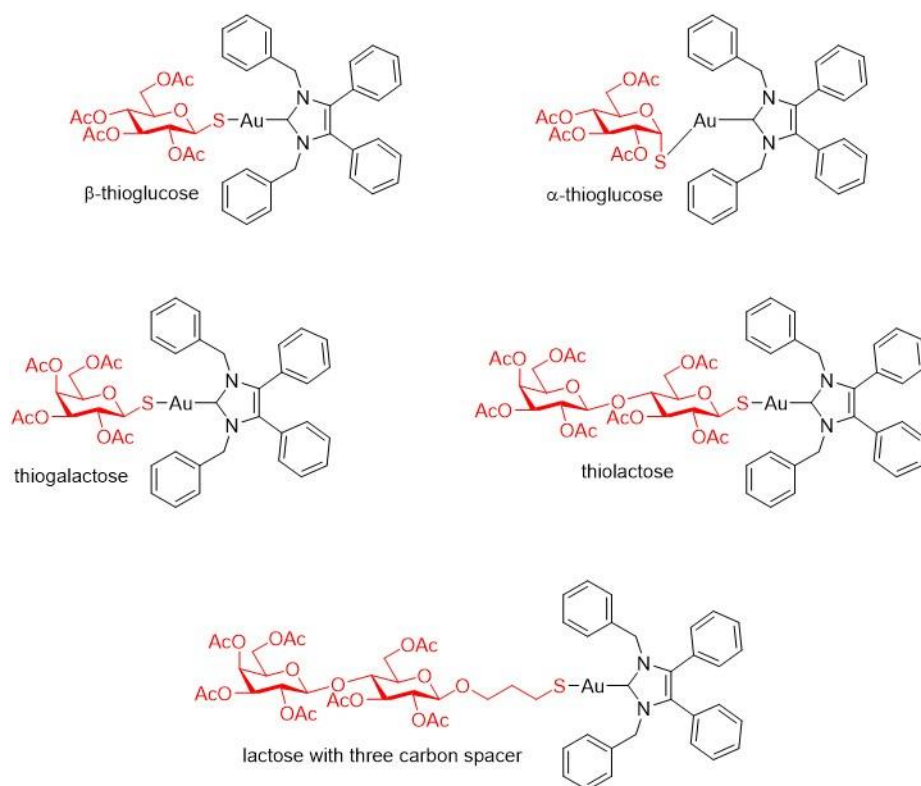
Figure 4.17. The structures of (1,3-dibenzyl-4,5-diphenyl-imidazon-2-ylidene)gold(I) complexes containing different sugars [122].

To further study the role of the thioglucose ligand of the AF analogue, Dada et al. studied the replacement of this ligand with other sugars that have been conjugated to anticancer drugs in order to take advantage of the GLUT-mediated cellular uptake, which could potentially lead to a heightened activity [122]. In addition to AF's β-thioglucose, the other sugar moieties they studied were α-thioglucose, galactose, lactose and also lactose with a three-carbon spacer between the sugar

and the metal (Figure 4.17). All of the compounds were synthesized, characterized, and evaluated for their cytotoxicity against the NCI-60 cancer cell line panel. Generally, all of the synthesized compounds demonstrated good activity against the tested cancer cell lines at medium to low micromolar concentrations, while the α-thioglucose analogue exhibited the best activity overall at low micromolar to nanomolar concentrations. It should be noted that, in addition to the α-thioglucose analogue, the lactose analogue without the three-carbon spacer also exhibited better activity than the β-thioglucose analogue. It is remarkable how, in this case, simply changing the stereochemistry of the anomeric site of the original thioglucose ligand resulted in enhanced cytotoxicity against multiple cancer cell lines, even more than replacing the ligand for other sugar moieties that interact with GLUT. This could be considered a plausible modification to the β-thiosugar ligand of AF in order to potentially improve its cellular uptake via an alternative transport route and, consequently, its anticancer potency [122].

4.3.6. AF in Anticancer Clinical Trials

AF has advanced to clinical trials for its potential as a cancer chemotherapeutic [124]. The Mayo Clinic in Rochester, MI completed a Phase 1 trial to evaluate treatment of ten patients with asymptomatic ovarian cancer with cancer antigen 125 (CA-125) elevation [125]. The patients received 3 mg AF orally twice per day for 28 days. Some patients reported experiencing diarrhea, nausea, vomiting, fatigue, thrombocytopenia, and thromboembolism, none of which exceeded grade 2 of severity. Overall, AF was well-tolerated. Four patients manifested stable disease, one patient was removed from the study due to cancer progression, and one patient died. The median progression-free survival was 2.8 months. The clinic has move forward with a Phase 2 trial to determine whether the combination of AF and sirolimus can provide effective treatment of patients with ovarian cancer. The study is ongoing and involves 22 patients and the main objective is to evaluate the tumor response rate, progression-free survival, overall survival, and adverse events of participants. The Mayo Clinic in Arizona is performing a PhaseI/II trial on 47 patients to study the side effects and best dose of AF when given in combination with sirolimus to determine the effectiveness of this approach on lung cancer patients that have metastasized and cannot be treated with other methods or have experienced cancer recurrence. The University of Ulm School of Medicine is performing a proof of concept Phase 1 and 2 trial to evaluate the safety of the coordinated undermining of survival paths by 9 repurposed drugs (aprepitant, minocycline, disulfiram, celecoxib, sertraline, captopril, itraconasole, and AF) combined with metronomic temozolomide for recurrent glioblastoma. This trial will involve ten patients that undergo different cycles of the combination of temozolomide with the different repurposed drugs over the course of a year. The University of Kansas Medical Center performed a phase I/II clinical trial with five chronic lymphocytic leukemia (CLL) patients and one small lymphocytic lymphoma (SLL) patient. The patients were given 6 mg of AF daily for 28-day cycles, with a dose increase to 9 mg after the first cycle if no grade ≥2 toxicity was observed. The best response was stable disease. CLL cells

were isolated from blood samples to evaluate the in vivo effect of AF. One day following the first dose administration of AF, there was an increase in the levels of ROS and similar increase in apoptosis. In addition, there were changes in genes regulating redox homeostasis. This is characteristic of the proposed mechanism of AF. However, by day 7, these changes reverted back to baseline. This suggests that there is an in vivo adaptive response to resist the effect of AF and consequently resulted in limited clinical activity of AF. No results were reported for the SLL patient [125]. The researchers plan to continue in vivo studies of AF on CLL patients at higher doses [126].

4.4. Fusing the Auranofin and Titanocene Moieties to Create a Bimetallic Complex with Heightened Cytotoxic Potency

An intriguing approach to exploit the distinct cytotoxic mechanism of action of Ti(IV) and Au(I) is synergizing their activity in the form of heterometallic compounds [5-8, 127-130]. These compounds build off of the titanocene structure. In the zero generation compounds, the gold binding moieties were conjugated to the Cp rings [8]. However, these compounds were not very stable in solution due to Cp ring dissociation. In the subsequent generations, the gold binding moieties were/are conjugated to groups that provide an oxygen ligation to the Ti(IV) and are far more stable [8]. Herein we will only focus on a select set of studies by Contel et al. centered on the fusion of the auranofin-like and titanocenyl moieties designed under the premise that two metals with different mechanism of actions will have a synergistic cytotoxic effect. In 2014, they prepared titanocene-gold complexes, one of which was the compound $Cp_2Ti(OC(O)-4-C_6H_4PPh_2AuCl)_2$ (Figure 4.17) [128]. Treatment of several cancer cell lines with this heterometallic compound and the titanocenyl-free version demonstrated a profound synergistic decrease in the cell viabilities for the heterometallic compound (Table 2). This very significant synergism is something that would most definitely not have been achieved by mere co-treatment of the titanocenyl and Au(I) components of these compounds. From a surface perspective, this work demonstrates that two metals can be better than one in killing cancer cells. We believe that there is more at play. The choice of ligands and how they were designed to carefully coordinate both Au(I) and Ti(IV) possibly affords greater ligand exchange inertness to both metal ions and, as a positive consequence, decreased debilitating serum protein interaction. This is true even when the Cp rings dissociate. These results could explain the better activity exhibited by these compounds versus the zero generation compounds and the enhanced synergistic effect. A 2015 follow-up study was performed with a heterometallic compound $Cp_2Ti(CH_3)OC(O)-4-C_6H_4SAuPPh_3$ (Figure 4.18), which features Au(I) in a ligation more analogous to AF [129]. This compound is very potently cytotoxic against the cancer cell lines examined (IC_{50} ~ mid nM to very low µM). Cellular uptake of the compound in Caki-1 cells (human renal cancer) demonstrated that the compound is quite robust as it appears to enter intact, with co-localization of both metals and a dose-dependent increase in their levels. This apoptotic compound features the signature activity of AF by inhibiting thioredoxin reductase and of Cp_2Ti^{2+} in being unable to induce a direct DNA strand break [129]. In vivo studies also showed an

important decrease of tumor size by 67% compared to the control, supporting the in vitro studies in which this compound is able to block the growth of renal cancer [114]. More recent studies in 2019 showed that $Cp_2Ti-OC(O)-4-C_6H_4SAuPPh_3$ (Figure 4.18) and an ethyl derivative $Cp_2Ti-OC(O)-4-C_6H_4SAuPEt_3$, can attack more than one characteristic of cancer such as migration, invasion and angiogenesis while being more selective that monometallic counterparts [7]. These heterometallic Au(I) and Ti(IV) hold great potential for clinical screening.

$Cp_2Ti(OC(O)-4-C_6H_4PPh_2AuCl)_2$

$Cp_2Ti(CH_3)OC(O)-4-C_6H_4SAuPPh_3$
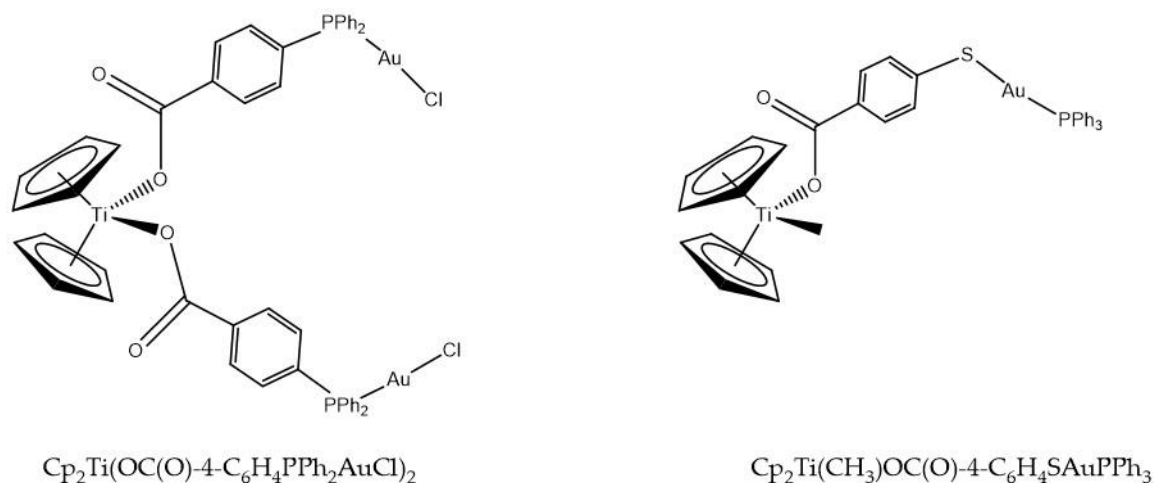
Figure 4.18. The chemical structures for $Cp_2Ti(OC(O)-4-C_6H_4PPh_2AuCl)_2$ and $Cp_2Ti(CH_3)OC(O)-4-C_6H_4SAuPPh_3$.

Table 2. Antiproliferative activities (µM ± SD) of Ti(IV)–Au(I) complexes against cancer cell lines.

Compounds	A498 Kidney	UO31 Kidney	Caki-1 Kidney	HEK-293T Kidney	PC3 Prostate	DU145 Prostate
$Cp_2Ti-(OC(O)-4-C_6H_4PPh_2AuCl)_2$	6.9 ± 2.2	0.3 ± 0.06	1.0 ± 0.29	20.1 ± 1.6	37.7 ± 7.1	6.6 ± 1.8
$HOC(O)-4-C_6H_4PPh_2AuCl$	21 ± 2.5	1.2 ± 0.8	19.2 ± 2.9	31 ± 0.9	78 ± 18.1	39 ± 5.7
$Cp_2Ti-OC(O)-4-C_6H_4SAuPPh_3$	ND	ND	0.12 ± 0.003	0.49 ± 0.008	ND	ND
$C_6H_4SAuPPh_3$	ND	ND	2.76 ± 0.35	1.11 ± 0.65	ND	ND
Cisplatin	37.2 ± 4.6	8.9 ± 2.7	29 ± 4.1	3.2 ± 0.13	14 ± 2.3	12.1 ± 3.9
Cp_2TiCl_2	>200	>200	>200	>200	>200	>200
Titanocene Y	29.6 ± 2.8	>200	29.4 ± 4.2	>200	58.1 ± 11.2	55.2 ± 7.9

4.5.   Conclusions and Future Directions

Empirically driven research has led to many breakthroughs in the medical field. It brought the serendipitous finding of the anticancer properties of cisplatin, which gave birth to a scientific Renaissance to explore other metals in medicine that led to the discoveries of Cp_2TiCl_2 and AF. Like cisplatin, Cp_2TiCl_2 and AF are classified as prodrugs. The distinct metal centers of these compounds confer different coordination chemistries and interactions with biomolecules, which subsequently results in different effects on cells. However, by dissecting the

biological speciation of these compounds and their mechanism of action within cells and in vivo, much insight has been gained about the limitations posed to their therapeutic potential and about how the ligands can be fine-tuned to play a more active role to increase potency and specificity for cancer cells. It has become more apparent that decreasing the ligand exchange lability of the titanocenyl moiety and the thio and phosphine ligands of AF is essential as is altering structural features of these ligands to minimize serum protein interactions that hinder their cellular uptake and/or alter their speciation by producing noncytotoxic species. In the case of the titanocene family of compounds, the titanocenyl moiety may in fact be very important to damaging DNA and leading to cell death and so minimizing the synergistic destabilization of these compounds by STf and citrate is necessary. For the AF family of compounds, preserving the core ligation is needed to prevent HSA induced dissociation of the compound. Functionalizing the ligands of both compounds with biological vectors or inorganic nanoparticles can aid in facilitating alternative cell uptake routes that can result in higher cellular levels of intact compounds. Deviating from the core ligation of the AF and Cp_2Ti^{2+} moieties can dramatically alter the cellular effect of Au(I) and Ti(IV) by not only improving the ligand-dissociation stability and biomolecular interactions of the metal ion [21, 89, 131-133] but also potentially changing the intracellular targets of the metals [9, 28, 34, 133-134].

4.6. REFERENCES

1. Bertini, I.; Gray, H. B.; Stiefel, E. I.; Valentine, J. S., *Biological Inorganic Chemistry: Structure and Reactivity*. University Science Books: California, 2007; p 95-135.
2. Abeysinghe, P. M.; Harding, M. M., *Dalton Trans.* **2007,** (32), 3474-82.
3. Bannon, J. H.; Fichtner, I.; O'Neill, A.; Pampillon, C.; Sweeney, N. J.; Strohfeldt, K.; Watson, R. W.; Tacke, M.; Mc Gee, M. M., *Br. J. Cancer* **2007,** *97* (9), 1234-41.
4. Beckhove, P.; Oberschmidt, O.; Hanauske, A. R.; Pampillon, C.; Schirrmacher, V.; Sweeney, N. J.; Strohfeldt, K.; Tacke, M., *Anticancer Drugs* **2007,** *18* (3), 311-5.
5. Curado, N.; Contel, M., CHAPTER 6 Heterometallic Complexes as Anticancer Agents. In *Metal-based Anticancer Agents*, The Royal Society of Chemistry: 2019; pp 143-168.
6. Curado, N.; Giménez, N.; Miachin, K.; Aliaga-Lavrijsen, M.; Cornejo, M. A.; Jarzecki, A. A.; Contel, M., *ChemMedChem.* **2019,** *14* (11), 1086-1095.
7. Elie, B. T.; Fernandez-Gallardo, J.; Curado, N.; Cornejo, M. A.; Ramos, J. W.; Contel, M., *Eur. J. Med. Chem.* **2019,** *161*, 310-322.
8. Mui, Y. F.; Fernandez-Gallardo, J.; Elie, B. T.; Gubran, A.; Maluenda, I.; Sanau, M.; Navarro, O.; Contel, M., *Organometallics* **2016,** *35* (9), 1218-1227.
9. Loza-Rosas, S. A.; Vazquez, A. M.; Rivero, K. I.; L.J., N.; Delgado, Y.; Benjamin-Rivera, J. A.; Vazquez-Maldonado, A. L.; Parks, T. B.; Munet-Colon, C.; Tinoco, A. D., *Inorg. Chem.* **2017,** *56*, 7788-7802.
10. Gaur, K.; Pérez Otero, S. C.; Benjamín-Rivera, J. A.; Rodríguez, I.; Loza-Rosas, S. A.; Vázquez Salgado, A. M.; Akam, E. A.; Hernández-Matias, L.; Sharma, R. K.; Alicea, N.; Kowaleff, M.; Washington, A. V.; Astashkin, A. V.; Tomat, E.; Tinoco, A. D., *JACS Au* **2021**, https://doi.org/10.1021/jacsau.1c00078.
11. Fernández-Vega, L.; Ruiz Silva, V. A.; Domínguez-González, T. M.; Claudio-Betancourt, S.; Toro-Maldonado, R. E.; Capre Maso, L. C.; Sanabria Ortiz, K.; Pérez-Verdejo, J. A.; Román González, J.; Rosado-Fraticelli, G. T.; Pagán Meléndez, F.; Betancourt Santiago, F. M.; Rivera-Rivera, D. A.; Martínez Navarro, C.; Bruno Chardón, A. C.; Vera, A. O.; Tinoco, A. D., *Inorganics* **2020,** *8* (2), 10.
12. Institute for Health Metrics and Evaluation, Global Burden of Disease. https://vizhub.healthdata.org/cod/ (accessed 29 November 2019).
13. Siegel, R. L.; Miller, K. D.; Jemal, A., *CA Cancer J. Clin.* **2019,** *69* (1), 7-34.
14. Approved drug products with therapeutic equivalence evaluations (Orange Book) https://www.fda.gov/drugs/resources-information-approved-drugs/approved-drug-products-therapeutic-equivalence-evaluations-orange-book (accessed 1 November 2019).
15. Rosenberg, B.; Vancamp, L.; Krigas, T., *Nature* **1965,** *205* (4972), 698-699.
16. Muggia, F.; Farrell, N., *Crit. Rev. Oncol. Hematol.* **2005,** *1* (53), 1-2.

17.   Dilruba, S.; Kalayda, G. V., *Cancer Chemother. Pharmacol.* **2016,** *77* (6), 1103-1124.

18.   Rabik, C. A.; Dolan, M. E., *Cancer Treat. Rev.* **2007,** *33* (1), 9-23.

19.   Siddik, Z. H., *Oncogene* **2003,** *22* (47), 7265.

20.   Fuertes, M. A.; Alonso, C.; Perez, J. M., *Chem. Rev.* **2003,** *103* (3), 645-62.

21.   Dabrowiak, J. C., *Metals in Medicine*. 2nd ed.; Wiley: 2017; p 452.

22.   Descôteaux, C.; Provencher-Mandeville, J.; Mathieu, I.; Perron, V.; Mandal, S. K.; Asselin, E.; Bérubé, G., *Bioorg. Med. Chem. Lett.* **2003,** *13* (22), 3927-3931.

23.   Van Themsche, C.; Parent, S.; Leblanc, V.; Descoteaux, C.; Simard, A. M.; Berube, G.; Asselin, E., *Endocr. Relat. Cancer* **2009,** *16* (4), 1185-95.

24.   Aris, S. M.; Farrell, N. P., *Eur. J. Inorg. Chem.* **2009,** *2009* (10), 1293-1293.

25.   Dhar, S.; Liu, Z.; Thomale, J.; Dai, H.; Lippard, S. J., *JACS* **2008,** *130* (34), 11467-11476.

26.   Cotton, F. A.; Wilkinson, G.; Murillo, C. A.; Bochman, M., *Adv. Inorg. Chem.* John Wiley & Sons, Inc.: United States of America, 1999.

27.   Buettner, K. M.; Valentine, A. M., *Chem. Rev.* **2011,** *112* (3), 1863-1881.

28.   Saxena, M.; Loza Rosas, S.; Gaur, K.; Sharma, S.; Perez Otero, S. C.; Tinoco, A. D., *Coord. Chem. Rev.* **2018,** *363*, 109-125.

29.   Valentine, A. M., *Encyclopedia of Inorganic Chemistry* **2006**.

30.   Housecroft, C. E.; Sharpe, A. G., *Inorg. Chem.* 4th ed.; Pearson: 2012.

31.   Graetzel, M.; Rotzinger, F. P., *Inorg. Chem.* **1985,** *24* (14), 2320-2321.

32.   Schmidt, J.; Vogelsberger, W., *J. Solut. Chem.* **2009,** *38* (10), 1267-1282.

33.   Guo, M.; Harvey, I.; Campopiano, D. J.; Sadler, P. J., *Angew. Chem.* **2006,** *45* (17), 2758-2761.

34.   Tinoco, A. D.; Thomas, H. R.; Incarvito, C. D.; Saghatelian, A.; Valentine, A. M., *PNAS* **2012,** *109* (13), 5016-5021.

35.   Guo, M. L.; Sun, H. Z.; Bihari, S.; Parkinson, J. A.; Gould, R. O.; Parsons, S.; Sadler, P. J., *Inorg. Chem.* **2000,** *39* (2), 206-215.

36.   Keppler, B. K.; Friesen, C.; Moritz, H. G.; Vongerichten, H.; Vogel, E., *Struct. Bond.* **1991,** *78*, 97-127.

37.   Köpf, H.; Köpf-Maier, P., *Angew. Chem.* **1979,** *18* (6), 477-478.

38.   Köpf-Maier, P.; Köpf, H. In *Transition and main-group metal cyclopentadienyl complexes: Preclinical studies on a series of antitumor agents of different structural type*, Berlin, Heidelberg, Springer Berlin Heidelberg: Berlin, Heidelberg, 1988; pp 103-185.

39.   Harding, M. M.; Mokdsi, G., *Curr. Med. Chem.* **2000,** *7* (12), 1289-303.

40.   Olszewski, U.; Hamilton, G., *Anti-Cancer Agents Med. Chem.* **2010,** *10* (4), 302-311.

41.   Toney, J. H.; Marks, T. J., *JACS* **1985,** *107* (4), 947-953.

42.   Williams, J.; Moreton, K., *Biochem. J.* **1980,** *185* (2), 483-488.

43.   Sun, H.; Li, H.; Sadler, P. J., *Chem. Rev.* **1999,** *99* (9), 2817-2842.

44.   Vincent, J. B.; Love, S., *Biochim. Biophys. Acta Gen. Subj.* **2012,** *1820* (3), 362-378.

45.   Bonvin, G.; Bobst, C. E.; Kaltashov, I. A., *Int. J. Mass Spectrom.* **2017,** *420* (Supplement C), 74-82.

46.   Sun, H.; Li, H.; Weir, R. A.; Sadler, P. J., *Angew. Chem.* **1998,** *37* (11), 1577-1579.
47.   Messori, L.; Orioli, P.; Banholzer, V.; Pais, I.; Zatta, P., *Febs Lett.* **1999,** *442* (2-3), 157-161.
48.   Guo, M.; Sun, H.; McArdle, H. J.; Gambling, L.; Sadler, P. J., *Biochemistry* **2000,** *39* (33), 10023-10033.
49.   Shen, Y.; Li, X.; Dong, D.; Zhang, B.; Xue, Y.; Shang, P., *Am. J. Cancer Res.* **2018,** *8* (6), 916-931.
50.   Tinoco, A. D.; Saxena, M.; Sharma, S.; Noinaj, N.; Delgado, Y.; Quiñones González, E. P.; Conklin, S. E.; Zambrana, N.; Loza-Rosas, S. A.; Parks, T. B., *JACS* **2016,** *138* (17), 5659-5665.
51.   Köpf-Maier, P., *Acta Histochem.* **1991,** *91* (1), 25-37.
52.   Guo, M.; Guo, Z.; Sadler, P. J., *J. Biol. Inorg. Chem.* **2001,** *6* (7), 698-707.
53.   Erxleben, A.; Claffey, J.; Tacke, M., *J. Inorg. Biochem.* **2010,** *104* (4), 390-6.
54.   Wang, H.; Zhong, J.; Xiao, K.; Tian, Z., *Sep. Sci. Plus* **2018,** *1* (2), 93-99.
55.   Christodoulou, C. V.; Eliopoulos, A. G.; Young, L. S.; Hodgkins, L.; Ferry, D. R.; Kerr, D. J.,   *Br. J. Cancer* **1998,** *77* (12), 2088-2097.
56.   Olszewski, U.; Deally, A.; Tacke, M.; Hamilton, G., *Neoplasia* **2012,** *14* (9), 813-822.
57.   Mokdsi, G.; Harding, M. M., *J. Inorg. Biochem.* **2001,** *83* (2–3), 205-209.
58.   Fasano, M.; Curry, S.; Terreno, E.; Galliano, M.; Fanali, G.; Narciso, P.; Notari, S.; Ascenzi, P., *IUBMB Life* **2005,** *57* (12), 787-796.
59.   Peters Jr., T., *All about albumin: Biochemistry, genetics, and medical applications*. Academic Press: San Diego, 1996.
60.   Ghuman, J.; Zunszain, P. A.; Petitpas, I.; Bhattacharya, A. A.; Otagiri, M.; Curry, S., *J. Mol. Biol.* **2005,** *353* (1), 38-52.
61.   Merlot, A. M.; Kalinowski, D. S.; Richardson, D. R., *Front. Physiol.* **2014,** *5,* 299.
62.   Heim, M. E.; Flechtner, H.; Keppler, B. K. In *Clinical Studies with Budotitane — A New Non-Platinum Metal Complex for Cancer Therapy*, Ruthenium and Other Non-Platinum Metal Complexes in Cancer Chemotherapy, Berlin, Heidelberg, 1989//; Baulieu, E.; Forman, D. T.; Ingelman-Sundberg, M.; Jaenicke, L.; Kellen, J. A.; Nagai, Y.; Springer, G. F.; Träger, L.; Will-Shahab, L.; Wittliff, J. L., Eds. Springer Berlin Heidelberg: Berlin, Heidelberg, 1989; pp 217-223.
63.   Schilling, T.; Keppler, K. B.; Heim, M. E.; Niebch, G.; Dietzfelbinger, H.; Rastetter, J.; Hanauske, A.-R., *Investigational New Drugs* **1996,** *13* (4), 327-332.
64.   Christodoulou, C. V.; Ferry, D. R.; Fyfe, D. W.; Young, A.; Doran, J.; Sheehan, T. M.; Eliopoulos, A.; Hale, K.; Baumgart, J.; Sass, G.; Kerr, D. J., *J. Clin. Oncol.* **1998,** *16* (8), 2761-2769.
65.   Korfel, A.; Scheulen, M.; Schmoll, H.-J.; Gründel, O.; Harstrick, A.; Knoche, M.; M Fels, L.; Skorzec, M.; Bach, F.; Baumgart, J.; Sass, G.; Seeber, S.; Thiel, E.; Berdel, W., *Clin. Cancer Res.* **1998,** *4*, 2701-8.
66.   Mross, K.; Robben-Bathe, P.; Edler, L.; Baumgart, J.; Berdel, W. E.; Fiebig, H.; Unger, C., *Onkologie* **2000,** *23* (6), 576-579.

67. Lümmen, G.; Sperling, H.; Luboldt, H.; Otto, T.; Rübben, H., *Cancer Chemother. Pharmacol.* **1998,** *42* (5), 415-417.

68. Kröger, N.; Kleeberg, U. R.; Mross, K.; Edler, L.; Hossfeld, D. K., *Onkologie* **2000,** *23* (1), 60-62.

69. Buettner, K. M.; Snoeberger, R. C.; Batista, V. S.; Valentine, A. M., *Dalton Trans.* **2011,** *40* (37), 9580-9588.

70. Ravera, M.; Cassino, C.; Monti, E.; Gariboldi, M.; Osella, D., *J. Inorg. Biochem.* **2005,** *99* (12), 2264-2269.

71. Pandrala, M.; Casanas-Montes, B.; Lopez Cubero, A.; Planas Fontánez, T. M.; Parham, L. R.; Vazquez, A. M.; Martinez, M.; Sharma, S.; Saxena, M.; Castro Lebron, G.; Colon, J. L.; Tinoco, A. D., **Manuscript in preparation**.

72. Abeysinghe, P. M.; Harding, M. M., *Dalton Trans.* **2007,** (32), 3474-82.

73. Caruso, F.; Rossi, M., *Mini. Rev. Med. Chem.* **2004,** *4* (1), 49-60.

74. Ellahioui, Y.; Prashar, S.; Gomez-Ruiz, S., *Inorganics* **2017,** *5* (1), 4.

75. de la Cueva-Alique, I.; Munoz-Moreno, L.; Benabdelouahab, Y.; Elie, B. T.; El Amrani, M. A.; Mosquera, M. E.; Contel, M.; Bajo, A. M.; Cuenca, T.; Royo, E., *J. Inorg. Biochem.* **2016,** *156*, 22-34.

76. Top, S.; Kaloun, E. B.; Vessieres, A.; Laios, I.; Leclercq, G.; Jaouen, G., *J. Organomet. Chem.* **2002,** *643*, 350-356.

77. Vessieres, A.; Plamont, M. A.; Cabestaing, C.; Claffey, J.; Dieckmann, S.; Hogan, M.; Muller-Bunz, H.; Strohfeldt, K.; Tacke, M., *J. Organomet. Chem.* **2009,** *694* (6), 874-879.

78. Gao, L. M.; Vera, J. L.; Matta, J.; Meléndez, E., *J. Biol. Inorg. Chem.* **2010,** *15* (6), 851-859.

79. Gao, L.; Maldonado, W.; Narváez-Pita, X.; Carmona-Negrón, J.; Olivero-Verbel, J.; Meléndez, E., *Inorganics* **2016,** *4* (4), 38.

80. Pérez-Quintanilla, D.; Gómez-Ruiz, S.; Žižak, Ž.; Sierra, I.; Prashar, S.; del Hierro, I.; Fajardo, M.; Juranić, Z. D.; Kaluđerović, G. N., *Chem. Eur. J.* **2009,** *15* (22), 5588-5597.

81. Kaluđerović, G. N.; Tayurskaya, V.; Paschke, R.; Prashar, S.; Fajardo, M.; Gómez-Ruiz, S., *Appl. Organomet. Chem.* **2010,** *24* (9), 656-662.

82. García-Peñas, A.; Gómez-Ruiz, S.; Pérez-Quintanilla, D.; Paschke, R.; Sierra, I.; Prashar, S.; del Hierro, I.; Kaluđerović, G. N., *J. Inorg. Biochem.* **2012,** *106* (1), 100-110.

83. Ceballos-Torres, J.; Virag, P.; Cenariu, M.; Prashar, S.; Fajardo, M.; Fischer-Fodor, E.; Gómez-Ruiz, S., *Chem. Eur. j* **2014,** *20* (34), 10811-10828.

84. Wani, W. A.; Prashar, S.; Shreaz, S.; Gomez-Ruiz, S., *Coord. Chem. Rev.* **2016,** *312*, 67-98.

85. Ceballos-Torres, J.; del Hierro, I.; Prashar, S.; Fajardo, M.; Mijatović, S.; Maksimović-Ivanić, D.; Kaluđerović, G. N.; Gómez-Ruiz, S., *J. Organomet. Chem.* **2014,** *769*, 46-57.

86. Cuffe, S.; Dowling, C. M.; Claffey, J.; Pampillón, C.; Hogan, M.; Fitzpatrick, J. M.; Carty, M. P.; Tacke, M.; Watson, R. W. G., *Prostate* **2011,** *71* (2), 111-124.

87. Bannon, J. H.; Fichtner, I.; O'Neill, A.; Pampillón, C.; Sweeney, N. J.; Strohfeldt, K.; Watson, R. W.; Tacke, M.; Mc Gee, M. M., *Br. J. Cancer* **2007,** *97* (9), 1234-1241.

88.   Schur, J.; Manna, C. M.; Deally, A.; Köster, R. W.; Tacke, M.; Tshuva, E. Y.; Ott, I., *Chem. Commun.* **2013,** *49* (42), 4785.

89.   Schur, J.; Manna, C. M.; Deally, A.; Köster, R. W.; Tacke, M.; Tshuva, E. Y.; Ott, I., *Chem. Commun.* **2013,** *49* (42), 4785-4787.

90.   Zou, T.; Lum, C. T.; Lok, C.-N.; Zhang, J.-J.; Che, C.-M., *Chem. Soc. Rev.* **2015,** *44* (24), 8786-8801.

91.   Berners-Price, S. J.; Sadler, P. J. In *Phosphines and metal phosphine complexes: Relationship of chemistry to anticancer and other biological activity*, Berlin, Heidelberg, Springer Berlin Heidelberg: Berlin, Heidelberg, 1988; pp 27-102.

92.   Kenny, S. L., *Gold: A Cultural Encyclopedia*. ABC-CLIO: 2011.

93.   Kean, W. F.; Kean, I. R., *Inflammopharmacology* **2008,** *16* (3), 112-25.

94.   Pricker, S. P., *Gold Bull.* **1996,** *29* (2), 53-60.

95.   Sutton, B. M.; McGusty, E.; Walz, D. T.; DiMartino, M. J., *J. Med. Chem.* **1972,** *15* (11), 1095-1098.

96.   Finkelstein, A. E.; Walz, D. T.; Batista, V.; Mizraji, M.; Roisman, F.; Misher, A., *Ann. Rheum. Dis.* **1976,** *35* (3), 251-257.

97.   Schattenkirchner, M.; Kaik, B.; Muller-Fassbender, H.; Rau, R.; Zeidler, H., *J. Rheumatol. Suppl.* **1982,** *8*, 184-189.

98.   Ward, J. R.; Williams, H. J.; Boyce, E.; Egger, M. J.; Reading, J. C.; Samuelson, C. O., *Am. J. Med.* **1983,** *75* (6A), 133-137.

99.   Schattenkirchner, M.; Bröll, H.; Kaik, B.; Müller-Faßbender, H.; Rau, R.; Zeidler, H., *Klin. Wochenschr.* **1988,** *66* (4), 167-174.

100.   Telleria, C. M., *J. Cancer Ther.* **2012,** *4* (7), ix-xi.

101.   Roder, C.; Thomson, M. J., *Drugs R. D.* **2015,** *15* (1), 13-20.

102.   Yeo, C. I.; Ooi, K. K.; Tiekink, E. R. T., *Molecules* **2018,** *23* (6), 1410.

103.   Simon, T. M.; Kunishima, D. H.; Vibert, G. J.; Lorber, A., *J. Rheumatol. Suppl.* **1979,** *5*, 91-97.

104.   Mirabelli, C. K.; Johnson, R. K.; Sung, C. M.; Faucette, L.; Muirhead, K.; Crooke, S. T., *Cancer Res.* **1985,** *45* (1), 32-9.

105.   Mirabell, C. K.; Johnson, R. K.; Hill, D. T.; Faucette, L. F.; Girard, G. R.; Kuo, G. Y.; Sung, C. M.; Crooke, S. T., *J. Med. Chem.* **1986,** *29* (2), 218-223.

106.   Rigobello, M. P.; Scutari, G.; Boscolo, R.; Bindoli, A., *Br. J. Pharmacol.* **2002,** *136* (8), 1162-8.

107.   Nobili, S.; Mini, E.; Landini, I.; Gabbiani, C.; Casini, A.; Messori, L., *Med. Res. Rev.* **2010,** *30* (3), 550-580.

108.   Rigobello, M. P.; Scutari, G.; Folda, A.; Bindoli, A., *Biochem. Pharmacol.* **2004,** *67* (4), 689-696.

109.   Chrysouli, M. P.; Banti, C. N.; Kourkoumelis, N.; Panayiotou, N.; Markopoulos, G. S.; Tasiopoulos, A. J.; Hadjikakou, S. K., *J. Inorg. Biochem.* **2018,** *179*, 107-120.

110.   Snyder, R. M.; Mirabelli, C. K.; Crooke, S. T., *Biochem. Pharmacol.* **1986,** *35* (6), 923-932.

111.   Snyder, R. M.; Mirabelli, C. K.; Crooke, S. T., *Biochem. Pharmacol.* **1987,** *36* (5), 647-654.

112.   Shaw, C. F., *Chem. Rev.* **1999,** *99* (9), 2589-2600.

113.   Bryan, D. L. B.; Mikuriya, Y.; Hempel, J. C.; Mellinger, D.; Hashim, M.; Pasternack, R. F., *Inorg. Chem.* **1987,** *26* (25), 4180-4185.

114.   Intoccia, A. P.; Flanagan, T. L.; Walz, D. T.; Gutzait, L.; Swagzdis, J. E.; Flagiello, J., Jr.; Hwang, B. Y.; Dewey, R. H.; Noguchi, H., *J. Rheumatol. Suppl.* **1982,** *8*, 90-8.

115.   Papp, K. A.; Shear, N. H., *Clin. Dermatol.* **1991,** *9* (4), 535-51.

116.   Garcia, A.; Carvalhaes, R.; Grazul, R.; Lopes, M. P.; Corrêa, C.; Santos, H.; Almeida, M.; Silva, H., *J. Biol. Inorg. Chem.* **2016,** *21* (2), 275-292.

117.   Commisso, C.; Davidson, S. M.; Soydaner-Azeloglu, R. G.; Parker, S. J.; Kamphorst, J. J.; Hackett, S.; Grabocka, E.; Nofal, M.; Drebin, J. A.; Thompson, C. B.; Rabinowitz, J. D.; Metallo, C. M.; Vander Heiden, M. G.; Bar-Sagi, D., *Nature* **2013,** *497* (7451), 633-7.

118.   Chaves, J. S. D.; Neumann, F.; Francisco, T.; Corrêa, C.; Lopes, M. T. P.; Silva, H.; Fontes, A.; Almeida, M., *Inorg. Chim. Acta* **2014,** *414*, 85–90.

119.   Dean, T. C.; Yang, M.; Liu, M.; Grayson, J. M.; DeMartino, A. W.; Day, C. S.; Lee, J.; Furdui, C. M.; Bierbach, U., *ACS Med. Chem. Lett.* **2017,** *8* (5), 572-576.

120.   Pratesi, A.; Cirri, D.; Ciofi, L.; Messori, L., *Inorg. Chem.* **2018,** *57* (17), 10507-10510.

121.   Hill, D. T.; Isab, A. A.; Griswold, D. E.; DiMartino, M. J.; Matz, E. D.; Figueroa, A. L.; Wawro, J. E.; DeBrosse, C.; Reiff, W. M.; Elder, R. C.; Jones, B.; Webb, J. W.; Shaw, C. F., *Inorg. Chem.* **2010,** *49* (17), 7663-7675.

122.   Dada, O.; Sánchez, G.; Tacke, M.; Zhu, X., *Tetrahedron Lett.* **2018,** *59* (30), 2904–2908.

123.   Walther, W.; Dada, O.; O'Beirne, C.; Ott, I.; Sánchez, G.; Schmidt, C.; Werner, C.; Zhu, X.; Tacke, M., *Lett. Drug Des. Discovery* **2017,** *14* (2), 125-134.

124.   ClinicalTrials.gov. https://clinicaltrials.gov (accessed 1 December 2019).

125.   Jatoi, A.; Radecki Breitkopf, C.; Foster, N. R.; Block, M. S.; Grudem, M.; Wahner Hendrickson, A.; Carlson, R. E.; Barrette, B.; Karlin, N.; Fields, A. P., *Oncology* **2015,** *88* (4), 208-213.

126.   Saba, N. S.; Ghias, M.; Manepalli, R.; Schorno, K.; Weir, S.; Austin, C.; Maddocks, K.; Byrd, J. C.; Kambhampati, S.; Bhalla, K.; Wiestner, A., *Blood* **2013,** *122* (21), 3819-3819.

127.   Wenzel, M.; Bertrand, B.; Eymin, M.; Comte, V.; Harvey, J. A.; Richard, P.; Groessl, M.; Zava, O.; Amrouche, H.; Harvey, P. D.; Le Gendre, P.; Picquet, M.; Casini, A., *Inorg. Chem.* **2011,** *50* (19), 9472-9480.

128.   Fernández-Gallardo, J.; Elie, B. T.; Sulzmaier, F. J.; Sanaú, M.; Ramos, J. W.; Contel, M., *Organometallics* **2014,** *33* (22), 6669-6681.

129.   Fernández-Gallardo, J.; Elie, B. T.; Sadhukha, T.; Prabha, S.; Sanaú, M.; Rotenberg, S. A.; Ramos, J. W.; Contel, M.,   *Chem. Sci.* **2015,** *6* (9), 5269-5283.

130.   Tabrizi, L.; Olasunkanmi, L. O.; Fadare, O. A., *Chem. Commun.* **2020,** *56* (2), 297-300.

131.   Meker, S.; Braitbard, O.; Hall, M. D.; Hochman, J.; Tshuva, E. Y., *Eur. J. Chem.* **2016,** *22* (29), 9986-9995.

132.   Tshuva, E. Y.; Ashenhurst, J. A., *Eur. J. Inorg. Chem.* **2009,** *2009* (15), 2203-2218.

133.   Cini, M.; Bradshaw, T. D.; Woodward, S., *Chem. Soc. Rev.* **2017,** *46* (4), 1040-1051.

134.   Parks, T. B.; Cruz, Y. M.; Tinoco, A. D., *Inorg. Chem.* **2014,** *53* (3), 1743-1749.

Chapter 5

Conclusions and publications

5.1. CONCLUSIONS

Ti has been considered a non-essential metal for a long time. But now, we can understand that this statement is not entirely true; even when it is not fully understood, Ti can directly interact con many biological molecules and participate in enzyme transport and delivery. Understanding its mechanism of action and biological effect on cancer and non-cancer cells will give us the knowledge to develop more potent and effective cancer cells.

The mechanistic insight of $[Ti(Deferasirox)_2]^{2-}$ complex in which Fe and Cu are involved were studied. We found how these two metals can trigger a transmetalation process, affecting cancer by metal depletion therapy. At the same time, Ti(IV) is released in the intracellular environment. Previous work shows that it affects nucleotides and thus DNA synthesis in a three-metal involved anticancer treatment. Additionally, the Fe-induce transmetalation process is presumed to increase the ROS production in mitochondrial and cytoplasm by forming active redox intermediates, possibly causing mitochondrial disruption and cell death. On the other side, Cu(II) binds Deferasirox forming cytotoxic species as in a pro-drug-like behavior to become a more potent pharmacologically active drug. Its concentration-dependent speciation and affinity of the ligand by the metal ion in physiological conditions demonstrate the capability of intracellular formation of this compound. Even low concentration can play a part in the dose-response mechanism of $[Ti(Deferasirox)_2]^{2-}$ against cancer cells. A summary of the combined Fe and Cu induced transmetalation mechanism is presented in **figure 5.1**. Part of this work was performed in the l'école nationale supérieure de chimie de Paris - PSL. Chimie ParisTech, thanks to the Chateaubriand fellowship of the embassy of France in the USA. This fellowship supported me to complete a four months internship.

After the mechanistic studies and to ensure compounds are getting to the expected target, drug delivery systems (DDS) were tested. Interestingly, two of the three-tested DDS failed in improving the biological activity of the compounds against cancer cells. Even when Ti(IV) 's delivered amount increases, the action remains under the accepted values. Except for the transferrin receptor peptide (HAIYPRHK) P7 -conjugated Deferasirox-Ti(IV) complex, which effectively delivers a higher amount of Ti(IV) and still guaranteeing and potentiating its action compared to the parent compound.

These studies demonstrated that it is not only how much metal is delivered; otherwise, how much metal biologically active reaches the desired target. P7 delivered the compound with more selectivity to cancer cells, and probably the

parent compound is intact in the intracellular environment, allowing it to show its action.

Ti-based compounds are still under development. Researchers are taking some approaches to synthesize new derivatives, multicentered-fused drugs and design new DDSs. Current results are promising, and more stable, potent, and selective compounds with lower IC_{50} values will come.
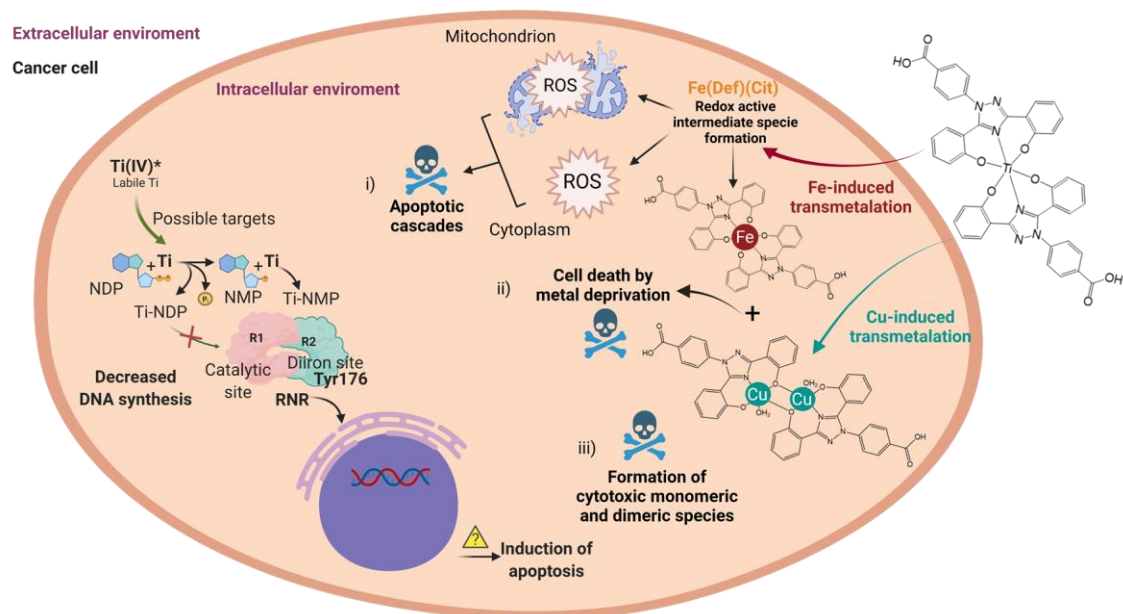

Figure 5.1. Proposed multi-focused mechanism of i) Fe-induced ROS imbalance, ii) Cell death metal deprivation, and iii) Cu(II) Deferasirox cytotoxic species formation. *Ti(IV) pathway model published in Gaur, K.; Tinoco, A.D. et al. *J. Am. Chem. Soc. Au.* **2021**, doi:10.1021/jacsau.1c00078.

5.2. List of publications

The following publications were the product of the research work during my Ph. D. time:

*: Denotes authorship.

-Rodríguez, I., **Fernández-Vega, L.**, Maser-Figueroa, A. N., Sang, B., González-Pagán, P., & Tinoco, A. D. Exploring Titanium (IV) Complexes as Potential Antimicrobial Compounds. *Antibiotics* **2022**, *11*(2), 158.

-Gaur, Kavita;* Cruz, Yahaira; Santiago Espinoza, Jose; Morales Rueda, Carlos; Loza-Rosas, Sergio; **Fernandez-Vega, Lauren**; Benjamín-Rivera, Josue; Alvarez, Adelis; Tinoco, Arthur. Exploring the pH dependent aqueous speciation of metal complexes through UV-Vis spectroscopy. *J. Chem. Educ* **2020**, 97(7), 1970–1975.

-**Fernández-Vega, L.*,** Ruiz Silva, V. A., Domínguez-González, T. M., Claudio-Betancourt, S., Toro-Maldonado, R. E., Capre Maso, L. C., ... & Pagán Meléndez, F. Evaluating Ligand Modifications of the Titanocene and Auranofin Moieties for the Development of More Potent Anticancer Drugs. Inorganics **2019**, 8(2), 10.

- **Fernández-Vega, L**.*; Gaur, K.*; Vázquez-Salgado, A.; Duran-Camacho, G.; Dominguez-Martinez, I.; Benjamín-Rivera, J.*; Carmona Sarabia, L.; Cruz García, A.; Pérez-Deliz, F.; Méndez Román, J., Iron and Copper Intracellular Chelation as an Anticancer Drug Strategy. *Inorganics* **2018,** *6*, 126.

-Das, S.; Parga, K.; Chakraborty, I.; Tinoco, A.D.; Delgado, Y.; Lopez, P.M.; **Fernández Vega, L.**; Sanakis, Y.; Ghosh, Y.; Ghosh, S.; Bankson, J.; Klostergaard, J.; Gonzalez-Mendez, R.; Raptis, R.G.* "Octanuclear iron-oxo clusters enhance contrast in magnetic resonance imaging *in vitro* and *in vivo.*" *Journal of inorganic biochemistry* **2018,** *186*, 176-186.

- **L. Fernández***, M. Ruidiaz, L. Pérez, A. Pérez-Gamboa, "Structural, spectroscopic and optical properties of 4-(6-(dimethylamino)benzo[d]thiazol-2-yl)benzonitrile as a model of system D-E-A by computational methods", *Prospectiva* **2018**, *16*, 114-123.

5.3.   List of presentations

-Fernández, L.V. "Reactive oxygen species (ROS) homeostasis imbalance as the mechanism of action of deferasirox and its Ti(IV) complex against lung cancer" Poster presentation given at the ACS spring meeting, San Diego, USA, March 2022.

-Fernández, L.V. "Expanding the knowledge of the mechanism of action and improvement of the selectivity of the Titanium(IV)-based complexes" Poster presentation given at the ISABC15 Nara, Japan, June 2019.

-Fernández, L.V. "Expanding the knowledge of the mechanism of action and improvement of the selectivity of the Titanium(IV)-based complexes" Flash talk given at the ISABC15 Nara, Japan, June 2019.

- Fernández, L. V. "Design of Deferasirox peptide-conjugated ligands for a selective delivery of anticancer Ti(IV) compounds." Congreso Estudiantil de Investigacion Graduada (CEIG) San Juan, Puerto Rico, October 2018.

-Fernández, L.V. "Design of Biomimicking Anticancer Drug Based on Peptide-Conjugated Ligands for Selective Delivery of Titanium(IV)." The poster presentation was given at the ISABC14 Toulouse, France, June 2017.

Appendix

Appendix 1. Permission from Inorganics under the Creative Commons Attribution License (attribution 4.0 International CC BY 4.0), *8,* 48. https://doi.org/10.3390/inorganics8090048

Every element presented from the following scientific review:

Benjamín-Rivera, J.A.; Cardona-Rivera, A.E.; Vázquez-Maldonado, Á.L.; Dones-Lassalle, C.Y.; Pabón-Colon, H.L.; Rodríguez-Rivera, H.M.; Rodríguez, I.; González-Espiet, J.C.; Pazol, J.; Pérez-Ríos, J.D.; Catala-Torres, J.F.; Carrasquillo Rivera, M.; De Jesus-Soto, M.G.; Cordero-Virella, N.A.; Cruz-Maldonado, P.M.; González-Pagan, P.; Hernández-Ríos, R.; Gaur, K.; Loza-Rosas, S.A.; Tinoco, A.D. Exploring Serum Transferrin Regulation of Nonferric Metal Therapeutic Function and Toxicity. *Inorganics* **2020**, *8,* 48. https://doi.org/10.3390/inorganics8090048

Appendix 2. Permission from Journal of the American Chemical Society, 138(17), 5659–5665. Copyright 2016 American Chemical Society.

Appendix 3. Permission from Elsevier, 109–125, Copyright (2018).

ELSEVIER LICENSE
TERMS AND CONDITIONS

Apr 05, 2022

This Agreement between Lauren Fernandez-Vega ("You") and Elsevier ("Elsevier") consists of your license details and the terms and conditions provided by Elsevier and Copyright Clearance Center.

License Number	5282631109890
License date	Apr 05, 2022
Licensed Content Publisher	Elsevier
Licensed Content Publication	Coordination Chemistry Reviews
Licensed Content Title	Exploring titanium(IV) chemical proximity to iron(III) to elucidate a function for Ti(IV) in the human body
Licensed Content Author	Manoj Saxena,Sergio A. Loza-Rosas,Kavita Gaur,Shweta Sharma,Sofía C. Pérez Otero,Arthur D. Tinoco
Licensed Content Date	May 15, 2018
Licensed Content Volume	363
Licensed Content Issue	n/a
Licensed Content Pages	17
Start Page	109
End Page	125

Appendix 4. Permission from Inorganic Chemistry, 56, 14, 7788-7802. Copyright 2017 American Chemical Society.

CCC
RightsLink®

🏠 Home   ❓ Help ∨   📞 Live Chat   👤 Sign in   👤➕ Create Account

Expanding the Therapeutic Potential of the Iron Chelator Deferasirox in the Development of Aqueous Stable Ti(IV) Anticancer Complexes

ACS Publications
Most Trusted. Most Cited. Most Read.

Author: Sergio A. Loza-Rosas, Alexandra M. Vázquez-Salgado, Kennett I. Rivero, et al

Publication: Inorganic Chemistry

Publisher: American Chemical Society

Date: Jul 1, 2017

Copyright © 2017, American Chemical Society

PERMISSION/LICENSE IS GRANTED FOR YOUR ORDER AT NO CHARGE

This type of permission/license, instead of the standard Terms and Conditions, is sent to you because no fee is being charged for your order. Please note the following:

- Permission is granted for your request in both print and electronic formats, and translations.
- If figures and/or tables were requested, they may be adapted or used in part.
- Please print this page for your records and send a copy of it to your publisher/graduate school.
- Appropriate credit for the requested material should be given as follows: "Reprinted (adapted) with permission from {COMPLETE REFERENCE CITATION}. Copyright {YEAR} American Chemical Society." Insert appropriate information in place of the capitalized words.
- One-time permission is granted only for the use specified in your RightsLink request. No additional uses are granted (such as derivative works or other editions). For any uses, please submit a new request.

If credit is given to another source for the material you requested from RightsLink, permission must be obtained from that source.

BACK   CLOSE WINDOW

Appendix 5. Permission from Jacs Au under the Creative Commons Attribution License (attribution 4.0 International CC BY 4.0), *1*(6), 865-878.

Every element presented from the following scientific review:

Gaur, K., Pérez Otero, S. C., Benjamín-Rivera, J. A., Rodríguez, I., Loza-Rosas, S. A., Vázquez Salgado, A. M., ... & Tinoco, A. D. Iron chelator transmetalative approach to inhibit human ribonucleotide reductase. *Jacs Au* **2021**, *1*(6), 865-878.

It is approved to use under the Creative Commons Attribution License described in the following link:

https://creativecommons.org/licenses/by-nc-nd/4.0/

All credits to the authors.

Appendix 6. Provisional patent on the HAIYPRHK (P7) Deferasirox bioconjugate and Ti(IV) complex.

Acknowledgement Receipt

The USPTO has received your submission at **17:50:17** Eastern Time on **25-MAY-2021** .

$ **75** fee paid by e-Filer via *RAM* with Confirmation Number: E20215OH50423103.

eFiled Application Information

EFS ID	42818395
Application Number	63192911
Confirmation Number	8286
Title	Development of a titanium(IV) peptide-iron/copper chelator compound for anticancer drugs that operate by iron/copper-based transmetalation and serve as a dual ribonucleotide reductase inhibitor
First Named Inventor	Arthur D. Tinoco
Customer Number or Correspondence Address	51353
Filed By	Roberto Jose Rios Cuevas
Attorney Docket Number	UPR-20-025
Filing Date	
Receipt Date	25-MAY-2021
Application Type	Provisional

Application Details

Sequence	Submitted Files	Page Count	Document Description	File Size	Warnings
1	SPECIFICATION.pdf	113	Specification	11040417 bytes	◆ PASS
No validation errors found.					
2	sb0015b.pdf	2	Certification of Micro Entity (Education Basis)	122114 bytes	◆ PASS
No validation errors found.					
3	ProvisionalSB.pdf	3	Provisional Cover Sheet (SB16)	1477272 bytes	◆ PASS
No validation errors found.					
4	fee-info.pdf	2	Fee Worksheet (SB06)	30013 bytes	◆ PASS
No validation errors found.					

This Acknowledgement Receipt evidences receipt on the noted date by the USPTO of the indicated documents, characterized by the applicant, and including page counts, where applicable. It serves as evidence of receipt similar to a Post Card, as described in MPEP 503.

New Applications Under 35 U.S.C. 111

If a new application is being filed and the application includes the necessary components for a filing date (see 37 CFR 1.53(b)-(d) and MPEP 506), a Filing Receipt (37 CFR 1.54) will be issued in due course and the date shown on this Acknowledgement Receipt will establish the filing date of the application.

National Stage of an International Application under 35 U.S.C. 371

If a timely submission to enter the national stage of an international application is compliant with the conditions of 35 U.S.C. 371 and other applicable requirements a Form PCT/DO/EO/903 indicating acceptance of the application as a national stage submission under 35 U.S.C. 371 will be issued in addition to the Filing Receipt, in due course.

New International Application Filed with the USPTO as a Receiving Office

If a new international application is being filed and the international application includes the necessary components for an international filing date (see PCT Article 11 and MPEP 1810), a Notification of the International Application Number and of the International Filing Date (Form PCT/RO/105) will be issued in due course, subject to prescriptions concerning national security, and the date shown on this Acknowledgement Receipt will establish the international filing date of the application.

If you need help:

- *To ask questions about Patent e-Filing, or to suggest improvements to the online system, or report technical problems, please call the Patent Electronic Business Center at (866) 217-9197 (toll free) or send email to EBC@uspto.gov.*
- *Send general questions about USPTO programs to the USPTO Contact Center (UCC) .*
- *For general questions regarding a petition, or requirements for filing a petition, contact the Office of Petitions Help Desk at 1 800-786-9199.*

Appendix 7. Experiment contributions in Tinoco lab papers

CO-ADD Screening Results[1]

The CO-ADD performs a first antimicrobial screening of compounds at a one-dose concentration of 32 µg/mL to assess general potency. Compounds that demonstrate inhibition of the growth of two or more of the microbes between 50% to 75% or of at least one microbe at greater than 75% are typically then advanced to a dose–response screening (0.25 to 32 µg/mL) and are also tested for human cell toxicity to evaluate their therapeutic index (selectivity against microbes versus human cells). Next, it is provided a summary of these two screenings, which lists the compounds numerically. The compounds Ti(Deferasirox)$_2$ (**10**), Ti(HBED) (**11**), K$_2$[Ti(naphthalene-2,3-diolate)$_3$] (**5**), K$_2$[TiO(Oxalate)$_2$] (**14**), and HBED (**8**) met the criteria to advance to the second screening. Although deferasirox (**4**) and [Cu(Deferasirox)(H$_2$O)]$_2$ (**15**) did not meet the criteria, they were also included in the second screening.

Table 6.1. Predicted or measured MIC (µg/mL) values for the compounds against the Gram-negative (G-ve) bacteria, Gram-positive (G+ve) bacteria, and the fungi. The maximum % inhibition (Dmax) exhibited by the compounds against each organism is included. MIC values that could be measured are highlighted in yellow. D$_{max}$ values of _50% are highlighted in gray. ND = Not determined.

| | G+ve | | G−ve | | | | | | | | Fungi | | | |
| | S. aureus (MRSA) | | A. baumannii | | E. coli | | K. pneumoniae | | P. aeruginosa | | C. albicans | | C. neoformans | |
	MIC	D$_{max}$	MIC	D$_{max}$	MIC	D$_{max}$	MIC	D$_{max}$	MIC	D$_{max}$	MIC	D$_{max}$	MIC	D$_{max}$
1	>32	10.59	>32	18	>32	6.14	>32	14.22	>32	10.27	>32	0.28	>32	−8.24
2	>32	12.55	>32	31.32	>32	6.86	>32	26.77	>32	14.61	>32	16.32	>32	−9.97
3	>32	−2.34	>32	−1.93	>32	−9.07	>32	4.11	>32	10.03	>32	6.23	>32	−7.23
4	>32	44.31	>32	18.95	>32	7.72	>32	20.2	>32	5.82	>32	4.31	>32	−25.58
5	>32	24.28	>32	68.29	>32	51.65	>32	52.86	>32	69.01	>32	3.5	>32	−17.49
6	>32	13.86	>32	17.87	>32	−0.01	>32	17.1	>32	9.76	>32	30.95	>32	−10.66
7	>32	38.01	>32	17.94	>32	10.41	>32	15.43	>32	7.99	>32	44.53	>32	−7.88
8	>32	52.5	>32	24.76	>32	2.67	>32	22.94	>32	13.43	>32	57.57	>32	−1.45
9	>32	7.82	>32	1.55	>32	−0.56	>32	6.35	>32	10.27	>32	4.27	>32	−1.7
10	16	98.2	>32	16.28	>32	20.44	>32	34.61	>32	7.57	>32	5.74	>32	−5.72
11	>32	61.46	>32	68.73	>32	48.02	>32	56.3	>32	72.48	>32	10.43	>32	−18.86
12	>32	3.66	>32	9.4	>32	2.6	>32	12.46	>32	9.57	>32	49.3	>32	−5.2
13	>32	51.55	>32	15.78	>32	23.76	>32	16.65	>32	16.01	>32	16.15	>32	6.5
14	>32	40.5	>32	8.2	>32	11.0	>32	17.2	>32	7.5	32	77.3	>32	ND
15	>32	26.9	>32	7.8	>32	−9.5	>32	7.7	>32	19.2	>32	34.0	>32	ND

Solubility and stability study of conjugate [Fe$_8$]-Tyr-HA[2]

The ferrozine assay showed that 2 was reasonably water soluble and yielded relatively high iron concentrations. Conjugate 2 reached a maximal soluble iron concentration of 5.51 ± 0.43mM or 0.17 ± 0.015mM compound concentration in water. The compound is extremely stable in water. At 3.3 µM it does not demonstrate any UV–Vis spectral changes even after 24 h in solution (S10). The stability of the compound at the same concentration was monitored under physiologically relevant conditions (pH 7.4, 25mM Tris buffer, 100mM NaCl, 10%

fetal bovine serum (FBS)) every 15 min for 2 h and then every hour up to 24 h (**Fig 6.1**). The shoulder at 280 nm, attributable to the Tyr-HA, remains virtually constant for 12 h. Between the 12 and 24 h time points the absorbance increases either due to slow binding to biomolecular species in the FBS or a gradual speciation change because of partial dissociation of Tyr-HA and compound aggregation as discussed in the analysis of the gel filtration chromatographic data. This FBS-induced aggregation will obviously affect the relaxivity, therefore contrast enhancement, achieved in vivo compared to those determined in vitro. No new absorbance shoulders or maxima appear during the spectral changes.
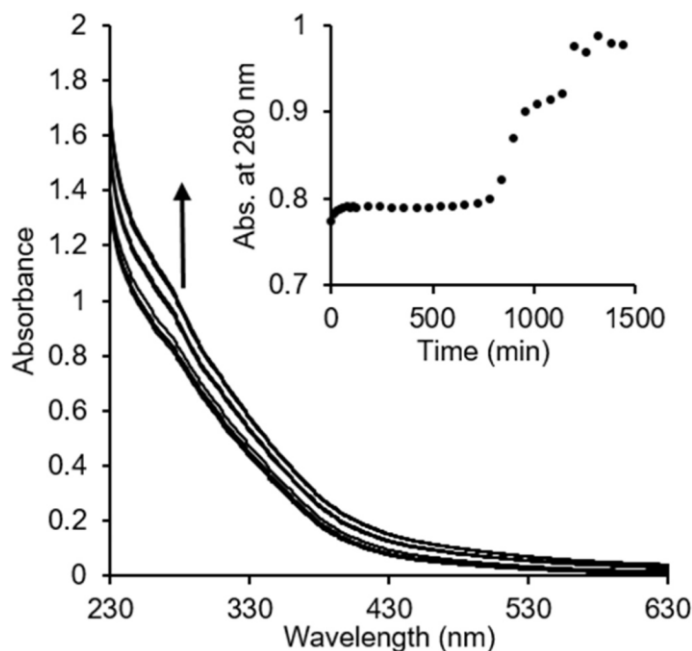

Figure 6.1. The stability of 3.3 µM conjugate 2 at pH 7.4 in 10% FBS monitored by changes in its UV–vis spectrum. Inset: Absorbance change at 280 nm over time.

Appendix 8. Thesis publication permission of the evaluating Ligand Modifications of the Titanocene and Auranofin Moieties for the Development of More Potent Anticancer Drugs paper (Chapter 4).

Permission from Inorganics under the Creative Commons Attribution License (attribution 4.0 International CC BY 4.0), *8*(2), 10; https://doi.org/10.3390/inorganics8020010.

Fernández-Vega, L.; Ruiz Silva, V.A.; Domínguez-González, T.M.; Claudio-Betancourt, S.; Toro-Maldonado, R.E.; Capre Maso, L.C.; Sanabria Ortiz, K.; Pérez-Verdejo, J.A.; Román González, J.; Rosado-Fraticelli, G.T.; Pagán Meléndez, F.; Betancourt Santiago, F.M.; Rivera-Rivera, D.A.; Martínez Navarro, C.; Bruno Chardón, A.C.; Vera, A.O.; Tinoco, A.D. Evaluating Ligand Modifications of the Titanocene and Auranofin Moieties for the Development of More Potent Anticancer Drugs. *Inorganics* **2020**, *8*, 10. https://doi.org/10.3390/inorganics8020010

It is approved to use under the Creative Commons Attribution License described in the following link:

https://creativecommons.org/licenses/by/4.0/

REFERENCES

1.   Rodríguez, I.; Fernández-Vega, L.; Maser-Figueroa, A. N.; Sang, B.; González-Pagán, P.; Tinoco, A. D., *Antibiotics* **2022,** *11* (2), 158.

2.   Das, S.; Parga, K.; Chakraborty, I.; Tinoco, A. D.; Delgado, Y.; López, P. M.; Vega, L. F.; Sanakis, Y.; Ghosh, S.; Bankson, J., *Journal of inorganic biochemistry* **2018,** *186*, 176-186.